ASD/XR-TR-75-22

TERRAIN FOLLOWING CONTROL BASED ON AN OPTIMIZED SPLINE MODEL OF AIRCRAFT MOTION

NOVEMBER 1975

TECHNICAL REPORT ON IN-HOUSE STUDIES

Approved for public release, distribution unlimited.

DEPUTY FOR DEVELOPMENT PLANNING
AERONAUTICAL SYSTEMS DIVISION
WRIGHT-PATTERSON AIR FORCE BASE, OHIO 45433

NOTICES

When Government drawings, specifications, or other data are used for any purpose other than in connection with a definitely related Government procurement operation, the United States Government thereby incurs no responsibility nor any obligation whatsoever; and the fact that the Government may have formulated, furnished or in any way supplied the said drawings, specifications, or other data, is not to be regarded by implication or otherwise as in any manner licensing the holder or any other person or corporation, or conveying any rights or permission to manufacture, use, or sell any patented invention that may in any way be related thereto.

This technical report has been reviewed and is approved for publication.

JAMES H. HALL
Colonel, USAF
Deputy for Development Planning

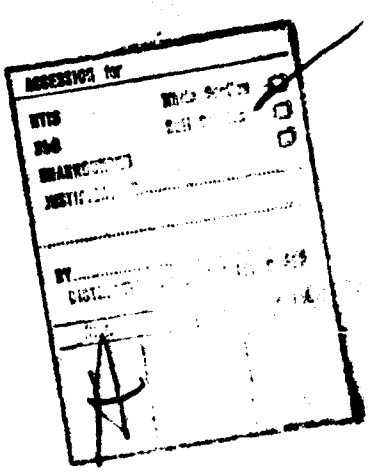

UNCLASSIFIED

SECURITY CLASSIFICATION OF THIS PAGE (When Data Entered)

REPORT DOCUMENTATION PAGE

READ INSTRUCTIONS BEFORE COMPLETING FORM

(14) 1. REPORT NUMBER: ASD/XR-TR-75-22

2. GOVT ACCESSION NO.

(9) 3. RECIPIENT'S CATALOG NUMBER

(6) 4. TITLE (and Subtitle): Terrain Following Control Based on an Optimized Spline Model of Aircraft Motion

5. TYPE OF REPORT & PERIOD COVERED: Technical Report

6. PERFORMING ORG. REPORT NUMBER

(10) 7. AUTHOR(s): James E. Punk

8. CONTRACT OR GRANT NUMBER(s)

9. PERFORMING ORGANIZATION NAME AND ADDRESS
Deputy for Development Planning (ASD/XR)
Aeronautical Systems Division
Wright-Patterson AFB, Ohio 45433

10. PROGRAM ELEMENT, PROJECT, TASK AREA & WORK UNIT NUMBERS
ASDP 0032 22600

11. CONTROLLING OFFICE NAME AND ADDRESS
Deputy for Development Planning (ASD/XR)
Aeronautical Systems Division
Wright-Patterson AFB, Ohio 45433

(11) 12. REPORT DATE: NOV [redacted] 75

13. NUMBER OF PAGES

14. MONITORING AGENCY NAME & ADDRESS (if different from Controlling Office)

15. SECURITY CLASS. (of this report): UNCLASSIFIED

15a. DECLASSIFICATION/DOWNGRADING SCHEDULE

(12) 192p.

16. DISTRIBUTION STATEMENT (of this Report)
Approved for public release, distribution unlimited.

17. DISTRIBUTION STATEMENT (of the abstract entered in Block 20, if different from Report)

18. SUPPLEMENTARY NOTES
This is a dissertation submitted in partial fulfilment of the requirements for the degree of Doctor of Philosophy (Aerospace Engineering) at the University of Michigan.

19. KEY WORDS (Continue on reverse side if necessary and identify by block number)
Terrain Following
Optimal Control
Cubic Splines
Low-Level Penetration
Mathematical Programming Problem
Automatic Control

20. ABSTRACT (Continue on reverse side if necessary and identify by block number)
The major portion of the computational processing of information in an aircraft terrain following system is optimized in order to provide the best commands to the longitudinal flight-control system based on available terrain data. Previous terrain-following processors have not optimized the flight path subject to all of the practical constraints. The scheme presented incorporates all of the major constraints into an optimization problem that can be solved to provide a reference path for the aircraft to follow.

DD FORM 1 JAN 73 1473 EDITION OF 1 NOV 65 IS OBSOLETE

403 875

UNCLASSIFIED

SECURITY CLASSIFICATION OF THIS PAGE (When Data Entered)

The optimal reference path satisfied two important requirements: 1) it stays as close to the terrain as possible while satisfying a minimum clearance constraint and the specified acceleration limits, and 2) it is a smooth path that the aircraft can follow extremely well by a very simple tracking system.

The optimization problem is either a quadratic or linear programming problem, depending upon the specific closeness performance criterion chosen. It appears that it can be solved in real time, even for a very high speed missile, by an airborne digital computer when accurate vehicle state and terrain information are available. The optimal solutions to the problem can also be used as "ideal" paths to provide standards for evaluating other types of terrain following systems.

ACKNOWLEDGMENTS

This report is a dissertation submitted in partial fulfilment of the requirements for the degree of Doctor of Philosophy (Aerospace Engineering) at The University of Michigan.

The author greatfully acknowledges the guidance of Dr. Elmer G. Gilbert and Dr. William F. Powers in the formulation of the studies and review of this report.

TABLE OF CONTENTS

PAGE

ACKNOWLEDGMENTS ii

LIST OF TABLES vi

LIST OF ILLUSTRATIONS vii

LIST OF APPENDICES ix

LIST OF SYMBOLS x

CHAPTER

1. INTRODUCTION 1

1.1 The Basic Terrain-Following Problem 1
1.2 Previous Terrain-Following Systems 2
1.3 The Information Processing Problem 4
1.4 The Specific Approach 6
1.5 Mathematical Complexities of the Optimization Problem 8
1.6 Overview 9

2. TERRAIN FOLLOWING CONCEPTS 11

2.1 Definitions 11

2.1.1 Acceleration limits 11
2.1.2 Clearance Curve 11
2.1.3 Ideal Path 13
2.1.4 Terrain Roughness 14
2.1.5 Path Curvature and Kink 14
2.1.6 Ride Hardness 15

2.2 Performance Criteria and Parameters 16

2.3 Terrain-Following Command Gereration 17

2.3.1 Flight-Path-Angle Controllers 17

2.3.1.1 Relative Altitude/Altitude-Rate System 18
2.3.1.2 Scanned-Range and Template Systems 19
2.3.1.3 Relative Angle Systems 21

2.3.2 Path Controllers 22

2.3.2.1 ADLAT System 22
2.3.2.2 Optimal Tracker System 24
2.3.2.3 Optimum Processor-Tracker System 26

PAGE

3. MODEL AND OPTIMIZATION FORMULATIONS 33

3.1 The Trajectory Model 33
3.2 The Optimal Control Problem 34
3.3 Discrete Equations of Motion 36
3.4 Discrete Performance Measure 39
3.5 Quadratic Programming Problem 40
3.6 Complementary Problem 41

4. FRAMING FOR DATA PROCESSING 44

4.1 The Characteristic Maneuver 44
4.2 Frame Advance 47
4.3 Frame Length 48
4.4 Frame Junctions 49
4.5 Control Point Spacing 51
4.6 Specification of Framing Structure 53

5. TERRAIN AND CLEARANCE CURVES 55

5.1 Cubic Splines 55
5.2 UNIVAC Spline Fitting Procedure 59
5.3 Direct Slope-Determination Spline Fits 61
5.4 End-Point Slope Estimates 63
5.5 Clearance Curve Determination 64

6. REFERENCE PATH DETERMINATION AND PARAMETRIC STUDIES . . 72

6.1 Penalty Function Approach 72
6.2 Quadratic Programming Approach 78
6.3 Performance Criteria Study 83

6.3.1 Quadratic and Linear Performance Measures 83
6.3.2 Min-Max Criterion 87

6.4 Frame Length Study 87
6.5 Control Point Spacing 94
6.6 Slope Constraints 97

7. TRACKER SYSTEM SIMULATIONS 100

8. REAL TIME AIRBORNE APPLICATIONS 112

8.1 Total Number of Sample Points 114
8.2 Computational Requirements 116
8.3 Evaluation of the Framing Structure for an Example Missile 117

PAGE

9. CONCLUSIONS AND RECOMMENDATIONS 125

9.1 Splines and Clearance Paths 125
9.2 Optimal Path Computations 126
9.3 Tracker System Performance 127
9.4 Overall System Performance 128
9.5 Recommendations 129

APPENDICES 132

REFERENCES 174

LIST OF TABLES

		PAGE
5-1	Comparison of the Differences in Clearance Curve Heights	71
6-1	Central Processor Solution Times	78
6-2	Cost Coefficient Comparison	84
6-3	Framing Structures for Reference Paths	86
6-4	Frame Length Study Data	89
6-5	Soft-Ride Computational Run Time Predictions	93
6-6	Control-Point Spacing Parametric Data	96
7-1	Tracker Gains and Performance	104
7-2	Tracker Performance Data	106
8-1	Framing Structures for Missile Paths	119
8-2	Missile Reference Path Performance and Computational Times	121

LIST OF ILLUSTRATIONS

		PAGE
2-1	Clearance Curves	12
2-2	Ideal Path	13
2-3	Flight-Path-Angle Controller Schematic	18
2-4	Relative Altitude / Altitude-Rate System	19
2-5	Template System	20
2-6	Relative-Angle System	21
2-7	ADLAT System Path	23
2-8	ADLAT Path Controller	24
2-9	Preprocessed Clearance Path	25
2-10	Optimal Tracker System	26
2-11	Minimum-Acceleration Constraint Enforcement	29
2-12	Digital Filtering Process	30
2-13	Digitally Filtered Data	31
3-1	Curvature Spline	36
4-1	Characteristic Maneuver	45
4-2	Data Frame Overlap	47
4-3	Frame Junction	50
4-4	Infeasible Solution at Frame Junction	51
4-5	Graduated-Control-Point Spacing	52
5-1	Cubic Spline Function	55
5-2	Unstable Spline Function	58
5-3	Typical Terrain Spline with Different End Slope Estimates	65
5-4	Extreme Test Terrain Spline with Different End Slope Estimates	66
5-5	Extreme Test Terrain Clearance Curves	67
5-6	1000-ft Clearance Path for Typical Terrain	68
5-7	Local Estimates of Clearance Differences	69
6-1	Bounded Parameter Search	74
6-2	Typical Penalty-Function Optimal Path	76
6-3	Penalty-Function Optimal Paths with Various Iteration Limits	77
6-4	Penalty-Function vs. Quadratic Programming Solutions	82
6-5	Control Comparison for Different Cost Coefficients	85
6-6	Min-Max vs. Quadratic Cost Solutions	88
6-7	Hard-Ride Frame Length Comparisons	90
6-8	Soft-Ride Frame Length Comparisons	92
6-9	Control-Point Spacing Comparisons	95
6-10	Dive Constraint Effects	98

		PAGE
7-1	General Tracker System Diagram	100
7-2	3-Channel Optimal-Path Tracker System	101
7-3	Soft-Ride Tracker Performance with 2000-ft Control Interval	107
7-4	Hard-Ride Tracker Performance with 2000-ft Control Interval	108
7-5	Hard-Ride Tracker Performance with 1000-ft Control Interval	109
7-6	Hard-Ride Tracker Performance with 500-ft Control Interval	110
8-1	Real Time Framing	112
8-2	Example Missile Optimal Path for Soft-Ride	120
8-3	Example Missile Optimal Path for Hard-Ride	122
8-4	Example Missile Optimal Path for Smooth Terrain	124
B-1	Characteristic Maneuver	144
C-1	Velocities and Accelerations	149
C-2	Radius of Curvature	150
E-1	Offset Loop	158
F-1	Positive Curvature Clearance Estimate	160
F-2	Negative Curvature Clearance Estimate	162
G-1	Stability Axis System	166
H-1	Maximum Clearance-Constraint Violation	170
H-2	Maximum Slope-Constraint Violation	172

LIST OF APPENDICES

		PAGE
APPENDIX A.	OPTIMIZATION PROBLEM EQUATION DERIVATIONS	132
	A.1 Path State Equations	132
	A.2 Cost Gradients	135
	A.3 Quadratic Programming Problem Equations	136
	A.4 Complementary Problem Equations	140
APPENDIX B.	CHARACTERISTIC MANEUVER FRAME LENGTH ESTIMATE . . .	144
APPENDIX C.	CURVATURE RELATIONSHIPS	149
APPENDIX D.	DIRECT SLOPE SPLINE FITTING METHOD	153
APPENDIX E.	OFFSET-LOOP-POINT REJECTION METHOD	158
APPENDIX F.	SLANT CLEARANCE ESTIMATE.	160
	F.1 Positive Curvature	160
	F.2 Negative Curvature	161
APPENDIX G.	AIRCRAFT SIMULATION	164
	G.1 General Aircraft Equations of Motion	166
	G.2 Normalization	169
	G.3 F-4C Aircraft Data	169
APPENDIX H.	CONSTRAINT VIOLATIONS BETWEEN SAMPLE POINTS	170

LIST OF SYMBOLS

E	Excess clearance constraint matrix
F	Clearance constraint vector
G	Standard gravitational acceleration unit (32.17 ft/sec^2)
H	Height of maximum expected terrain obstacle
I	Identity matrix
J	Performance measure
K-ft	1000 feet
L	Linear performance measure coefficient
M	Min-max performance measure coefficient
$\overline{M}$	Complementary problem matrix
N	Number of sample points
Q	Quadratic performance measure coefficient
R	Range along the horizontal
RMS	Root mean squared sample statistic: $x_{RMS} = (\frac{1}{N} \sum_{i=1}^{N} x_i)^{\frac{1}{2}}$
S	Slope constraint matrix
T	Terrain curve height
V	Total velocity magnitude
W	Slope constraint vector
a	Acceleration
a_N	Normal acceleration
c	Clearance curve height
c_Q	Performance measure coefficient for the quadratic term
c_L	Performance measure coefficient for the linear term

c_M	Performance measure coefficient for the min-max term
c_{min}	Minimum clearance distance above the terrain
c_{ref}	Reference clearance distance above the terrain
c	Excess clearance distance of the path above the reference clearance curve
fps	Feet per second
h	Height or altitude
h_c	Clearance height above the terrain
i	Index number
j	Jerk (time derivative of acceleration)
k	Curvature of the path or curve (second derivative of height with respect to range)
m	Min-max performance parameter, for upper bound on clearance
n	Index number
nm	Nautical miles
p	Kink (third derivative of path height with respect to range)
q	Complementary problem vector
r_c	Instantaneous radius of curvature
s	Slope of the path
t	Time variable
u	Vector of unit elements
$\hat{u}$	Slack variable vector
w	Complementary problem dual variable vector
x	Independent variable for the cubic spline

y	Dependent variable for the cubic spline
z	Spline coefficient vector
γ	Flight-path angle
Δ	Range interval between sample points
σ	Normalized range variable
σ_T	Standard deviation of terrain height samples
δ_c	Commanded control surface deflection angle (for pitch)
θ	Aircraft pitch angle
ϵ	"is an element of"
$( )'$	Transpose of a matrix or vector
	(Also, the derivative of a variable with respect to range)
$(\dot{})$	Derivative of a variable with respect to time
1_d	Vector of unit elements with dimension "d"

1. INTRODUCTION

Terrain following systems evolved in the late 1950s, after very effective defenses against high-altitude aircraft had developed. Low-altitude high-speed flight became the best means for an aircraft to evade detection and destruction by enemy defenses. Many modern military aircraft (fighters, bombers, and transports) now have terrain following systems. The F-111, B-52, and the C-5A are examples of these. Future aircraft, such as the B-1, missiles, and possibly remotely piloted vehicles (RPVs) will have terrain following systems. It is also possible that commercial aircraft may use similar techniques for landing approaches in the future. Thus, the terrain following problem has become important for many types of aircraft.

1.1 The Basic Terrain Following Problem

The basic terrain following problem is to determine the proper commands to the control system in order to achieve a flight path that minimizes the probability of destruction of the aircraft. The destruction can result either from enemy defenses or from impact on the terrain. This definition presents a very complex problem that depends directly on the enemy defenses and on how well a particular terrain following scheme is actually implemented. The problem is further complicated by acceleration and flight-path angle constraints that may be imposed upon the aircraft. Additionally, some terrain following systems can be operated either in an automatic mode or in a manual mode. During the manual mode, the pilot provides command inputs to the control system after viewing a display generated by the terrain following system. The immense complexity of the

basic problem prevents its direct overall solution; the problem requires division into subproblems that can be solved with the available mathematical tools and technology. Accordingly, only a major subproblem of the basic problem is treated here and will be defined precisely after some general background information is discussed.

1.2 Previous Terrain Following Systems

In the literature, a wide variety of major topics concerning terrain following has been covered. These topics include performance measures, probability of kill, probability of impact on the terrain, displays, human factors, terrain classification, flight test data, simulation data, turbulence effects, and radar characteristics. The reader may consult Reference 4 for a more detailed summary and a bibliography that cover these diverse topics.

The first-generation terrain following systems are basically aircraft flight-path-angle controllers [3, 4, 16]. These angle controllers compute a desired flight-path angle based on the relative locations of critical terrain features. Deviations from the desired flight-path angle create pitch commands to the aircraft flight-control system.

The second-generation terrain followers control the path of the vehicle more directly [2, 4, 11, 23]; the pitch commands are generated to produce specific types of paths. In order to obtain lower paths, some systems use segments of terrain data, rather than only critical terrain points. Path control results in a natural division of the problem into the path-determination and the tracking subproblems.

Much of the early development was devoted merely to obtaining

systems that performed in a reasonable fashion. Later, attempts were made to improve performance of the various subsystems. One example of subsystem improvement is the optimal tracker developed by General Electric Company [23, 24, 25]. In another, Greaves [11] optimized both the tracker and the path-determination scheme, but as two separate subproblems. To date, the latter has come closest to optimizing the overall system. There are two major similarities between the work by Greaves and that reported here: both schemes are intended as feasible real-time controllers, and both formulate the path optimization as a quadratic programming problem with linear inequality constraints. The primary differences are in the approach to optimality, the path data processing method, and the implementation of the tracking system. The various types of systems are discussed in more detail in Chapter 2, where appropriate terms are defined.

As indicated previously, the basic problem is too complex for overall optimization with present theory and techniques. The dynamics of the aircraft are nonlinear and the addition of the many constraints makes the mathematical problem untractable. The two major contributions of this dissertation are the precise definition of a mathematical optimization problem that encompasses a major portion of the terrain following problem, and the parametric study of the solutions of that problem with all of its constraints. Each solution of the problem is a smooth reference path that follows the terrain as closely as possible and is a path that an aircraft can follow very well. The simplifying assumptions required to make the problem tractable are deemed to be more consistent with practical limitations than those of previous

approaches. For example, there is no assumption of constant horizontal velocity; neither is there an attempt to make the aircraft follow a path that it cannot reasonably be expected to follow. The set of allowable controls does not permit discontinuous accelerations that defy implementation, but provides both acceleration and acceleration-rate limits.

1.3 The Information Processing Problem

The method of subdivision of the basic problem into subproblems affects the performance of the resulting terrain following system, as will be indicated in the following discussion. The scope of the problem will be first narrowed to a much more manageable extent by four basic assumptions:

1) A reliable set of discrete terrain data points is available,
2) The motion of the aircraft is restricted to a vertical plane so that only longitudinal motion is considered,
3) A priori knowledge of enemy defense systems is not available, and
4) The automatic mode, with no pilot in the control loop, is to be used.

These assumptions, which will be discussed in more detail below, limit the problem to the following "information processing problem": given a set of terrain data points, determine the input commands to the longitudinal control system of the aircraft such that the resulting aircraft path is as low as possible, within the following constraints:

1) The flight path is not lower than a specified minimum-clearance distance above the terrain points,

2) Specified normal acceleration limits are not exceeded by the aircraft, and

3) Flight-path angle, or slope, limits (if specified) are not exceeded.

The usual source of terrain information in a system is a forward-looking radar. Conceivably, other sources, such as satellites and accurate terrain maps, can be used also. The effects of radar "shadowing", which occurs because the radar cannot see the back sides of hills, are not considered directly in this study. Any terrain-following system that uses a forward-looking radar suffers from this same handicap -- in any case, whatever data are available should be processed in the best manner.

The term "terrain avoidance" has been applied consistently to systems that involve lateral motion of the aircraft, to enable the vehicle to fly around high peaks rather than over them. The term "terrain following" has usually been restricted to longitudinal-motion systems. Only terrain following is studied here, although most of the concepts could certainly be extended to terrain-avoidance systems.

For general usage, it is reasonable to assume that a terrain-following system should be able to operate effectively without any knowledge of the enemy defenses. This requires a choice of performance measure that is insensitive to the defensive configuration. The natural choice for such a performance measure is to require the vehicle to fly as low as possible as often as possible -- or in other words, each clearance height sample should be weighted equally.

Modifications to this procedure are easily possible, especially if good rationale for weighting some regions more heavily than others is known. If some a priori knowledge of the defense structure is known, certainly the heavily defended regions could be given higher performance weighting coefficients. However, these ideas will not be pursued further in this thesis.

The uniform global approach to closeness (treating sample points equally) is at variance with the assumptions made by Greaves [11]. He assumes that the highest point of the terrain segment being optimized is the most critical. Furthermore, he does not impose a non-zero minimum-clearance distance constraint, although he might easily do so with his method; apparently, pure vertical translation of his optimal path would be required to provide a safety clearance.

The automatic mode is considered more important for low-altitude high-speed flight because pilot reaction times can adversely affect the system performance. This does not imply that the automatic mode would be used only for high-speed flight, but high-speed does provide the most severe test of a terrain-following system.

1.4 The Specific Approach

Within the framework of the information processing problem, the further subdivision of problems for the proposed system can now be stated:

1) Construct a terrain representation curve,
2) Determine a minimum-clearance curve,
3) Optimize a path subject to
   a) the constraint that the path is above the minimum-clearance curve,

b) acceleration constraints, and

c) flight-path slope constraints, and

4) Determine command signals to the aircraft control system based on the optimal flight path.

The major subproblem is the determination of a path for the aircraft that satisfies all of the constraints and lies as "close" as possible to the terrain. Since the nonlinear aircraft equations of motion are too cumbersome for efficient computation, a very simple path model is chosen into which the specified constraints can be directly incorporated. The solution of the problem with the simplified model is a reference flight path that the aircraft can essentially follow. Therefore, the tracking problem becomes relatively simple.

The minimum-clearance constraint is obviously a safety consideration. A terrain curve is desired, rather than just discrete points, so that the effects of minimum clearance distance can be investigated in detail. Most systems merely translate the terrain curve upward by the specified reference-clearance distance to obtain a clearance path. But, if the slopes of the terrain are large, some points of the resulting curve will be closer to the nearest terrain curve points than the reference-clearance distance, as illustrated in Figure 2-1 where the reference-clearance distance is c_{min}. The terms used in the figure are defined in Section 2.1.3, while the clearance effects are investigated in Chapter 5, along with the fitting of cubic splines through data points.

The acceleration and flight-path-slope constraints are frequently imposed for pilot comfort and performance, although they could also be due to aircraft structural or performance limitations.

1.5 Mathematical Complexities of the Optimization Problem

The inclusion of the clearance, slope, and acceleration constraints in the mathematical optimization problem creates a very difficult problem. Due to the clearance and slope constraints, the resulting optimal control problem becomes one with state variable inequality constraints (SVICs). There has been limited success with general optimization algorithms that handle SVICs. Methods that handle these constraints directly require a priori assumptions of when and how many times the constraints are "active" (satisfied by an equality). The method of Denham and Bryson [10] and that of Hennig [13] are examples of these. For the terrain-following problem in which many contacts with the constraint boundaries are likely, the number and locations of the contacts are extremely difficult to predict in advance. It very nearly requires guessing the complete solution in advance.

Jacobson and Lele [15] have attempted to circumvent these difficulties by converting from state inequality constraints to slack variables. For the same reason, Martensson [20] converts the state inequality constraints into control variable constraints, which can be treated more easily. The slack variable approach has inherent computational problems, while Martensson's conversion, for this particular problem, leads to incompatible control constraint equations (there is no feasible control at times). Other special techniques, such as decomposition into subarcs [7], have been attempted by other authors, but they are limited to special types of problems.

The greatest success with SVICs has been in treating them indirectly with penalty function methods [5, 19]. This was the first approach

considered. It was successful, but it required very large computing times. The details are reviewed in Section 6.1. The second approach was much more effective. In it the optimization problem is formulated first as an optimal control problem with differential state equations, continuous controls, and an integral performance measure. A cubic-spline trajectory model reduces the problem to a finite dimensional optimization, without sacrificing any of the essential character of the aircraft flight path. Then, the state equations are written as linear difference equations, and the control is a set of discrete values. These results simplify the computations; however, a still greater simplification is produced by replacing the integral performance measure by a discrete performance measure which is evaluated by sampling the path at intervals. These procedures which discretize with respect to range result in either a quadratic or linear programming problem. Both linear and quadratic programming algorithms treat the inequality constraints directly and offer large savings in computational time. Furthermore, good linear and quadratic programming algorithms are readily available [14, 27, 28].

1.6 Overview

The second chapter defines some terrain-following terminology and summarizes the basis of existing types of terrain-following systems. Chapter 3 contains the formulation of the optimization problem that is the essence of the optimal-path following scheme. The usual terrain-following system does not have all of the terrain data available at one time; new data is received periodically as the aircraft proceeds along the terrain. This process leads to a sequence of data frames

and successive optimizations. The framing process and the parameters involved are described and analyzed in Chapter 4. Chapter 5 contains an analysis of fitting cubic spline functions through the terrain data points to obtain a continuous curve. The continuous curve is used to analyze construction of a minimum-clearance reference path, and this path is then compared to a translated terrain curve. In Chapter 6, the solutions of the optimization problems are given in parametric studies of various framing structures. Analysis of the tracking problem--that of determining commands to the aircraft flight-control system such that it will closely follow the optimal path -- is in Chapter 7. Chapter 8 addresses some of the considerations for real-time onboard implementation of the optimal-path following scheme. Finally, conclusions are drawn and recommendations are made in Chapter 9.

2. TERRAIN FOLLOWING CONCEPTS

In the past many attempts have been made to evaluate terrain-following system performance and to establish criteria that are meaningful for more than one particular system. The determination of criteria is a very difficult problem considering the differences that can occur in terrains, in aircraft, in defense systems, and in the implementation of the various systems. The intent here is not to discuss past evaluations in great detail, but to give sufficient background in some of the more general criteria so that the effectiveness of the system proposed here may be judged more readily. Following some definitions of terminology used in terrain-following analysis and a brief discussion of performance criteria, some of the concepts of previous terrain following systems are discussed.

2.1 Definitions

The following are definitions of terms that will be used frequently throughout this thesis.

2.1.1 Acceleration Limits. The acceleration limits for terrain following usually are specified in incremental G's (1G = 32.17 ft/sec^2). Positive G's are measured upward and level flight has a zero G reference value. The incremental G's should not be confused with the normal load factor, which has a one G reference value for level flight.

2.1.2 Clearance Curve. The terms clearance curve and clearance altitude refer to a curve and its points that are a specified "minimum-clearance" distance, c_{min}, from the terrain points. The curve represents a lower bound for the aircraft flight path. The

clearance curve is distinct from the desired reference curve or reference path specified in other terrain following systems. That reference curve does not represent a lower bound on the aircraft flight path, but is at a desired clearance distance, c_{rof}, above the terrain. Some excursions of the aircraft flight path below the reference curve can be expected. Typically, points on the reference curves have been measured vertically above the terrain points. If the clearance curve is measured in this manner, it is simply a vertical translation of the terrain. Such a curve will be referred to as the vertical-clearance curve. Obviously, if the terrain slope is large, the clearance distance to the nearest point on the terrain curve will be <u>less</u> than c_{min}, as indicated in Figure 2-1. The

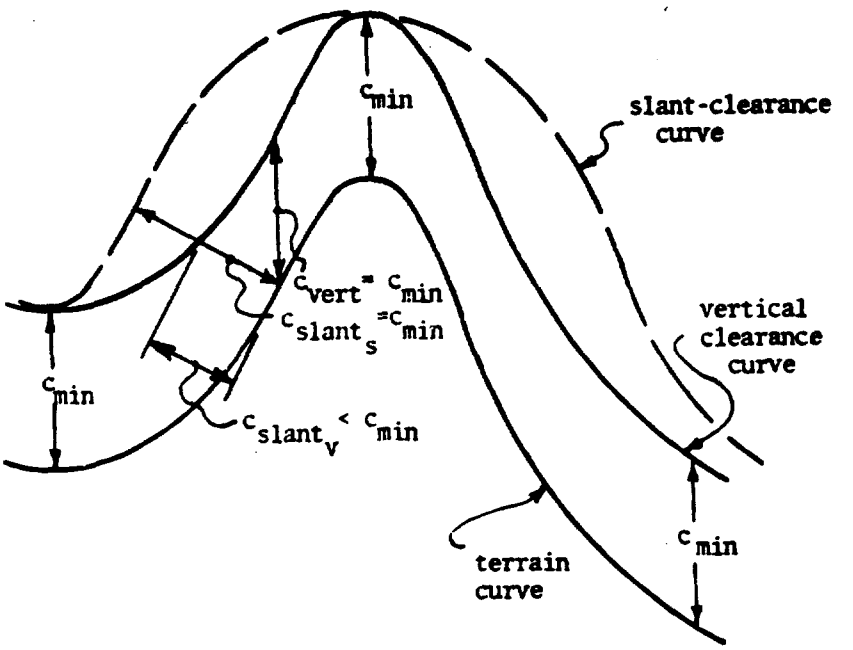

Figure 2-1 Clearance Curves

clearance to the nearest point on the terrain curve will be termed the "slant" clearance distance, c_{slant}, and is measured perpendicular to the terrain curve at any point. For the sake of analysis, continuous curves will be fitted through terrain and clearance path points. This fitting process, as well as the computation of a slant-clearance path with $c_{slant} = c_{min}$, is described in detail in Chapter 5. Also, the differences in the two types of clearance paths are analyzed there. The general term "clearance curve" will be used to refer to the curve regardless of how the clearance distance is measured.

2.1.3 Ideal Path. A path that is frequently used as an evaluation tool in terrain following is the ideal path. Unfortunately, this path does not have a unique definition in the literature. It has been determined in different ways by different authors, but the common requirement for this path is that the performance constraints are satisfied. The constraints are on either vertical or normal acceleration, on flight-path slopes, and on minimum-clearance distance. Figure 2-2 shows a typical ideal path.

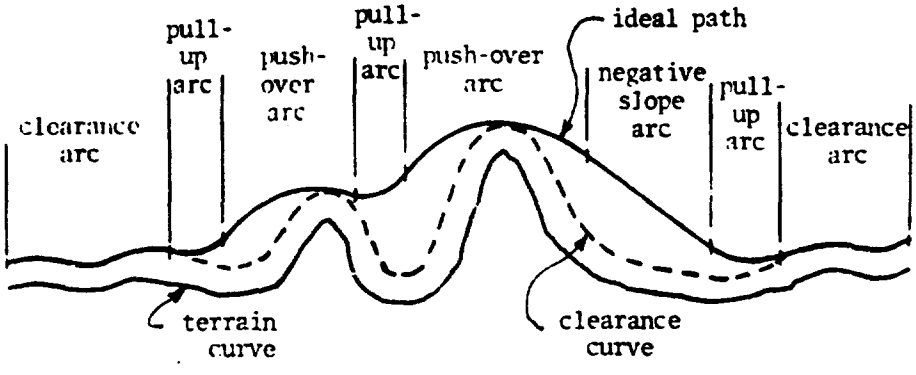

Figure 2-2 Ideal Path

2.1.4 Terrain Roughness. Various measures of terrain roughness have been proposed. One simple measure [4, page 37] has been the mean of the terrain point heights, where each sample point height, T_n, is measured from the zero reference level -- that of the lowest terrain point in the set.

$$T_{MEAN} = \frac{1}{N} \sum_{n=1}^{N} T_n \tag{2-1}$$

This measure conveys very limited information about the terrain; a more descriptive measure of roughness is the standard deviation of the terrain segment based on N sample points from the terrain.

$$\sigma_T = \sqrt{\frac{1}{N} \sum_{n=1}^{N} (T_n - T_{MEAN})^2} \tag{2-2}$$

Although the decision is somewhat arbitrary the following ranges are adopted here to define roughness as a function of σ_T:

Smooth -- 0 to 200 ft.

Moderate -- 200 to 500 ft.

Rough -- over 500 ft.

These ranges are in general agreement with current terrain analyses.

2.1.5 Path Curvature and Kink. The term "curvature", in this thesis, is defined as the second derivative of the path height with respect to horizontal range. This definition differs from that for the usual mathematic curvature, which is identically equal to the last term of term of Eq. (2-3). Here the curvature of a flight path is related to the aircraft speed along the path and to the acceleration normal to the path, by the approximation

$$\frac{d^2h}{dR^2} \triangleq k = \frac{a_N}{V^2} \sec^3\gamma \approx \frac{a_N}{V^2} \tag{2-3}$$

where the flight-path angle is γ. The derivation of this equation and the following one are in Appendix C. The approximation is exact only when the flight path is horizontal, but it is fairly accurate for small flight-path angles. The curvature is also related to the instantaneous radius of curvature, r_c, and the flight-path angle by the equation

$$r_c = \frac{1}{k} \sec^3 \gamma \tag{2-4}$$

The derivative of curvature with respect to range is defined as the "kink", p. Kink is analagous to jerk, j (the rate of change of acceleration in the time domain). Kink is proportional to the jerk and inversely proportional to the cube of the velocity.

$$p \triangleq \frac{dk}{dR} = \frac{d^3h}{dR^3} = \frac{j}{V^3} \tag{2-5}$$

2.1.6 Ride Hardness. The hardness of the ride is related to the acceleration limits imposed upon the aircraft. The term is usually qualitative rather than quantitative. The larger the span of acceleration allowed by the limits, the "harder" is the ride. To be more specific, in this thesis, precise values for the acceleration limits are assigned for the various rides. The first set of incremental-G limits is that given for the F-111, Mark II System [3], while the second set is for a hypothetical missile:

	Set 1	Set 2
Hard Ride	-1.0 to +2.0 G's	-5.0 to +15.0 G's
Medium Ride	-0.5 to +2.0	
Soft Ride	-0.25 to +2.0	-1.0 to + 3.0

The negative limits are generally more restrictive because of the pilot or because of some vehicle configuration. The pilot is physiologically much more adaptable to positive G's than to negative G's, while some jet engine inlet configurations are unsuited to the airflow patterns resulting from negative G's.

2.2 Performance Criteria and Parameters

Some of the criteria frequently used for improving and evaluating terrain following performance, as indicated in the Terrain Following Criteria Handbook [4] and by Brostrom [6] have been

1) Minimization of RMS clearance altitude deviation from a reference clearance altitude,
2) Attainment of level flight over dominant peaks,
3) Minimization of RMS normal acceleration,
4) Reduction of the maximum clearance altitude deviation from the reference clearance curve,
5) Reduction of the minimum and maximum vertical accelerations and vertical velocities, and
6) Subjective evaluations of flight path time histories.

Most of these are concerned with keeping the flight path as low as possible, but items 3) and 5) are concerned with reduction of ride hardness and maximization of flight range. Jeffrie [16] recommends the comparison of the flight path with the ideal path rather than the clearance curve, as in item 4), above. He shows statistical comparisons that indicate clearance deviations become much less sensitive to the particular terrain when the ideal path is used as a reference rather than the clearance curve. This is not surprising,

for the ideal path acts as a low-pass filter in filtering out the high terrain frequency components, as shown by Weir [31].

The parameters that affect the performance of all terrain following systems are

a) Aircraft forward velocity,

b) Aircraft normal acceleration limits,

c) Flight-path angle,

d) Minimum-clearance distance,

e) Terrain roughness and frequency content, and

f) Defensive threat situation.

A good terrain following system should allow for some adjustment in all of the above parameters, or it will be too specialized.

2.3 Terrain-Following Command Generation

There has been no standard for classifying the various systems that have been developed, but one approach is to classify them either as flight-path-angle controllers or as path controllers. Early systems were path-angle controllers, where the path itself was only indirectly affected by the direct control of the aircraft attitude. Later efforts developed controllers that analyzed paths directly before determining the proper attitude the vehicle should have to produce a good approximation of the desired path.

2.3.1 Flight-Path-Angle Controllers. The flight-path-angle controllers have been systems that generate commands based on critical features of the terrain. The commands are based either on the relative range or the relative angular position of the critical feature [3, 4, 16], and the general configuration is indicated in block diagram of Figure 2-3.

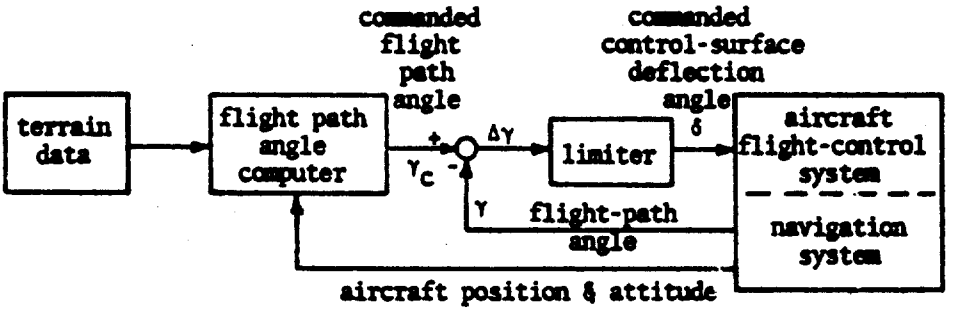

Figure 2-3 Flight-Path-Angle Controller Schematic

The first type of controller to be discussed below is the simplest since it does not require a forward-looking radar. This type uses only a radar altimeter terrain sensor. The two remaining types of angle-controllers are designed for forward-looking radar systems.

2.3.1.1 Relative Altitude/Altitude-Rate Systems. Typical missile terrain-following systems use terrain data which consist only of the vehicle altitude relative to the terrain, h_c, and the time rate of change of that relative altitude, $\dot{h}_c$. This type of system has very little predictive capability, since the only terrain data used is for the terrain immediately below the aircraft. A block diagram of this system is shown in Figure 2-4. The difference between the relative altitude, h_c, and the desired reference value represents an error in current position. The altitude rate data provide a measure of the relative angular difference between the vehicle flight path and the local terrain slope. There are a wide variety

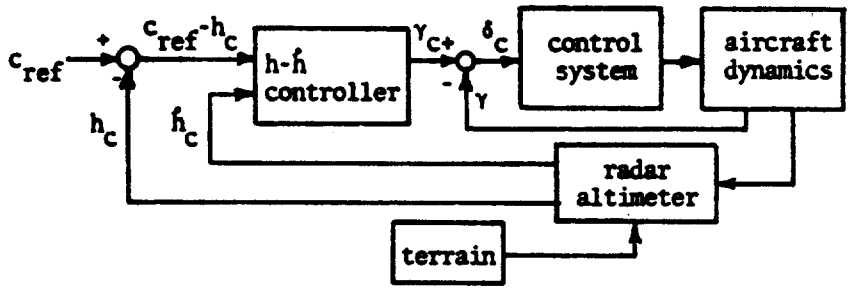

Figure 2-4 Relative Altitude/Altitude-Rate System

of ways of combining these two signals in the controller to produce a commanded flight path angle. Typically an equation such as Eq. (2-6) is used.

$$\gamma_c = \alpha \dot{h} + \beta (h_c - c_{ref}) \qquad (2\text{-}6)$$

Frequently, the negative α and β gains are fixed and limiters bound both the flight-path angle and surface deflection commands. This type of system has found application in missiles where space and weight limitations are severe and vehicle maneuverability is high.

2.3.1.2 Scanned-Range and Template Systems. In the range-type systems, the response to a terrain feature depends upon its relative range from the aircraft. Computational devices, such as the "template" illustrated in Figure 2-5, are used to compute command signals. The template is not a physical device, but is used only for mathematical computation. The template is fixed with respect to the aircraft axes and is contained entirely within a specified angular sector ($\beta_1 + \beta_2$) ahead of the aircraft. The template is

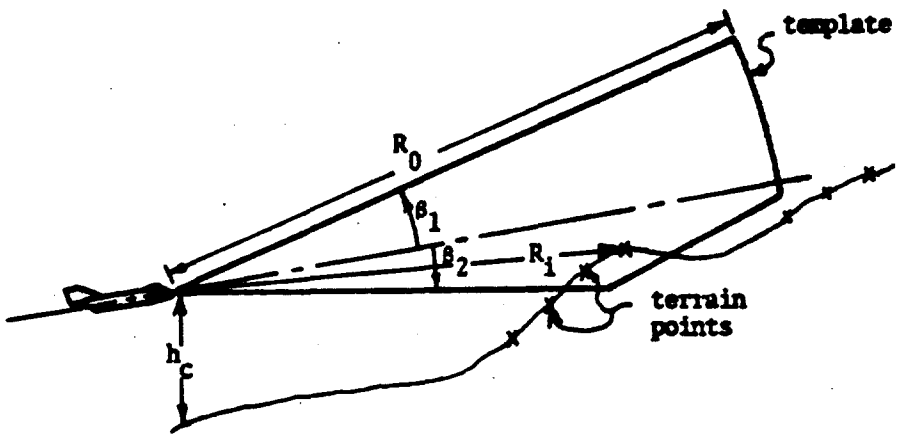

Figure 2-5 Template System

terminated at a specified maximum range, R_0, and is truncated by a ramp at the far lower corner. The actual dimensions of the template must be tailored for the particular radar and aircraft systems. The shape of the template is designed to separate terrain points into two groups: those that require pull-up commands to provide adequate clearance, and those that still can be cleared when push-over commands are given. First, the set of ranges, R_i, corresponding to terrain points inside the template is considered for the pull-up computation.

$$\gamma_c = \max_i \{\alpha_R(R_i - R_0)\} + \alpha_H(h_c - c_{ref}) \qquad (2\text{-}7)$$

where α_R and α_H are negative constant coefficients, h_c is the current clearance height above the terrain, and c_{ref} is the specified reference clearance height. The maximization in Eq. (2-7) indicates that the critical point is the terrain point in the template nearest to the aircraft. The first term of the equation provides for

clearance over the critical point, while the second term compensates for current altitude deviations from the reference clearance height. When no terrain points lie inside the template, but there are good radar returns from points outside the template, a pitch-down command is created from an equation similar to Eq. (2-7). However, the selection of the most critical point outside the template is more complex and may differ for different systems.

Both the template system and the relative-angle system, described below, use a "back-up" computation for times when good radar returns are not available from the forward-looking radar, such as when cresting a peak or when flying over water. The back-up system is usually an h-$\dot{h}$ controller that uses a command of the form in Eq. (2-6).

2.3.1.3 Relative-Angle Systems. The relative-angle systems have had greater usage than the relative-range systems. The F-111, C-5, F-4, and B-52 terrain-following systems are all relative-angle systems. These systems react to terrain points that lie in the range interval $[R_{min}, R_{max}]$, as illustrated in Figure 2-6.

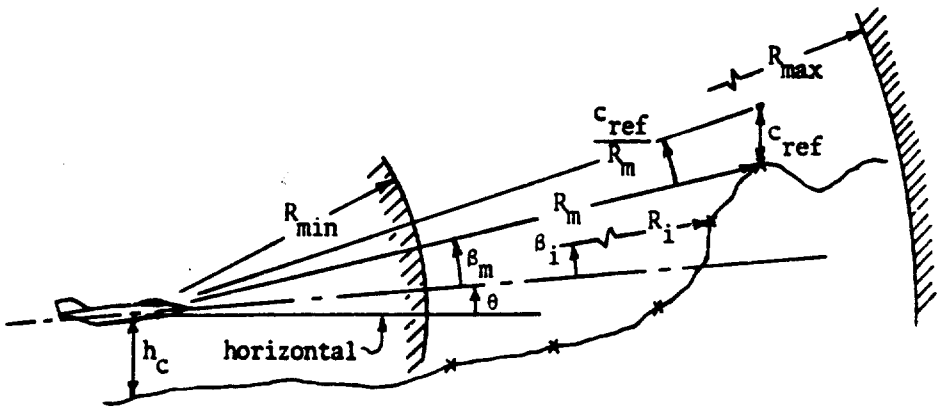

Figure 2-6 Relative-Angle System

The most critical terrain point in the interval is determined from Eq. (2-8).

$$\beta_m = \max_i \{\beta_i\} \tag{2-8}$$

where the index i refers to points in the range interval [R_{min}, R_{max}]. The critical point, at (R_m, β_m), determines the commanded flight-path angle:

$$\gamma_c = \alpha \left(\theta + \beta_m + \frac{c_{ref}}{R_m} - F_s\right) \tag{2-9}$$

where α is a constant coefficient, θ is the aircraft pitch angle, and the F_s shaping function is a function of the range R_m, the aircraft velocity, and the aircraft acceleration limits. The combination of α and F_s is chosen to provide the proper "amount" of prediction for a particular system. The amount of prediction required varies inversely with the range and the maneuverability of the aircraft.

2.3.2 Path Controllers. Three types of path controllers are discussed below. The first was developed by Cornell Laboratories (Calspan) [2,4], and is called the ADLAT system. The second is an "optimal" tracker system developed by General Electric Company for the Air Force Flight Dynamics Laboratory [23, 24, 25]. The last is one proposed by Greaves [11], which uses both an "optimum" path determination and an "optimum" tracker system.

2.3.2.1 ADLAT System. The Advanced Low Altitude Techniques (ADLAT) system [2] is one of the earliest path controllers. It utilizes two parabolic path segments as shown in Figure 2-7.

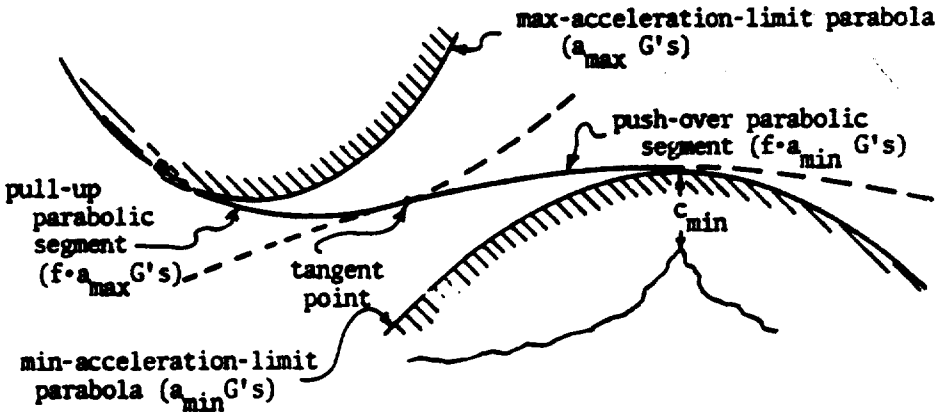

Figure 2-7 ADLAT System Path

The segments are pieced together so that they are tangent at the transition point. The first segment is tangent to the aircraft flight path and the second is horizontal at the "dominant" terrain obstacle. Each parabola represents a constant acceleration arc. The ratio of the accelerations on the two arcs is the same as the ratio of the two acceleration limits. It is possible for the two arc geometry to degenerate into a geometry which involves only a single push-over arc. If the aircraft were fairly high with respect to the obstacle, the order of the arcs might be reversed from that shown in the figure. However, if the system is operating properly, it should never allow the aircraft to get into a position where the limit areas that are cross-hatched in Figure 2-7 overlap.

Figure 2-8 illustrates the controller which is similar to an angle controller except the commanded angle is extracted from a stored set of sampled flight-path angles computed from the ADLAT parabolic path segments. The sampled set is updated periodically.

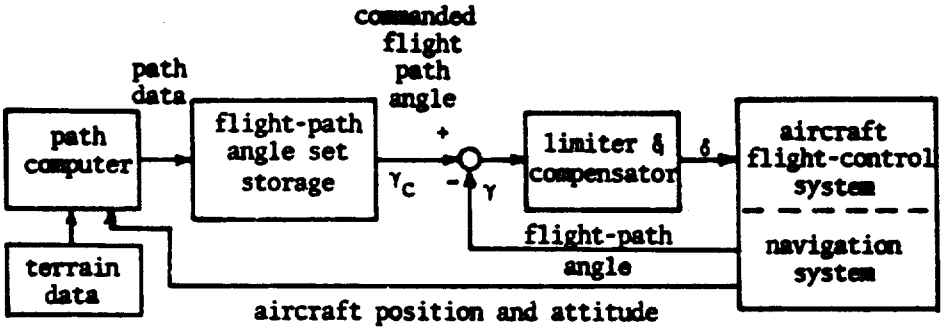

Figure 2-8 ADLAT Path Controller

Compensation is also added to the command signal to account for lags in the overall aircraft control system.

2.3.2.2 Optimal Tracker System. The system developed by General Electric [23, 24, 25] uses a stored segment of terrain data. Some preliminary processing of the terrain data is done to produce a clearance curve as indicated in Figure 2-9. The result is a path lying somewhere between a vertical-clearance curve and an ideal path. The path is translated upward from the terrain curve by the distance c_{min}, but in addition, parabolic segments, representing maximum pushover arcs, are inserted in front of the peaks by a backward sweep of the data in a special processor. In theory one would like to have the actual ideal path produced, (as will be described next in the Greaves approach), but this involves a much more complex piecing of arcs, as indicated in Figure 2-2. The processed clearance path is used in the General Electric system as a desired tracking signal for an optimal tracker. The tracker

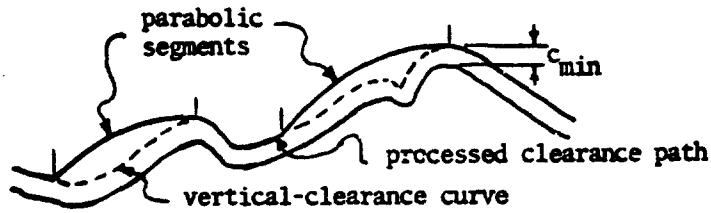

Figure 2-9 Preprocessed Clearance Path

is really only optimal in a limited sense. The aircraft motion is modeled as a simple third-order linear system. Optimal feedback gains for the usual quadratic cost tracking problem are found by the methods of optimal control using the Riccati equation. Appropriate correlation between the boundary conditions and cost coefficients produce constant gains for the third order model. The prediction signal required for the solution of the optimal tracking problem is obtained by a fast-time backward integration of the adjoint equations. This signal and the constant-gain feedback signals provide the input signal to the aircraft flight-control system, as indicated in the block diagram of Figure 2-10. The overall system, however, is only optimal to the extent that the preprocessed clearance path coincides with the ideal path, and insofar as the linear third-order system closely approximates the nonlinear aircraft system.

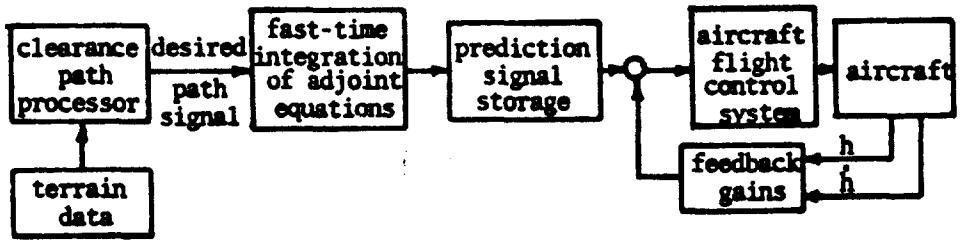

Figure 2-10 Optimal Tracker System

2.3.2.3 Optimum Processor-Tracker System. The system developed by Greaves [11] has both a path-determination optimizer and an optimal tracker. The path processor is a nonlinear digital filter that performs a series of operations on sets of discrete-range path points. The filter starts with the set of terrain points and produces a set of path points that satisfy specified clearance and acceleration constraints while remaining "close" to the terrain points.

A series of iterations is involved; for each iteration, an operator "optimally" enforces a particular type of constraint at each point of violation in the current path point set. After all violations of one type of constraint are eliminated, the next type of constraint is considered. The sequence of constraints is ordered so that no new violation of previously satisfied constraints occur.

The input set of path points for each operator, O_j, is designated $\{h_i\}$, and the output set is $\{y_i\}$, where i is the horizontal range index.

$$\{y_i\} = O_j \{h_i\} \tag{2-11}$$

If ∇_j indicates the set of points at which violation of the j^{th} type of constraint occur, then the O_j operator solves a "local" optimization problem at the highest point, h_n, in the set ∇_j. The optimization problem is to minimize

$$J_n = \sum_{i=n-1}^{n+1} (y_i - h_i + \frac{1}{2} y_i^2) \tag{2-10}$$

subject to the j^{th} type of constraint and a clearance constraint. Thus, the O_j operator eliminates a type j constraint violation at a specific range point by moving path points upward to maintain the clearance constraint. The operator is used repetitively on the path point set, but it only changes points in the three-point "neighborhood" of the violation at any one step. The details for the O_1 operator are described below.

The input set used to begin the procedure is the terrain heights, T_i, plus any specified minimum clearance, c_{min}.

$$\{h_i\}_0 = \{T_i + C_{min}\} \tag{2-12}$$

Greaves works with zero minimum clearance, but it is trivial to extend the procedure to non-zero values. The clearance constraint that the final set of points must satisfy is

$$y_i \geq T_i + c_{min} \tag{2-13}$$

and is maintained during each iteration step by the "non-lowering" requirement:

$$y_i \geq h_i \tag{2-14}$$

The first operator, O_1, enforces the minimum-acceleration constraint:

$$\tau^2 a_{min} \leq h_{n+1} - 2h_n + h_{n-1} \tag{2-15}$$

where τ is the time interval required to traverse the horizontal interval between terrain points (with the horizontal speed assumed to be constant). This constraint essentially considers the acceleration at the central point "n" to be equal to the constant acceleration on a parabolic path through three points.

$$a_n \triangleq \frac{1}{\tau^2} (h_{n+1} - 2h_n + h_{n-1}) \tag{2-16}$$

The O_1 operator solves a local optimization problem at the highest point, h_n, in Ψ_1. The optimization problem is to minimize J_n of Eq. (2-10) subject to the constraints of Eqs. (2-14) and (2-15). This operation is repeated on the path set until Ψ_1 is empty. Then the maximum-acceleration constraint operator is used to minimize J_n subject to Eq. (2-14) and a maximum-acceleration limit. Slope and jerk constraint operators are also considered by Greaves, but for simplicity they are not discussed here.

The mathematical results of the optimization problem for operator O_1 can be interpreted geometrically, as illustrated in Figure 2-11. A parabola that has a curvature corresponding to the minimum-acceleration limit is used as a violation indicator. The original points are the h_i and the processed points are the y_i. In Case 1, both adjacent points lie below (or on) the constraint parabola when the vertex of the parabola is located at the point of violation. The minimum J_n of Eq. (2-16) occurs when the two adjacent points are

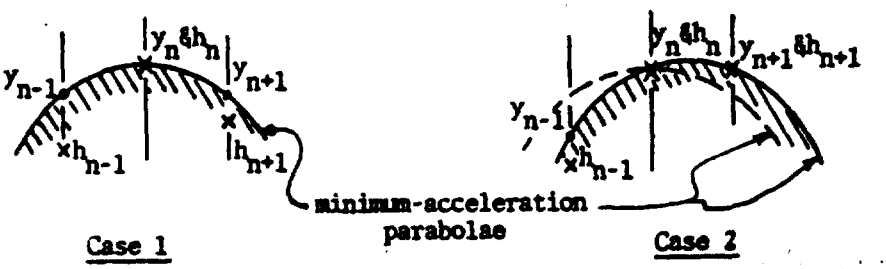

Figure 2-11 Minimum-Acceleration Constraint Enforcement

raised to equal levels on the parabola. If one of the adjacent points lies above the initial parabola location, as in Case 2, the parabola is repositioned to pass through the highest adjacent point, as well as the violation point. The solution is then obtained when the remaining point is raised to the parabola.

The complete iterative process is illustrated in Figure 2-12. The original terrain data points are shown, followed by the sets of path points that result from the enforcement of each type of acceleration constraint. The points are indicated by numbers, with the letter subscripts indicating the order of the step which resulted in its final placement. For example, step "a" is the first step and results in the adjustment of points 6 and 8, while step "b" repositions only point 5. The curves shown are orientation references only; the filtering process works only with the discrete points.

Greaves admits that it is difficult to determine the overall sense of optimality in his path processor, since a lengthly series of local optimization problems are performed. The sequence of

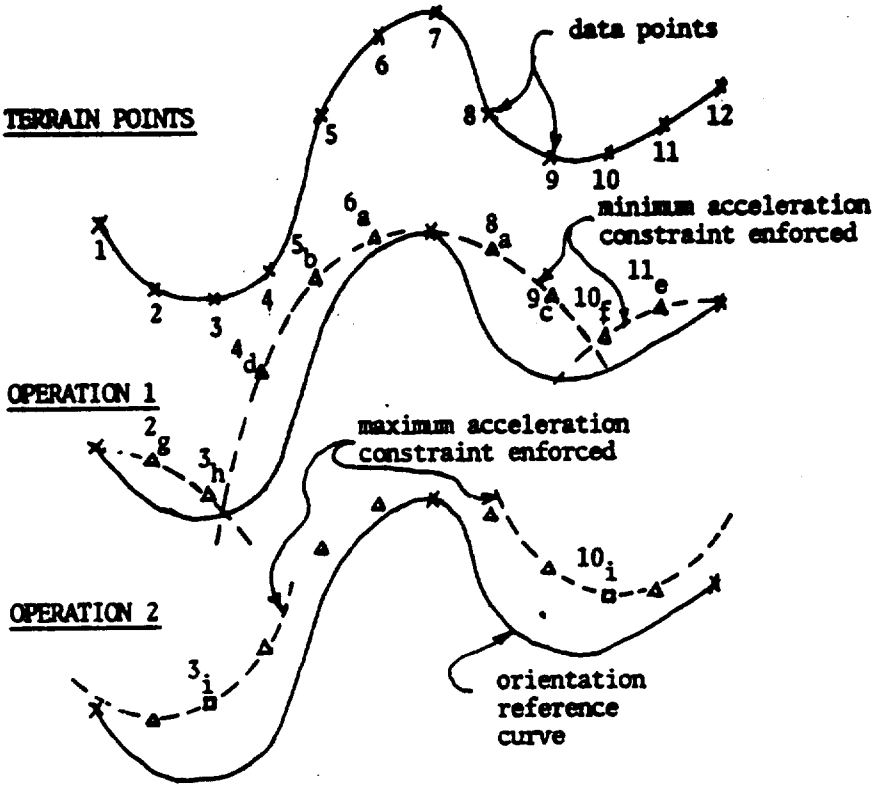

Figure 2-12 Digital Filtering Process

optimizations is equivalent to minimizing a "global" performance measure of the form

$$Z = \sum_{i=1}^{N} [\omega_i (y_i - h_i) + \frac{1}{2} (y_i - h_i)^2] \qquad (2\text{-}17)$$

Unfortunately the weighting coefficients, ω_i, are not known prior to the optimization, and they depend upon the particular terrain data used.

Although Greaves' procedure is closer than any predecessors to the overall objective of creating the best path for the vehicle to follow, it still suffers conceptually from two disadvantages:

1) the sense of overall optimality is obscure, and 2) because of the simplified (three point) treatment of the acceleration constraints, a smooth path through the final data points may not satisfy the normal acceleration constraints between sample points. This latter assertion is illustrated in Figure 2-13, where acceleration can be related directly to the path curvature. The data points shown are a subset

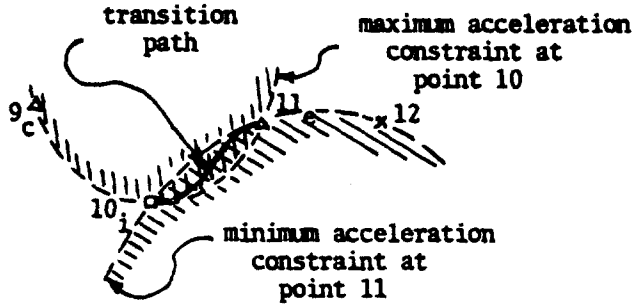

Figure 2-13 Digitally Filtered Data

of those from the final result in Figure 2-12. The points satisfy the acceleration constraints when considered three at a time; however, if a smooth curve is fitted through all four points, there must be some transition from maximum curvature to minimum curvature. But that type of transition path must violate the corresponding curvature limits somewhere between points 10 and 11 in the figure.

The optimal tracker system for the digitally filtered path is similar to the General Electric tracking system, even though the path processors are considerably different in the two systems. The system diagram is basically the same as that shown in Figure 2-10 for the General Electric system. Greaves' system does use a

fourth-order linear system model for the tracker, rather than a third-order model. The fourth-order model is a better approximation for a nonlinear aircraft system, but nevertheless, the corresponding optimal tracker system is still only optimal in an approximate sense, because it uses a linear model.

The optimal-spline-path following system described in the following chapters attempts a simpler, more practical coupling of the path determination and tracking problems. The computed paths will be smoother than the processed paths of the system described above and have a more practical curvature profile.

3. MODEL AND OPTIMIZATION PROBLEM FORMULATIONS

This chapter formulates an optimization problem that incorporates all of the essential ingredients for terrain following in a very simple way. The first step is to construct a simple trajectory model for the aircraft motion. This model will be used in an optimal control problem that strives to keep the aircraft as "close" to the terrain as possible without violating clearance, acceleration and slope constraints. Initially, the problem is considered in the most natural space, the space of continuous functions. Then, to provide computational simplicity, the problem is discretized. The discretization is accomplished using splines, which retain the essential characteristics of continuous functions even though they are defined by discrete values. This procedure maintains a close relationship between the mathematical problem and the problem of controlling aircraft motion. After the discrete equations of motion are developed, the performance measure is discretized also, by sampling. The resulting optimal control problem is either a quadratic or linear programming problem. The quadratic programming problem can be solved by algorithms that treat it directly, or it can be converted into the linear "Complementary Problem" prior to the application of an algorithm. Any of the programming problems can be solved much more rapidly than the original optimal control problem.

3.1 The Trajectory Model

The trajectory model that is used here is a triple integrator system defined in the range domain, rather than in the time domain. The range domain is ideal for terrain following because that is the

natural domain of the terrain. In the range domain, one does not need to consider the fluctuations in the time-rate of motion over the terrain due to aircraft velocity changes. The trajectory equations are

$$h' \triangleq \frac{dh}{dR} = s \tag{3-1}$$

$$s' \triangleq \frac{ds}{dR} = k \tag{3-2}$$

$$k' \triangleq \frac{dk}{dR} = p \tag{3-3}$$

for each range R in the interval $\Gamma = [R_0, R_N]$, where h is the height on the path, s is the slope, k is the curvature, and p is the "kink". The variables h, s, and k are continuous, while p is piecewise continuous. The curvature is analgous to acceleration and the kink is analagous to jerk (the derivative of acceleration with respect to time). To make the model paths correspond well to aircraft trajectories, limits on both the curvature and the kink are considered in the following problems.

3.2 The Optimal Control Problem

The trajectory model will be incorporated into the optimal control problem. To solve the dilema of how to define closeness to the terrain, a general performance measure is studied. It is constructed in terms of the excess clearance variable

$$e = h - c \tag{3-4}$$

where c is the height of the minimum-clearance curve. The performance function is defined over the range interval Γ.

$$J = \int_{R_0}^{R_N} (Qe^2 + Le)dR + M \max_{\Gamma} \{e\} \tag{3-5}$$

The choice of coefficients Q, L, and M determine whether this performance measure is quadratic (M=0), linear (Q = M=0), min-max (Q = L=0), or a combination of these.

The optimal control problem is to determine the curvature function k that minimizes J subject to the differential constraints of Eqs. (3-1) to (3-3) with specified initial conditions h_0, s_0, k_0, and subject to the following inequality constraints, for all $R \in \Gamma$

$$e \geq 0 \tag{3-6}$$

$$s_{min} \leq s \leq s_{max} \tag{3-7}$$

$$k_{min} \leq k \leq k_{max} \tag{3-8}$$

$$p_{min} \leq p \leq p_{max} \tag{3-9}$$

The limits on the curvature are determined from the normal acceleration limits and aircraft speed by the approximation of Eq. (2-3)

$$k_{lim} = \frac{a_{n_{lim}}}{V_{nom}^2} \tag{3-10}$$

This approximation is accurate only as long as the path slope is small. However, the approximation is good because the limits tend to be encountered at the tops of peaks and the bottoms of valleys where the flight path is nearly horizontal. The kink limits are related to jerk limits, which usually are not specified for an aircraft. However, jerk affects the ride comfort for a pilot and the performance of the tracking system that attempts to follow the reference path. Therefore, bounds on the jerk, or kink, are desirable and are discussed further in Chapter 4.

3.3 Discrete Equations of Motion

The integration of differential equations on a digital computer is a time consuming process. Also, the search of function space for an optimal control can be very slow compared to discrete parameter optimization. Therefore, the use of discrete range equations of motion and a discrete range control set greatly simplifies the optimal computations for this problem.

Spline curves are very useful in fitting smooth curves through data points [1]. The cubic spline is composed of cubic polynomial segments pieced together to provide continuous first and second derivatives at the junctions. The path model is to be represented by a cubic spline. Thus, the path slope is a quadratic spline, the curvature is a linear spline, and the kink is a piecewise constant function. The curvature is to be considered the control variable and is illustrated in Figure 3-1. A set of range values, R_i, is arbitrarily chosen for the spline "knots" (segment junctions). The interval between knots need not be equal, although it is often convenient to use uniform spacing.

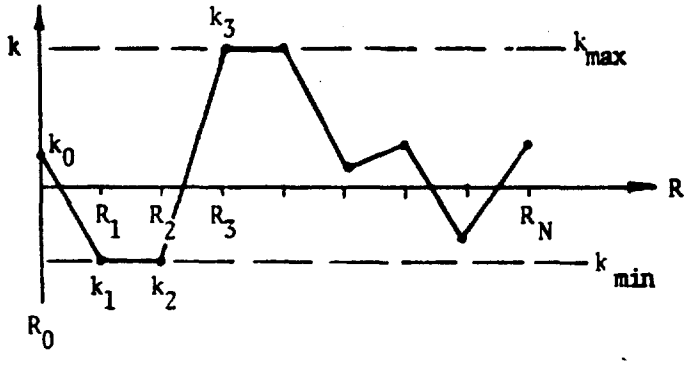

Figure 3-1 Curvature Spline

The k_i curvature values at the knots, along with the R_i, completely specify the curvature function on the interval Γ. Furthermore, the kink can also be specified in terms of the knot values and the interval lengths, $\Delta_i = R_i - R_{i-1}$,

$$p = \frac{k_{i+1} - k_i}{\Delta_{i+1}} \qquad \text{for } Rc(R_i, R_{i+1}) \tag{3-11}$$

Obviously, the kink is equal to the slope of each straight line segment in Figure 3-1. With the addition of initial values h_0 and s_0, the path height and slope can be written as difference equations that incorporate the spline continuity requirements.

$$s_i = s_{i-1} + \frac{1}{2}\Delta_i(k_i + k_{i-1}) \tag{3-12}$$

$$h_i = h_{i-1} + s_{i-1}\Delta_i + \frac{1}{6}\Delta_i^2(k_i + 2k_{i-1}) \tag{3-13}$$

The corresponding discrete kink equation is

$$p_i = \frac{k_i - k_{i-1}}{\Delta_i} \tag{3-14}$$

Note that each of these last three equations defines an affine function of the set of k_i curvature values. If the equations are a applied recursively, each of the values h_i, s_i, and p_i can be written in terms of the initial conditions and the k_i values, for i=1, 2, ..., N. The vector-matrix form is

$$h = Ek + f \tag{3-15}$$

$$s = Sk + b \tag{3-16}$$

$$p = Pk + d \tag{3-17}$$

where h, s, k, p, f, b, and d are N-dimensional vectors and E, S, and P are NxN matrices that have a triangular form. The elements of E, S, P, f, b, and d are computed recursively from the interval lengths Δ_i and the initial conditions h_0, s_0, and k_0. The equations for these elements are developed in Appendix A. It is possible to sample the variables at points other than the knots, but this complication will not be considered here. The excess-clearance sample vector can be written

$$e = h-c = Ek+f-c \tag{3-18}$$

where c is an N-vector of the clearance curve sample values. The inequality constraints of Eqs. (3-8), (3-6), (3-7), and (3-9) can be written in a single inequality

$$\begin{bmatrix} I \\ -I \\ E \\ S \\ -S \\ P \\ -P \end{bmatrix} k \leq \begin{bmatrix} uk_{max} \\ -uk_{min} \\ f-c \\ us_{max}-b \\ b-us_{min} \\ up_{max}-d \\ d-up_{min} \end{bmatrix} \tag{3-19}$$

where I is the NxN identity matrix and u is an N-vector of unit elements. Eq. (3-19) enforces the constraints only at the N knots, but this still implies satisfaction of the limits on curvature and kink over the entire interval Γ, as can be observed from Figure 3-1. However, the clearance and slope constraints are not necessarily satisfied over the intervals between knots. Definite bounds on the

amount of constraint violation can be computed; equations for these bounds are developed in Appendix H. The violations will normally be quite small.

3.4 Discrete Performance Measure

Invariably, in evaluating terrain following performance, investigators resort to sampling the trajectories to evaluate the system, Thus, it is not unnatural to use a discrete range performance measure, especially when using discrete range equations of motion. The use of the discrete measure also reduces the computation required. The discrete performance measure is a sampled version of Eq. (3-5):

$$J = \sum_{n=1}^{N} \left[\frac{1}{2} Q_n e_n^2 + L_n e_n\right] + M \max_n \{e_n\} \qquad (3\text{-}20)$$

An equivalent vector-matrix measure is obtained using Eq. (3-18) for e

$$J = L' k + \frac{1}{2} k' Qk + M \max_{\text{component}} \{Ek\} \qquad (3\text{-}21)$$

where L is an N-vector computed from the Q_n, L_n, E, f and h_c; Q is a symmetric NxN matrix computed from the Q_n and E.

In the early stages of this study, penalty function approaches were tried to enforce the clearance constraint. This involved the addition to Eq. (3-20) of a term of the form $P_n e_n^2$, which was added only for $e_n<0$. This approach resulted in a "soft" constraint that allow some violations of the clearance constraint. Although the violations were reasonably small, it was not possible to determine a priori a bound on the violations. When it became apparent that the

discrete formulation resulted in a quadratic programming problem, the clearance constraints could be treated directly and the penalty function approach was abandoned.

3.5 Quadratic Programming Problem

The quadratic programming problem follows directly from the discretized equations (3-19) and (3-21), with a scalar variable "m" introduced to treat the min-max term. The problem is to determine the (N+1) dimensional K vector

$$K = \begin{bmatrix} k \\ m \end{bmatrix} \tag{3-22}$$

that minimizes

$$J = L'k + \frac{1}{2} k'Qk + Mm$$

$$= [L'M]K - \frac{1}{2} K' \begin{bmatrix} Q & 0 \\ 0 & 0 \end{bmatrix} K \tag{3-23}$$

subject to

$$C' K \leq D \tag{3-24}$$

where the C and D are formed from the matrices of Eq. (3-19), plus appropriate coefficients for m if the min-max term of Eq. (3-23) is used ($M \neq 0$). The additional constraint set that is added to Eq. (3-19) to produce Eq. (3-24) is an upper bound on the excess clearance at each of the knots:

$$e \leq u\, m \tag{3-25}$$

or

$$Ik - um \leq f-c \tag{3-26}$$

where u is an N-vector of unit elements. Any of the constraints

that are not needed for a particular aircraft or mission can be eliminated from the matrices to reduce the problem dimension.

It should be noted that the above problem will be a linear programming problem when the quadratic performance coefficients, Q_n, are set to zero. Many algorithms are available to solve the linear programming problem [14]. The above form of the quadratic programming problem can be solved by two different approaches: there are algorithms that treat the above form directly [29], or the Lemke approach [26] is to convert the quadratic problem into a higher-dimensional linear programming problem, called the "Complementary Problem." If the min-max term is not used, so that the quadratic coefficient matrix Q is positive definite, Shankland's algorithm [29] can be used to solve the quadratic problem directly. The Complementary Problem has special structure that is handled readily by special linear programming algorithms, such as Ravindran's [26]. The algorithms are discussed in more detail in Chapter 6.

3.5 The Complementary Problem

The basic formulation from which the Lemke development starts is a slightly different form of the quadratic programming problem. It is converted into a linear programming problem by the use of slack variables and the Kuhn-Tucker conditions of optimality [8]. The particular quadratic problem is to minimize

$$J = L'x + \frac{1}{2}x'Qx \tag{3-27}$$

subject to

$$Gx \geq H \tag{3-28}$$

and

$$x \geq 0 \tag{3-29}$$

Eq. (3-28) is converted from an inequality constraint to an equality by the introduction of a "$\hat{u}$" slack variable vector, which is also constrained to have non-negative components.

$$\hat{u} = G\,x - H \tag{3-30}$$

$$\hat{u} \geq 0 \tag{3-31}$$

When the Kuhn-Tucker conditions [8, pp 54-56] are applied, the result is a system of linear equations with some undetermined multipliers v and y (these are frequently called the dual variables). plus non-negativity constraints on all the variables, and an additional orthogonality requirement:

$$\begin{bmatrix} v \\ \hat{u} \end{bmatrix} = \begin{bmatrix} Q & -G' \\ G & 0 \end{bmatrix} \begin{bmatrix} x \\ y \end{bmatrix} + \begin{bmatrix} L \\ -H \end{bmatrix} \tag{3-32}$$

$$\hat{u},\ v,\ x,\ y \geq 0 \tag{3-33}$$

$$v'\,x + \hat{u}'\,y = 0 \tag{3-34}$$

Eq. (3-32) can be written in a more concise form by grouping the variables into two vectors:

$$w \triangleq \begin{bmatrix} v \\ \hat{u} \end{bmatrix} \tag{3-35}$$

$$z \triangleq \begin{bmatrix} x \\ y \end{bmatrix} \tag{3-36}$$

$$\overline{M} \triangleq \begin{bmatrix} Q & -G' \\ G & 0 \end{bmatrix} \tag{3-37}$$

$$q \triangleq \begin{bmatrix} L \\ -H \end{bmatrix} \tag{3-38}$$

Now we consider the final formulation.

The Complementary Problem is to determine the unique w and z vectors that satisfy Eqs. (3-39), (3-40), and (3-41).

$$w = \bar{M} z + q \tag{3-39}$$

$$w,z \geq 0 \tag{3-40}$$

$$w' z = 0 \tag{3-41}$$

Eq. (3-39) can also be written in the linear programming form:

$$\begin{bmatrix} -\bar{M} & I \end{bmatrix} \begin{bmatrix} z \\ w \end{bmatrix} = q \tag{3-42}$$

The constraints of Eqs. (3-40) and (3-41) make it a special linear programming problem in which either each component of z or the corresponding component of w must be zero. Ravindran used this special property for a modified "Revised-Simplex" algorithm to solve this complementary problem. The non-negativity requirements involve a biasing of each of the curvature values for the terrain following problem.

$$x_i = k_i - k_{min} \qquad \text{for } i=1, 2, \ldots, N \tag{3-43}$$

When the min-max variable is used, it does not require a bias, as it is already positive.

The Ravidran algorithm can solve either the linear or quadratic programming problem. This flexibility makes it useful for testing the different performance criteria; thus, it is the primary algorithm used in the parametric studies of Chapter 6.

4. FRAMING FOR DATA PROCESSING

It is impractical to solve a single optimization problem for the entire flight of an aircraft. The great number of samples that would be required would produce an optimization problem of extremely high dimension. Furthermore, all of the required terrain data may not be available at the beginning of the flight. The method for handling these problems is a framing procedure. Frames of terrain data are considered serially as the aircraft advances over the terrain, and an ideal path is produced for each frame by solving an optimization problem of the type considered in Chapter 3. The details of the framing procedure are described in the following sections. To reduce computational requirements, it is desirable to use the minimum amount of data that will still produce good performance. To estimate the required amount of data and other framing parameters, the idea of a "characteristic maneuver" is introduced.

4.1 The Characteristic Maneuver

The unpredictability of many terrains makes the determination of an adequate frame length difficult. The characteristic maneuver is developed here for estimating this frame length in a fairly simple manner. A "maximum-expected-obstacle height", H, is specified, and then the minimum range interval required to clear the obstacle and return to level flight is computed. Any curvature and slope constraints imposed on the flight path must be considered in the computation. For simplicity, only the curvature limits will be considered here because slope constraints are frequently not imposed. The geometry of the characteristic maneuver is illustrated in Figure 4-1, where the symmetric path and curvature profiles are shown.

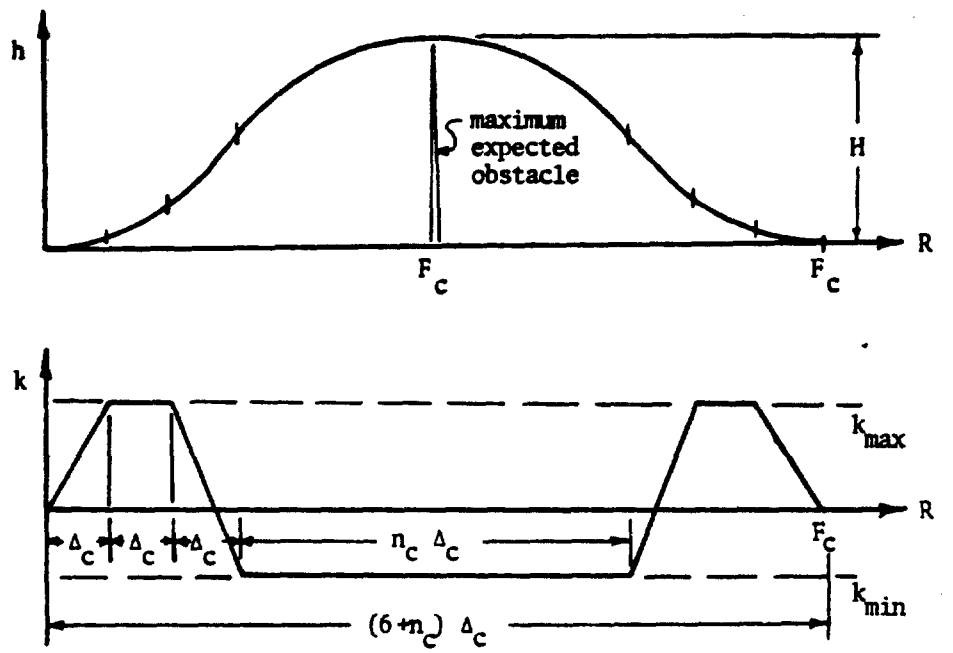

Figure 4-1 Characteristic Maneuver

The parameters of the maneuver are Δ_c, F_c, n_c, H, k_{max}, and k_{min}. The curvature limits, k_{max} and k_{min}, are computed from normal acceleration limits and aircraft speed. Since negative acceleration is usually limited to a smaller magnitude than the positive acceleration, the length of the pushover arc, $n_c\Delta_c$, is longer than the pullup arc length, Δ_c, while the transition arcs also have a length, Δ_c. Note that the positive and negative areas under the curvature profile in the figure must be equal for the aircraft to return to level flight. In the computations, the value of n_c will be considered a real number rather than an integer. The equations for n_c, Δ_c, and F_c are developed by piecewise integration in Appendix B.

$$\Delta_c = \sqrt{\frac{24H}{48\, k_{max}(1-\frac{k_{max}}{k_{min}}) + k_{min}}} \tag{4-1}$$

$$F_c = \Delta_c \left(5 - 4\,\frac{k_{max}}{k_{min}}\right) \tag{4-2}$$

$$n_c = -\left(4\,\frac{k_{max}}{k_{min}} + 1\right) \tag{4-3}$$

The parameter Δ_c, called the characteristic interval, represents the maximum size control interval that can be used while performing the maneuver in the minimum frame length, F_c. If a Δ is selected that is greater than Δ_c the pullup maneuver will cause the path to rise higher than H before level flight can be attained, or level flight can be achieved only at a range greater than $F_c/2$. Values of Δ smaller than Δ_c can be used to perform a similar maneuver, but intermediate control values between k_{min} and k_{max} may be required at some points. To be certain that the characteristic maneuver can be performed within a frame length that is an integral multiple of the control interval Δ, one can use the following equations:

$$F = \Delta\,(6+n) \tag{4-4}$$

where the integer "n" satisfies

$$n \geq n_c \tag{4-5}$$

The characteristic maneuver analysis yields a good, simple estimate of frame length. However, it is based on the clearance of a single obstacle, and there may be times when multiple obstacles of real terrains may degrade the performance. There are other framing

aspects which also affect the performance. These will be discussed in the following sections.

4.2 Frame Advance

The frame advance process is illustrated in Figure 4-2. At one

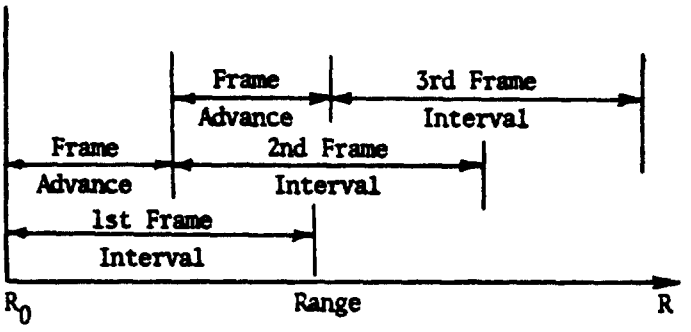

Figure 4-2 Data Frame Overlap

extreme, there is no overlap of frames; the second frame begins where the first ended, and the frame advance is equal to the frame length. This reduces the number of optimizations to a minimum, but it is largely an open loop system as far as terrain and clearance curve information is concerned. There is no adjustment to the data during the full frame interval. If the terrain data were perfect, non-overlapping frames would work well, but the present state of the art in terrain-following radars is such that good returns are not always available. Returns are also subject to the phenomenon called "radar shadowing", in which part of the terrain blocks the radar energy from reaching portions of the terrain at greater ranges. From a practical viewpoint, it is desirable to update portions of the terrain data as new data become available, before a full data frame is completely

traversed by the aircraft. To allow maximum feedback of terrain information the frame advance distance should approach zero, but the frames must advance at a rate which is at least as great as the aircraft speed. This establishes a minimum frame advance rate: however, the frame computational time must also be known to compute the frame advance distance. It is possible to advance the frames more rapidly than the aircraft speed to allow some idle time between successive frame computations. Since the computation time for different frames will usually vary, some idle time should nominally be allowed.

4.3 Frame Length

Although the required frame length can be estimated from the characteristic maneuver described previously, there are a few other frame-length aspects that should be mentioned. The characteristic frame length, F_c, is the estimate of minimum frame length, but there is also an upper bound on the frame length that is dictated by the source of terrain data. The amount of data to be optimized in a single frame must lie somewhere between these two extremes. To reduce the computation required, the frame length should be chosen near the characteristic value. Furthermore, the data at the far end of the frame may be less accurate than that near the aircraft, which is another reason that processing time should not be devoted to any "excess" information.

There can be an interaction between frame length and frame advance that affects the predictive capability of the system. The objective is to keep the frame length long enough, and the frame advance short enough that the predictive capability of the process is sufficient

for the particular terrain that is encountered. This capability is affected by the following factors:

a) Aircraft speed,

b) Acceleration limits,

c) Slope limits,

d) Kink limits, and

e) Terrain roughness and frequency content.

The characteristic frame length computation requires an estimation of the maximum expected obstacle height, H. If the specific terrain segment to be traversed is known, an appropriate height can be readily determined from the terrain data. However, in many cases the exact terrain information may not be available in advance. A possible method of estimating an H, in this case, is to select $H = 3\sigma_T$, where σ_T is the best estimate of the terrain standard deviation (the roughness) in the general area of the flight.

4.4 Frame Junctions

Since one of the objectives of the terrain-following control system considered here is to provide a fairly smooth command signal to the aircraft flight-control system, care must be taken to minimize discontinuities at frame junctions. Some of the possible ways of joining frames can be visualized by referring to Figure 4-3. The paths in the frame advance interval are of primary interest. Ideally the computation of the optimal path for Frame 2 would start from point A, the actual position of the aircraft at range R_1. Unfortunately, the computation of the optimal path for Frame 2 must begin when the aircraft is at range R_o, and must be complete by the time the aircraft reaches R_1,

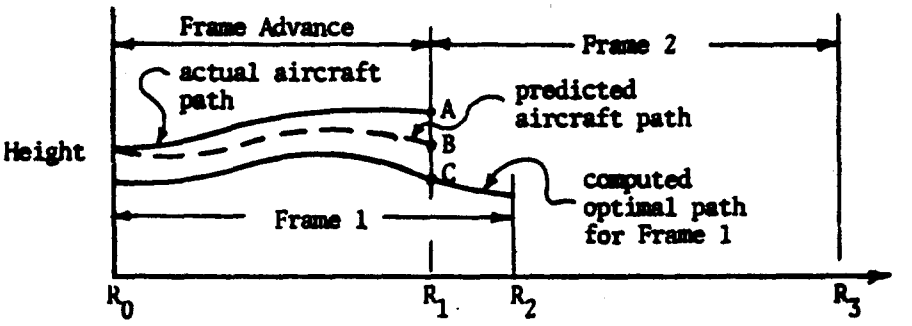

Figure 4-3 Frame Junction

so that the commands are available for the path immediately following that position. Therefore, computations for any frame must be based on a predicted position at the beginning of that frame.

One possible way of beginning the Frame 2 computation is to predict the aircraft's position by some set of prediction equations, based on the aircraft's position at R_0 and the commands generated by the optimal path of Frame 1. This is indicated as the point B in Figure 4-3. The disadvantage of doing that, even though it may more accurately represent the true aircraft position, is that the optimal paths of Frame 1 and Frame 2 would be disjoint.

A more reasonable and simplier approach is to use point C on the Frame 1 optimal path as the starting point for the optimal path of Frame 2. In this way the optimal path will be continuous from frame to frame, rather than disjoint. Furthermore, the slope and curvature of the optimal path can be made continuous by matching the Frame 2 values with those of Frame 1. Then the initial control point is fixed rather than varied in determining the optimal path for each frame. This is the procedure that is used in the parametric studies of Chapter 6.

If the command signals to the aircraft flight-control system are based on a feedback controller, i.e., a signal proportional to the difference in the optimal path and the actual aircraft path, then these are continuous also because the aircraft values would be continuous. A possible difficulty would result for a terrain data update in which the new terrain is significantly higher than the old. This is illustrated in Figure 4-4, where the initial point C for Frame 2 lies below the minimum clearance path. This creates difficulties for the programming algorithms, as it is likely that there will be no feasible solution that satisfies all of the clearance constraints. Quasi-solutions that "approximately" satisfy the constraints are required in this case and will be discussed in Section 6.2.

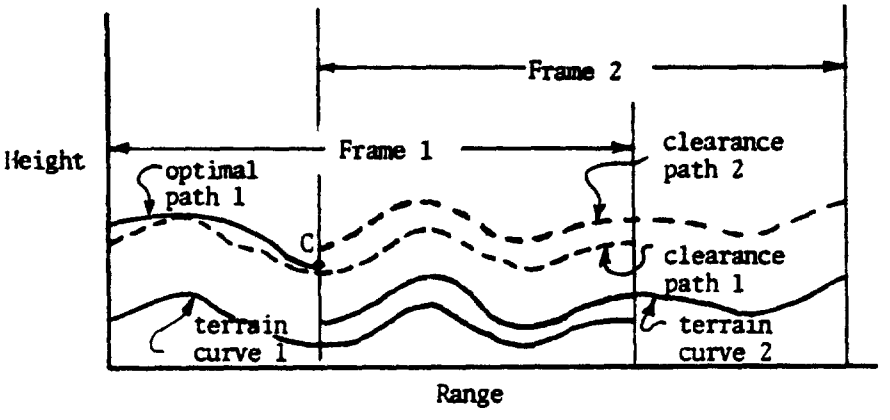

Figure 4-4 Infeasible Solution at Frame Junction

4.5 Control Point Spacing

The number of control points used per frame should be large enough to allow adequate control flexibility. Fine spacing of the

control points allows the greater flexibility, but it also places stronger demands on the flight-control system, as the rate of command signal change will be greater. Furthermore, the number of control points and constraint points needed to span the frame is also greater, which in turn requires greater amount of computation to solve the optimization problem. While it is convenient to use uniform control point spacing, it may not be necessary, or even possible for long data frames, if all computation is to be done in real time. The spacing can be graduated so that it is finely spaced in the near frame (close to the aircraft) and coarsely spaced in the far frame, as shown in Figure 4-5. The rationale for this is that only gross positional changes need to be considered in the far frame where updated data will be available for refinement in subsequent frames. The main reason for the far frame data is to predict far enough ahead that the aircraft will not fly into an untenable position, from which it cannot recover. If the spacing is too coarse, however, a loss of control flexibility will raise the mean clearance level for the flight.

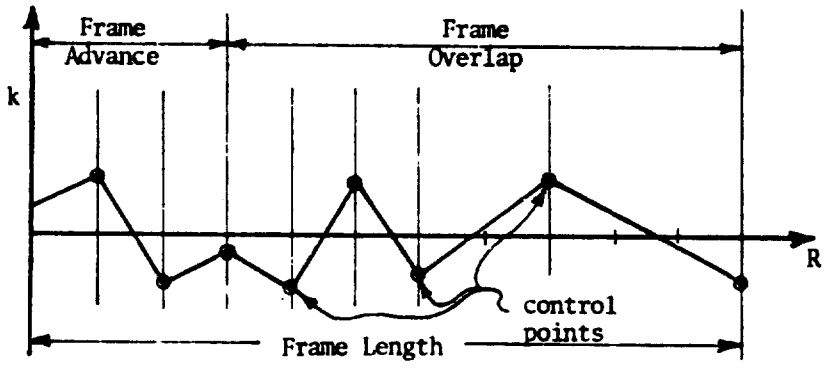

Figure 4-5 Graduated-Control-Point Spacing

The limits on kink are inherently related to the control interval and the curvature limits, as indicated previously in Eq. (3-14), and in a slightly different form in the following equations.

$$p_{lim} = \frac{k_{max} - k_{min}}{\Delta} \tag{4-6}$$

$$p_{max} = p_{lim} \tag{4-7}$$

$$p_{min} = -p_{lim} \tag{4-8}$$

Two approaches to treating the kink limits are available. The limits may be enforced directly in the optimization problem by including them in the constraint set. Alternatively, it may be possible to choose the control interval such that the inherent kink limits are acceptable for the specified curvature limits. Either of the two alternatives must be investigated in terms of the optimization problem dimensions, which depend upon both the number of sample points and which types of constraints are enforced.

All of the various parameters that affect the framing process are listed in the following section, while the parametric studies are discussed in Chapters 6 and 7. The studies include frame length, control point spacing, computational times, and frame advance rates.

4.6 Specification of Framing Structure

The solution of the optimization problem requires the specification of many parameters and their numerical values. To completely specify a framing structure the following parameters are required:

1) Frame length,
2) Frame advance distance,
3) Limits on path curvature,
4) Minimum-clearance distance and type of clearance,
5) Number and spacing of control points,
6) Performance measure sample points,
7) Terrain sample points,
8) Clearance constraint sample points,
9) Performance measure coefficients,
10) Limits on path slope (optional),
11) Limits on kink (optional), and
12) Slope constraint sample points.

Note that the acceleration constraints need not be specified directly, if the path curvature is the primary consideration. For a specified frame structure, different nominal flight speeds can be used if the corresponding inherent acceleration limits are acceptable, as determined by

$$a_{lim} = k_{lim} V_{nom}^2 \qquad (4\text{-}9)$$

The most convenient method of sampling is to use the same sample interval for each of the variables mentioned above. The numerical equations used are simplified by this procedure. However, there may be some tradeoffs between the complexity of the equations and the number of samples required, if some of the variables can be sampled at slower rates. These tradeoffs are heavily dependent upon the particular framing structures being considered and are beyond the scope of this study.

5. TERRAIN AND CLEARANCES CURVES

Although the performance is measured and the constraints are enforced only at discrete points, the investigation of the clearance distance to the nearest terrain point requires a continuous curve representation for the terrain. Many possible representations can be chosen; however the one selected here is a cubic spline function. One of the reasons for choosing a cubic spline, with continuous first and second derivatives, is that this closely corresponds in smoothness to the optimal path that will be subsequently determined from the terrain curve. Also, the techniques for fitting cubic splines through data points are well developed and have been very successful in a wide variety of applications [1].

5.1 Cubic Splines

A cubic spline function is a sequence of cubic polynomial segments joined to form a continuous function that has continuous first and second derivatives. The general function form is given in Eq. (5-1) and is illustrated in Figure 5-1.

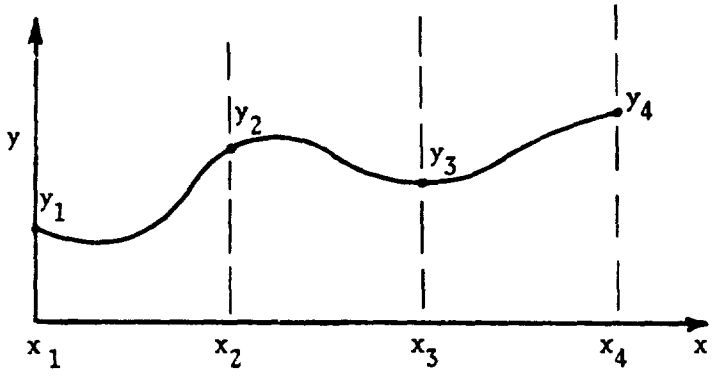

Figure 5-1 Cubic Spline Function

$$y(x) = y_i + A_i\left(\frac{x-x_i}{a_i}\right) + B_i\left(\frac{x-x_i}{a_i}\right)^2 + C_i\left(\frac{x-x_i}{a_i}\right)^3 \quad \text{for } i=1,2,\ldots n-1 \qquad (5\text{-}1)$$

where

$$a_i \triangleq x_{i+1} - x_i \qquad (5\text{-}2)$$

The junction points, (x_i, y_i), are called "knots". Many different approaches to fitting the cubic spline function to discrete data have been used [1,22,28,30]. No single approach is followed here; the best features of routines by various authors are used.

One fitting method varies the positions of the knots and fits the curve close to the data points in a weighted-least-square sense [22]. However, assuming the terrain data points are the best estimates for the actual terrain, the curve should pass through the data points. To guarantee this, the data points are selected as the knots. Then the fitting process is merely the determination of the set of coefficients for each segment of the curve. For n data points, there is a set of three coefficients (A_i, B_i, C_i) for each of the n-1 segments. Note that there is no requirement that the intervals between data points, a_i, are equal, even though this is often convenient. The continuous derivatives of the spline function are

$$y'(x) = \frac{1}{a_i}\left[A_i + 2\,B_i\left(\frac{x-x_i}{a_i}\right) + 3\,C_i\left(\frac{x-x_i}{a_i}\right)^2\right] \qquad (5\text{-}3)$$

$$y''(x) = \frac{1}{a_i^2}\left[2\,B_i + 6\,C_i\left(\frac{x-x_i}{a_i}\right)\right] \qquad (5\text{-}4)$$

To determine the coefficients, continuity conditions on y,y' and y'' are applied at each of the n-2 interior knot positions, using

the relationships: at $x=x_i$, $(x-x_i)/a_i = 0$, and at $x=x_{i+1}$, $(x-x_i)/a_i = 1$.

For $i=1,2,\ldots,n-2$

$$A_i + B_i + C_i = y_{i+1}-y_i = Y_i \tag{5-5}$$

$$A_i + 2B_i + 3C_i = a_i y'_{i+1} = H_i A_{i+1} \tag{5-6}$$

$$2B_i + 6C_i = a_i^2 y''_{i+1} = 2H_i^2 B_{i+1} \tag{5-7}$$

where

$$Y_i \triangleq y_{i+1}-y_i \tag{5-8}$$

$$H_i \triangleq \frac{a_i}{a_{i+1}} \tag{5-9}$$

This set of equations can be placed in a more convenient computational form by replacing Eq. (5-6) with Eq. (5-10), which is obtained by subtracting Eq. (5-5) from Eq. (5-6). Also, if Eq. (5-7) is divided by two and Eq. (5-10) is subtracted from that result, Eq. (5-11) is obtained. The resulting set of recursive equations is

$$A_i + B_i + C_i = Y_i \quad \text{for } i = 1,2,\ldots,n-1 \tag{5-5}$$

$$B_i + 2C_i - H_i A_{i+1} = -Y_i \quad \text{for } i = 1,2,\ldots,n-2 \tag{5-10}$$

$$C_i + H_i A_{i+1} - H_i^2 B_{i+1} = Y_i \quad \text{for } i = 1,2,\ldots,n-2 \tag{5-11}$$

Eq. (5-5) is also applied for the last segment ($i = n-1$) so that the curve passes through y_n. The total number of unknown coefficients is $3(n-1)$, but only $3(n-2)+1$ conditions have been specified. Therefore, two additional conditions must be given to uniquely determine a cubic spline function through the n points.

If both conditions are specified at one end point, the fitting process is simpler, but the curve can exhibit instabilities; i.e., it may oscillate wildly between data points as illustrated in Figure 5-2. This condition can be easily avoided by selecting one condition at each end point of the curve. The digital computer algorithm used in the following cubic spline studies was taken from the UNIVAC 1108 Math-Stat Library [30]. It allows the user the option of using either the first or second derivatives at each end point. It is usually more convenient to use the first derivative conditions shown in Eqs. (5-12) and (5-13).

$$A_1 = a_1 y'_1 \tag{5-12}$$

$$B_{n-1} + 2C_{n-1} = a_{n-1} y'_n - Y_{n-1} \tag{5-13}$$

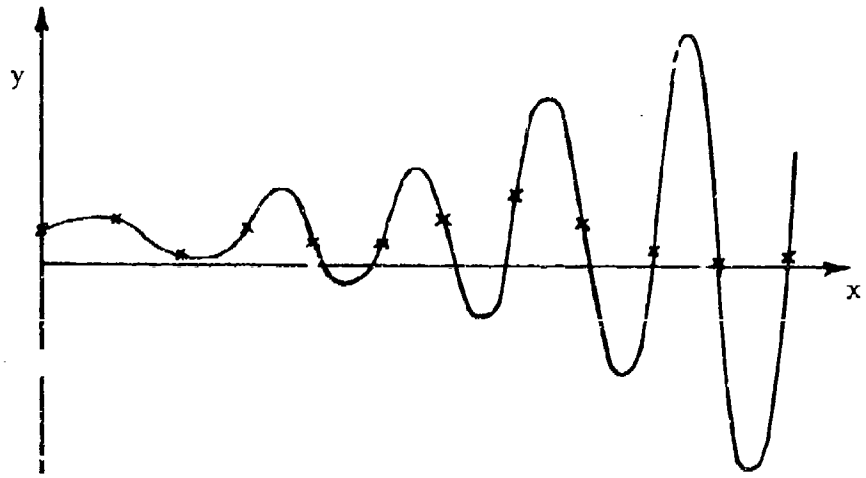

Figure 5-2 Unstable Spline Function

5.2 UNIVAC Spline Fitting Procedure

The UNIVAC cubic spline fitting procedure uses Eqs. (5-5), (5-10), (5-11), (5-12) and (5-13) to form a set of 3(n-1) equations that can be written using a "tri-diagonal" matrix form:

$$\begin{bmatrix} 1 & 0 & 0 & 0 & \dots & & & & & \\ 1 & 1 & 1 & 0 & \dots & & & & & \\ 0 & 1 & 2 & -H_1 & 0 & \dots & & & & \\ 0 & 0 & 1 & H_1 & -H_1^2 & 0 & & & & \\ \dots & 0 & 1 & 1 & 1 & 0 & \dots & & & \\ & \dots & 0 & 1 & 2 & -H_2 & 0 & \dots & & \\ & & & \vdots & & & & & & \\ & & \dots & 0 & 1 & 1 & 1 & 0 & \dots & \\ & & & \dots & 0 & 1 & 2 & -H_{n-2} & 0 & 0 \\ & & & & \dots & 0 & 1 & H_{n-2} & H_{n-2}^2 & 0 \\ & & & & & \dots & 0 & 1 & 1 & 1 \\ & & & & & & \dots & 0 & 1 & 2 \end{bmatrix} \begin{bmatrix} A_1 \\ B_1 \\ C_1 \\ A_2 \\ B_2 \\ C_2 \\ \vdots \\ \vdots \\ A_{n-1} \\ B_{n-1} \\ C_{n-1} \end{bmatrix} = \begin{bmatrix} a_1 y'_1 \\ Y_1 \\ -Y_1 \\ Y_1 \\ Y_2 \\ -Y_2 \\ \vdots \\ -Y_{n-2} \\ Y_{n-2} \\ Y_{n-1} \\ a_{n-1} y'_n - Y_{n-1} \end{bmatrix} \tag{5-14}$$

"Bi-diagonalization", or "upper-triangularization", of this matrix is possible by the following procedure, which will also be mathematically summarized after the description:

a) First designate the second row of the matrix as the i^{th} row,

b) Subtract the equation immediately above the i^{th} row from it,

c) Replace the i^{th} row equation by the resulting equation of step b) after it is divided by the value of the first non-zero element, c_i, and

d) Now designate the row immediately below as the new i^{th} row and repeat the process, starting at step b) above.

The matrix then has the form

$$\begin{bmatrix} 1 & c_1 & 0 & \dots & & & \\ 0 & 1 & c_2 & 0 & \dots & & \\ 0 & 0 & 1 & c_3 & 0 & \dots & \\ & \dots & 0 & 1 & c_4 & 0 & \dots \\ & & & & \vdots & & \\ & & & \dots & 0 & 1 & c_{3n-4} \\ & & & & \dots & 0 & 1 \end{bmatrix} \begin{bmatrix} z_1 \\ z_2 \\ z_3 \\ z_4 \\ \vdots \\ z_{3n-4} \\ z_{3n-3} \end{bmatrix} = \begin{bmatrix} w_1 \\ w_2 \\ w_3 \\ w_4 \\ \vdots \\ w_{3n-4} \\ w_{3n-3} \end{bmatrix} \tag{5-15}$$

where the 3(n-1)-dimensional z vector consists of A_i, B_i, and C_i coefficients that are to be determined and the w vector consists of appropriate linear combinations of the elements of the left-hand-side vector of Eq. (5-14).

The bi-diagonalization process is easily summarized by the following recursive equations:

$$c_1 = 0 \tag{5-16}$$

$$w_1 = a_1 \, y'_1 \tag{5-17}$$

for i = 1, 2, ..., n-1

$$c_{3i-1} = \frac{1}{1-c_{3i-2}} \tag{5-18}$$

$$w_{3i-1} = \frac{Y_{i-1}-w_{3i-2}}{1 - c_{3i-2}} \tag{5-19}$$

for i = 1, 2, ..., n-2

$$c_{3i} = \frac{-H_i}{2 - c_{3i-1}} \tag{5-20}$$

$$w_{3i} = \frac{-Y_i - w_{3i-1}}{2 - c_{3i-1}} \tag{5-21}$$

$$c_{3i+1} = \frac{-H_i^2}{H_i - c_{3i}} \tag{5-22}$$

$$w_{3i+1} = \frac{Y_i - w_{3i}}{H_i - c_{3i}} \tag{5-23}$$

Once the above set of c_i and w_i values is computed by "forward" recursion, the final coefficient, C_{n-1}, is known:

$$C_{n-1} \triangleq z_{3n-3} = w_{3n-3} = \frac{Y_{n-1} - w_{3n-4} + a_{n-1} y'_n}{2 - c_{3n-4}} \tag{5-24}$$

Then the "backward" recursion can be performed to evaluate the remaining polynomial coefficients, z_k:

$$\text{for } k = 3n-4,\ 3n-5,\ 3n-6,\ \ldots,\ 1$$

$$z_k = w_k - c_k z_{k+1} \tag{5-25}$$

5.3 Direct Slope-Determination Spline Fits

The above process for spline representation required the storage of five values for each data point: the data point coordinates x_i, y_i plus the A_i, B_i, and C_i coefficients. Poirier [22] indicates that some of this information is redundant. It is possible to completely reconstruct the spline (and its derivatives) from only x_i, y_i and y'_i, a total of 3n rather than 5n values.

$$y(x) = (1 - 3\sigma^2 + 2\sigma^3)y_i + (3\sigma^2 - 2\sigma^3)y_{i+1} + [(\sigma - 2\sigma^2 + \sigma^3)y'_i + (\sigma^3 - \sigma^2)y'_{i+1}]\, a_i \tag{5-26}$$

where

$$\sigma \triangleq \frac{x - x_i}{a_i} \qquad \text{for } x \in [x_i, x_{i+1}] \tag{5-27}$$

The corresponding set of equations for the determination of the derivatives, y'_i, that satisfy cubic spline continuity requirements can also be put into a bi-diagonal form, as shown in Appendix D.

$$\begin{bmatrix} 1 & c_2 & 0 & \dots & & & \\ 0 & 1 & c_3 & 0 & \dots & & \\ \dots & 0 & 1 & c_4 & 0 & \dots & \\ & \dots & 0 & 1 & c_5 & 0 & \dots \\ & & & & \vdots & & \\ & & & \dots & 0 & 1 & c_{n-2} \\ & & & & \dots & 0 & 1 \end{bmatrix} \begin{bmatrix} y'_2 \\ y'_3 \\ y'_4 \\ \vdots \\ \vdots \\ y'_{n-2} \\ y'_{n-1} \end{bmatrix} = \begin{bmatrix} w_2 \\ w_3 \\ w_4 \\ \vdots \\ \vdots \\ w_{n-2} \\ w_{n-1} - c_{n-1} y'_n \end{bmatrix} \tag{5-28}$$

The corresponding forward recursion equations are

$$c_1 \triangleq 0 \tag{5-29}$$

$$w_1 \triangleq y'_1 \tag{5-30}$$

for $i = 1, 2, 3, \dots, n-2$:

$$c_{i+1} = \frac{H_i}{2(1+H_i) - c_i} \tag{5-31}$$

$$w_{i+1} = \frac{3(\Sigma_i + H_i \Sigma_{i+1}) - w_i}{2(i + H_i) - c_i} \tag{5-32}$$

where

$$\Sigma_i \triangleq \frac{Y_i}{a_i} = \frac{y_{i+1} - y_i}{x_{i+1} - x_i} \tag{5-33}$$

The backward recursion equation is

for $i = n-1, n-2, \dots, 2$:

$$y'_i = w_i - c_i y'_{i+1} \tag{5-34}$$

While this direct-slope determination method uses the same general procedures as the UNIVAC routine, it has the advantages of both requiring less spline coefficient storage and requiring the computation of fewer coefficients. The UNIVAC method requires computation of 9(n-1) values: the c_i, w_i, and z_i, 3(n-1) of each. The latter method requires only 3(n-2) values: the c_i, w_i and y'_i, (n-2) of each.

5.4 End-Point Slope Estimates

The two fitting methods require end point slopes to uniquely define the fit. For terrain systems, only the data points themselves usually are available, but the slopes can easily be estimated from these by using two, three, or four data points at each end of the terrain segment. This corresponds to first, second, and third order slope estimates, respectively, as follows:

$$y'_a = \frac{y_2-y_1}{x_2-x_1} \tag{5-34}$$

$$y'_b = \left(\frac{1}{x_3-x_2}\right)\left[(y_3-y_1)\frac{(x_3-x_1)}{(x_2-x_1)} - (y_2-y_1)\frac{(x_2-x_1)}{(x_3-x_1)}\right] \tag{5-36}$$

$$y'_c = \frac{(y_2-y_1)\dfrac{(x_4-x_3)}{(x_2-x_1)^2} + (y_3-y_1)\dfrac{(x_4-x_2)}{(x_3-x_1)^2} + (y_4-y_1)\dfrac{(x_3-x_2)}{(x_4-x_1)^2}}{\left(\dfrac{x_4-x_3}{x_2-x_1}\right) + \left(\dfrac{x_4-x_2}{x_3-x_1}\right) + \left(\dfrac{x_3-x_2}{x_4-x_1}\right)} \tag{5-37}$$

The indices are ordered starting with 1 at either end point and counting toward the interior of the data interval.

Terrain data from a typical test terrain located in Pennsylvania (designated 6201) [4] is used in the studies that follow. It

is classified as moderately rough, σ_T = 367 feet. The splines are relatively insensitive to the order of the slope estimate for the typical terrain profile, as shown in Figure 5-3. Therefore, an extreme test profile (σ_T = 963 ft) was constructed in an attempt to differentiate between the three types of estimates. The plots for this case are shown in Figure 5-4 and do show some differences at the right end. However, there is no clear choice of a best fit, so the final choice for actual implementation could be made based on the ease of implementation, which would be the simplest one, Eq. (5-35).

5.5 Clearance Curve Determination

In the determination of the clearance curve, the effect of different types of clearance measurements is of interest. The measurement considered most accurate is the slant clearance (clearance to the nearest terrain point), but the easiest one to use and the one most frequently used in terrain following is the vertical clearance. The two types will be compared in this section.

It is fairly simple to compute the locus of points that have a specific normal offset distance from a cubic spline terrain curve. Such a locus is generated by continuously moving a line segment of the specified clearance length along the terrain curve so that it is always normal to the terrain. A 3000-foot-offset curve is shown in Figure 5-5 for the extreme-test segment constructed earlier. As indicated in the figure there are problems when the instantaneous radius of curvature of the terrain curve becomes smaller than the specified offset distance. Loops with cusps are produced on the offset curve. The obvious method for obtaining a clearance curve

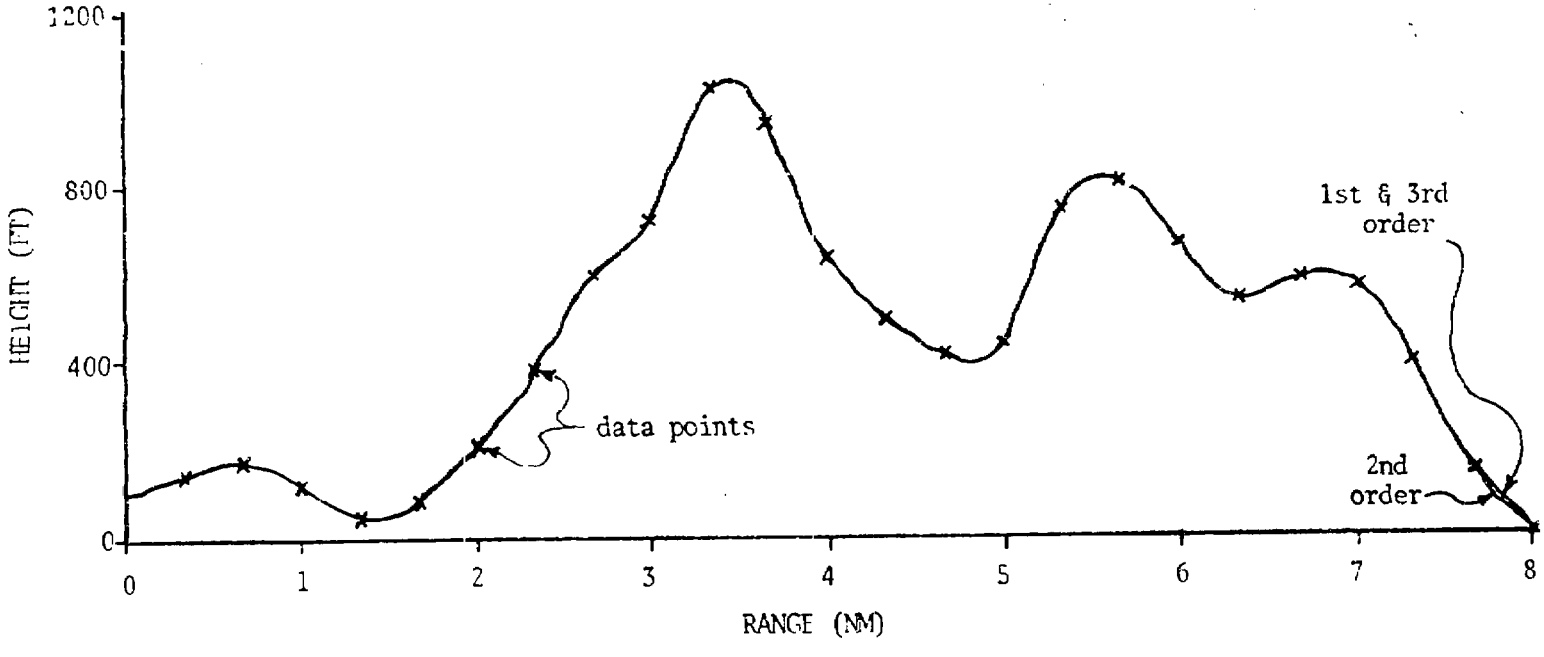

Figure 5-3 Typical Terrain with Different End Slope Estimates

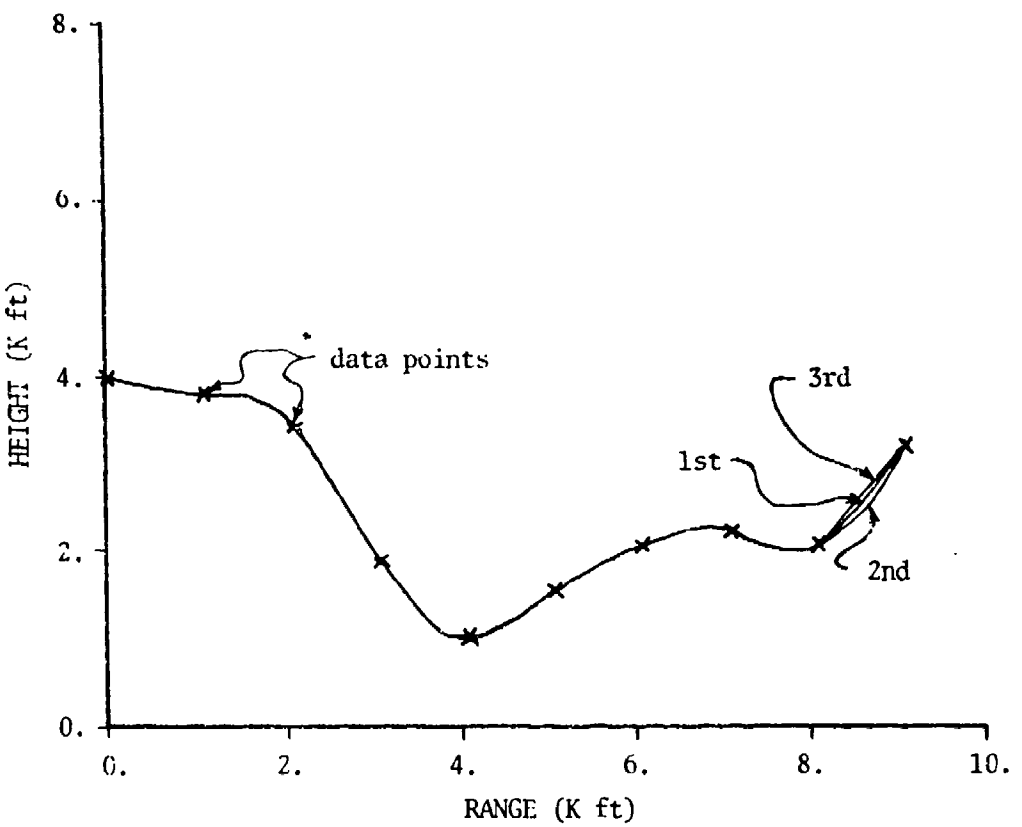

Figure 5-4 Extreme Test Terrain with Different End Slope Estimates

from the offset curve would be to reject those points on the offset curve that are on the loops or near the crossover point. The cusp at the crossover point is undesirable for a smooth clearance curve. Proper selection of points from the offset curve for cubic splining was the approach finally considered in this study. The elimination of "improper" points on the offset curve is not a simple procedure, but a method for doing this is presented in Appendix E. The slant clearance curve shown in Figure 5-5 was obtained by this method, which is considered a minor part of the study, since the presence of loops would be very unlikely for practical data point spacings and real terrains.

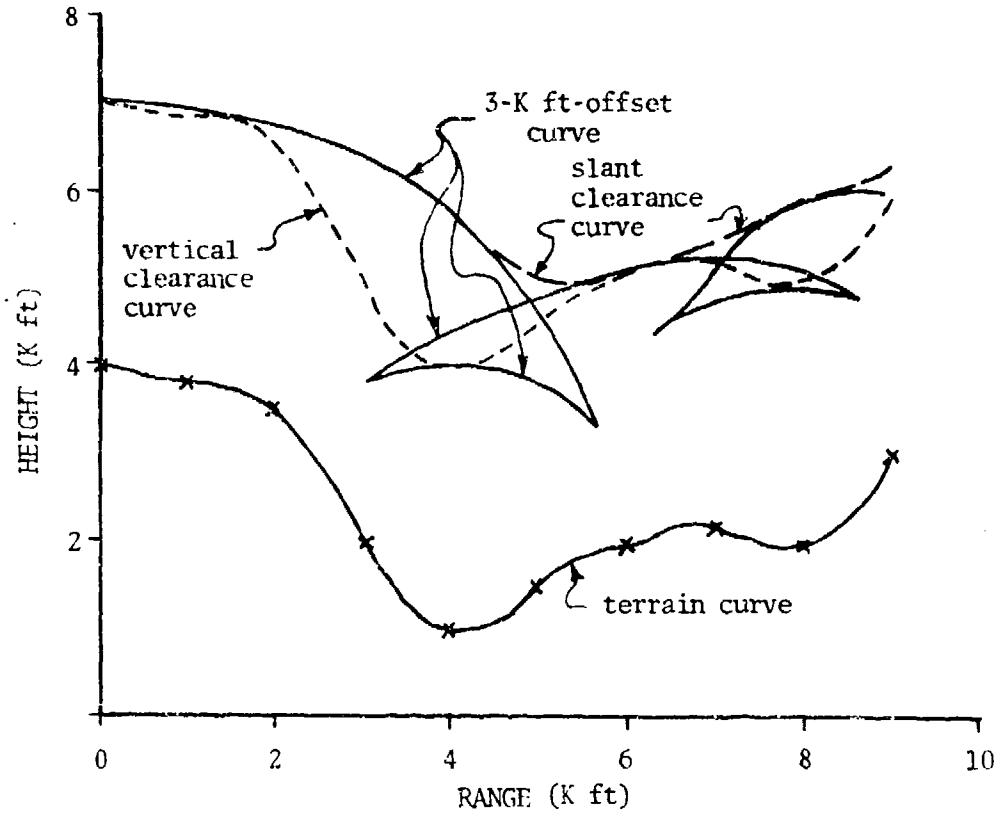

Figure 5-5 Extreme Test Terrain Clearance Curves

Also shown in Figure 5-5 is the vertical clearance curve which is just an upward translation of the terrain curve. The differences are pronounced for the extreme case shown; they would not be as different for typical terrains, as indicated in Figure 5-6.

An alternate approach to using the offset curve to construct a slant clearance curve is to use a "local" estimate of the vertical difference between the slant clearance and the vertical clearance curves. The term local refers to the fact that the slope and curvature at a single point on the terrain curve would be used for the estimate, while the true differences are determined by many

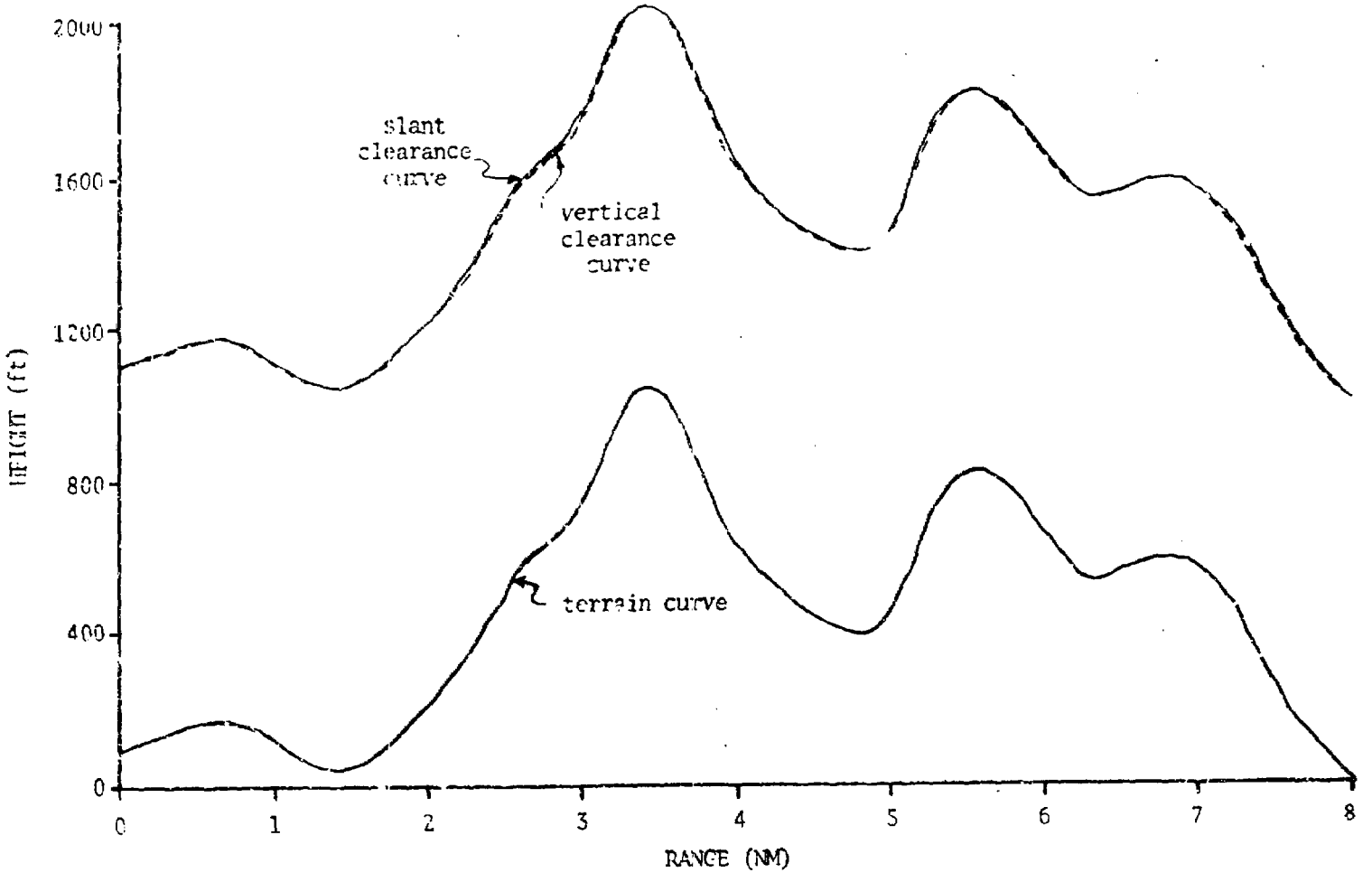

Figure 5-6 1000-ft Clearance Paths for Typical Terrain

points. The estimates are illustrated in Figure 5-7, and are based on the assumption that the instantaneous radius of curvature is constant over the interval ΔR. This is not true for a typical terrain curve, but it is necessary in order to obtain a simple estimate. The constant radius of curvature does not imply constant "curvature" ($k = \frac{d^2h}{dR^2}$), as seen by the relationship

$$r = \frac{1}{k} \sec^3\gamma \tag{5-38}$$

where γ is the path angle, which varies with range. Note that the radius of curvature is also negative when the curvature is negative. The estimate can be obtained from the CST triangle in Figure 5-7 by the cosine law, as shown in Appendix F.

$$c_c = n + \delta - \frac{r\theta}{n} - \text{sgn}\,(r)\sqrt{\left(\frac{r\theta}{n} - n\right)^2 - 2r(n - \theta)} \tag{5-39}$$

where n is the normal (slant) clearance distance and

$$\theta \triangleq n \cos\gamma \tag{5-40}$$

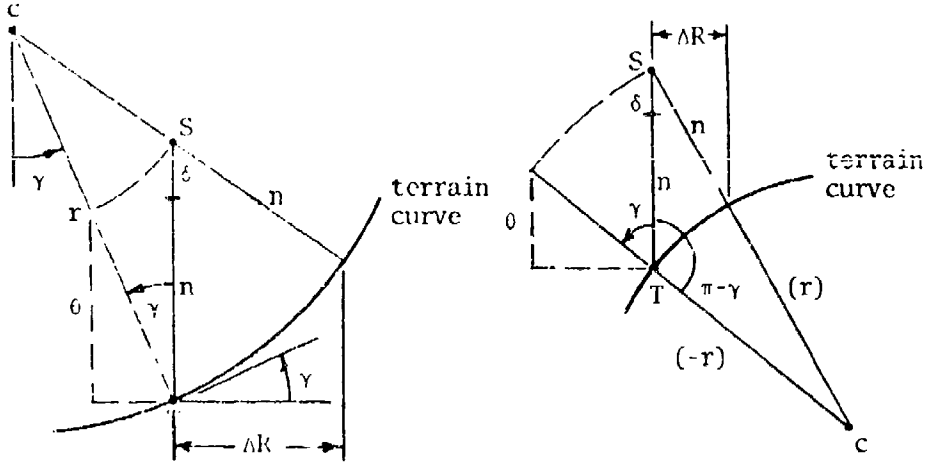

a. positive curvature b. negative curvature

Figure 5-7 Local Estimates of Clearance Differences

There is a simpler approximation if the magnitude of x, as defined by Eq. (5-41), is very small compared to unity.

$$x \triangleq \frac{2rn^2(n-\theta)}{(r\theta-n^2)^2} = \frac{2nw(n-\theta)}{(\theta-nw)^2} \tag{5-41}$$

where

$$w \triangleq \frac{n}{r} = \frac{k\theta^3}{n^2} \tag{5-42}$$

Then

$$c_e = n + \frac{rn(n-\theta)}{(r\theta-n^2)} = \frac{n^2(1-w)}{(\theta-wn)} \tag{5-43}$$

The total vertical clearance distance for the estimated curve is c_e.

A comparison of the three types of clearance curves is made in Table 5-1. The slant-clearance curve is used as a standard of reference; the differences between each of the other two clearance curves and it are listed. The data in the table are given for two terrain profiles: the extreme test segment and the typical terrain segment, which were shown in Figures 5-5 and 5-6, respectively. Because of its local nature, the estimated clearance frequently corresponds to the clearance distance for the lower portion of a loop when loops are present on the offset curve. This is an undesirable feature, as can be seen from the extreme-test terrain clearance data, but the typical terrain clearance data shows that the estimated clearance is an excellent approximation of the slant clearance when loops are not present in the offset curve. Since the estimated clearance requires significantly less computation, it would be a good selection for the reference clearance path in rough terrain. Estimated clearance is used for the clearance curves in the parametric studies in Chapters 6 and 7.

Table 5-1 Comparison of the Differences in Clearance Curve Heights

VC - Vertical-Clearance Curve

SC - Slant-Clearance Curve

EC - Estimated-Clearance Curve

	Typical Terrain		Extreme Test Terrain	
Range	VC-SC	EC-SC	VC-SC	EC-SC
	(All Values in Feet)			
2000	- .20	- .10	- 89.3	- 52.5
4000	- .28	.00	- 50.8	+ 1.6
6000	- .00	.00	- 215.5	+ 25.3
8000	- .80	.00	-1400.3	-1159.5
10000	- .26	.00	-1722.5	-1716.8
12000	- .86	.00	- 395.5	- 102.7
14000	-2.34	+ .02	- 102.8	+ 124.6
16000	-5.74	+ .02	- 118.4	- 104.9
18000	-3.02	.00	- 927.8	- 883.3
20000	-7.06	+ .06	- 424.6	0.0
22000	-4.08	- .02		
24000	-6.52	- .02		
26000	-8.72	+ .08		
28000	-1.14	.00		
30000	- .86	.00		
32000	-4.66	+ .04		
34000	-7.20	- .02		
36000	- .18	.00		
38000	-4.00	+ .02		
40000	- .36	.00		
42000	- .36	.00		
44000	- .68	.00		
46000	-6.44	.00		
48000	-5.32	+ .02		
50000	-3.10	+ .02		

6. REFERENCE PATH DETERMINATION AND PARAMETRIC STUDIES

The previous chapters developed the optimization problem for the determination of a reference path and discussed the parameters affecting that problem. In this chapter various solutions of the optimization problem are considered, as well as some of the characteristics of the algorithms that are used to compute those solutions. Two basic approaches to solving the problem are discussed: the first is a penalty function method of treating clearance constraints, the second and preferred approach is to treat the constraints directly by the mathematical programming method. The discussion of the penalty function approach is brief and is included only because it is one that is frequently used with state variable inequality constraints, and some interesting characteristics are observed when using it.

6.1 Penalty Function Approach

The first approach is an exterior penalty-function method utilizing a general parameter-search optimization algorithm. The penalty function limits the clearance constraint violations and search-direction limits enforce the curvature constraints. A Davidon rank-one search algorithm [9] is used. The rank-one algorithm is not as commonly used as the Davidon rank-two algorithm, which requires a one-dimensional optimization along the search direction in parameter space. The rank-one algorithm was selected because it has a self-adjusting step size that does not require a

one-dimensional optimization along each search direction and it was felt that fewer iterations would be required. Both algorithms use estimates of the variance (the inverse of the Hessian matrix) to establish search directions in the parameter space. The rank-one method updates the variance estimate with a matrix of rank-one, based on the gradient vector. Details of the method are found in Reference 9.

The penalty function creates convergence problems near the final solutions, because of the artificially steep cost surfaces introduced by the penalty term. This is a problem discussed by Beltrami [5] and others [17]. To further complicate convergence, the parameter limits on curvature also interrupt the normal search procedure. The Davidon routine was modified to reduce the effective dimension of the search whenever a parameter space boundary was encountered. This was done by reducing the rank of the variance estimate appropriately. However, once the rank was reduced, the search remained on the corresponding boundary. To allow for flexibility so that the search could leave the boundary, special tests and procedures to increase the rank of the variance had to be incorporated. The technique is illustrated in Figure 6-1, for a search in a two-dimensional space. The level curves of the cost function are sketched and the negative gradient directions are indicated by arrows along a possible search path. If one of the boundaries is encountered during the search, the method searches the boundary surface by reducing the variance in rank (to a rank of

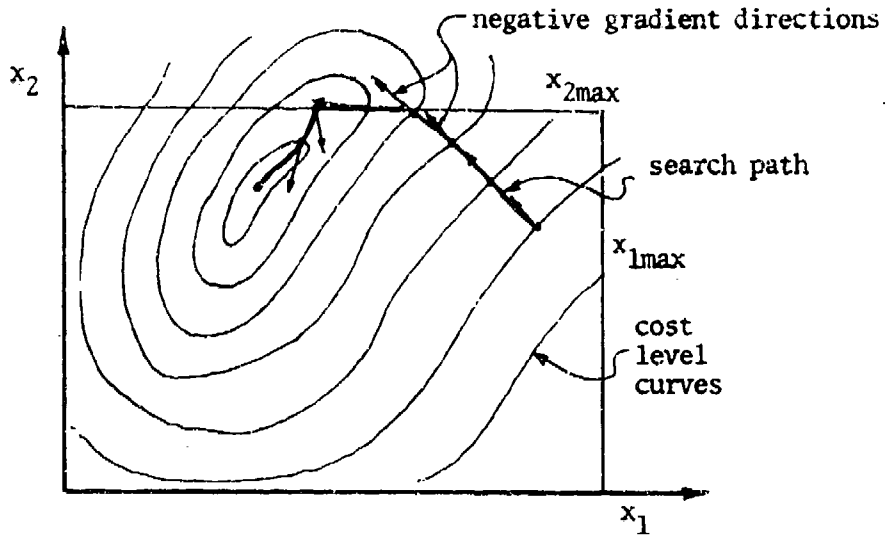

Figure 6-1 Bounded Parameter Search

one, in the example). Any time the negative cost gradient points out of the allowable parameter space the search continues on the boundary, but if the negative gradient points inward the variance rank is increased again to allow the search to leave the boundary. The procedure works fairly well, but when coupled with the penalty function ill-conditioning there are regions where the method tends to jump on and off the boundary as it jumps back and forth across the penalty function valley. This difficulty could probably be eliminated by an acceleration scheme such as those discussed by Beltrami [5], and Kelley and Denham [17]. Sequential increases in the penalty function coefficient improve the convergence for some problems, but stepping the coefficient does not help significantly for this problem. This is due to the nature of the parameter cost relationship. Trajectories which lie very close to one

another in position space may differ in all the curvature parameters -- not just in one or two. Small changes in the near frame parameters cause larger changes in the far frame trajectory because of the double integration of the control function. So it is not easy to go from the solution for one penalty coefficient to that of another, because of the complicated interaction of sensitivities and constraints.

The moderately rough terrain segment shown previously in Figure 5-3 is used to test all of the optimization approaches considered in this chapter. A typical penalty function solution is shown in Figure 6-2. The framing structure for this solution is Structure 1 in Table 6-3 on page 86, which gives the structures for all of the cases considered in this chapter. The number of iterations required for the solution to converge is very large for some frames when the penalty function approach is used. However, the rate of convergence is rather rapid at first and then slows considerably as the number of iterations increases. This fact is confirmed by Figure 6-3, which depicts solutions with various limits imposed upon the number of iterations in each optimization frame. Very little improvement is observed in the path when more than 80 iterations per frame are allowed. The case with a 150 limit has slightly greater clearance violation, but the path also goes slightly lower into the valleys than that for the 80-limit case. There is essentially no difference between the 500-limit path and the path without limits shown in Figure 6-2. Therefore, the large

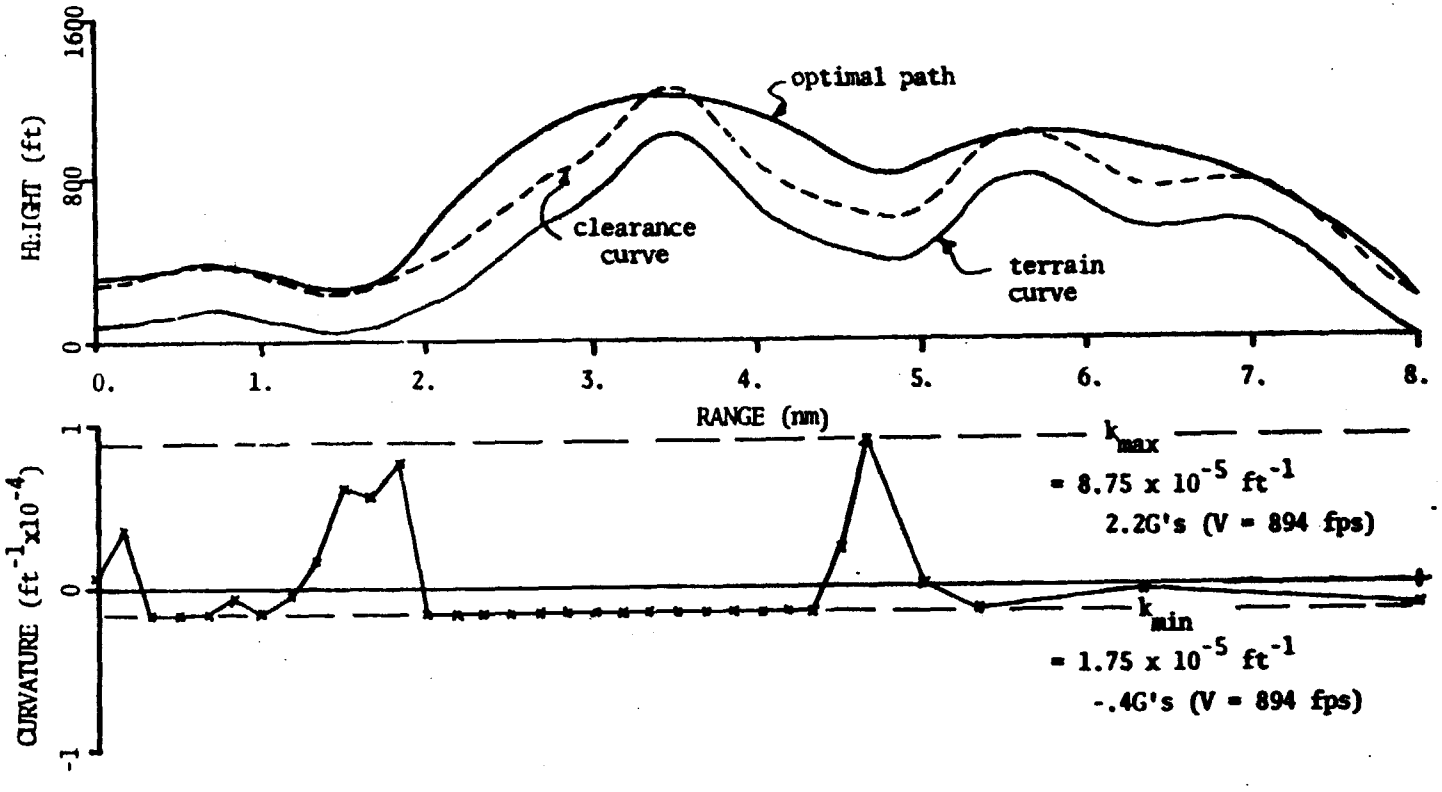

Figure 6-2 Typical Penalty-Function Optimal Path

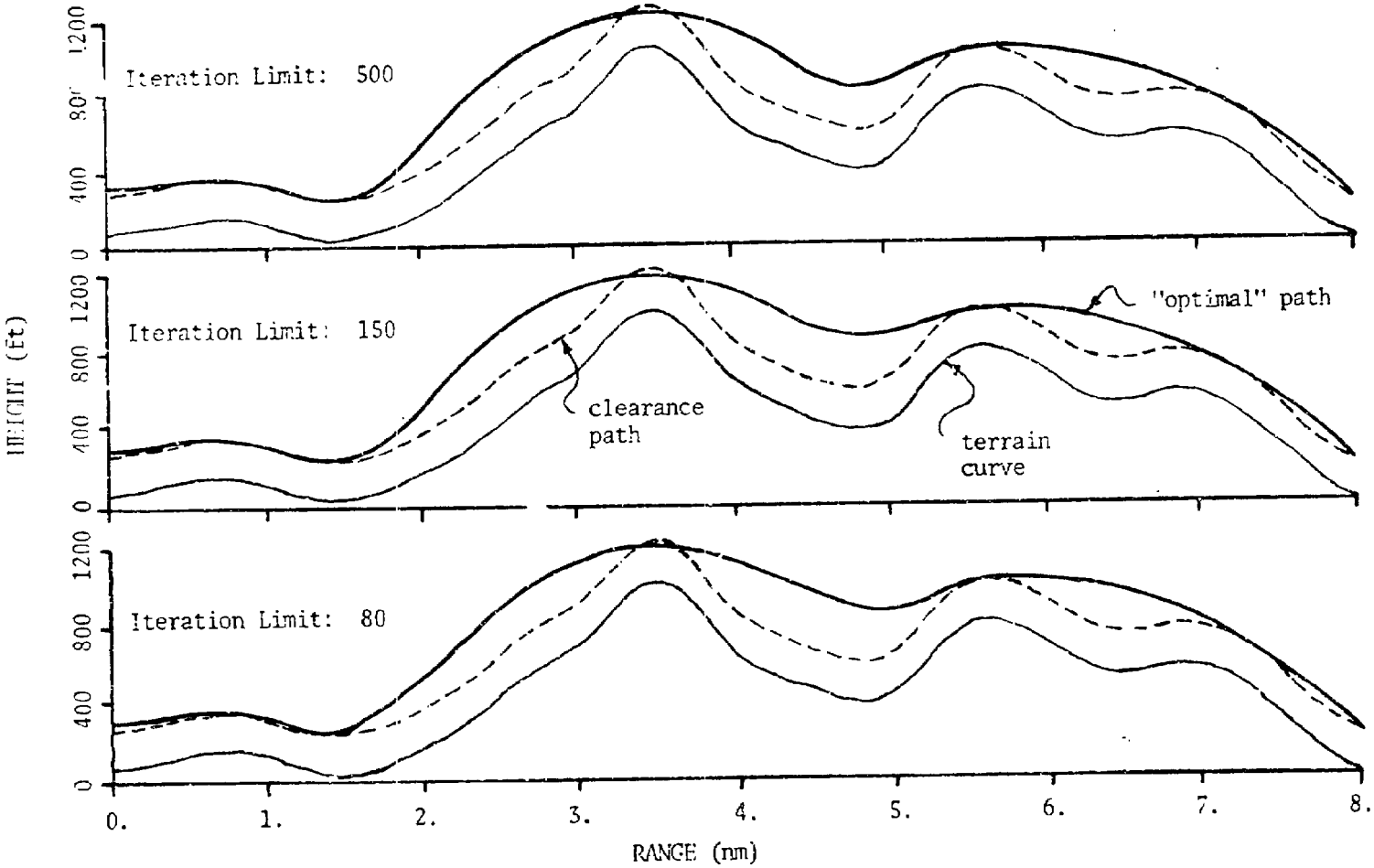

Figure 6-3 Penalty-Function Optimal Paths with Various Iteration Limits

number of iterations are not really needed for reasonable performance. The final path refinement is not significant, while the computation time required for it is large. The solution times corresponding to the various limits are given in Table 6-1 for framing Structure 1 (Table 6-3). These times are compared to the solution times for the quadratic programming routines which will be discussed below.

Table 6-1 Central Processor Solution Times

Approach	Iteration Limit Per Frame	Average Time Per Frame (Sec)
Penalty Function	80	2
	150	3
	500	8
	none	11
Quadratic Programming		
Shankland	none	1
Lemke-Ravindran	none	1

The penalty function approach requires more computer time and does not have well defined lower clearance bounds; therefore, the programming solutions are a much better approach.

6.2 Quadratic Programming Problem Approach

Two quadratic programming algorithms are used to obtain solutions to the optimization problem. Shankland's algorithm [29] uses the direct quadratic programming formulation described in Section 3.4, while the Lemke-Ravindran algorithm [26] is based on the complementary problem of Section 3.5.

Shankland's method seeks to find a solution by iteratively enforcing various sets of the inequality constraints as equality constraints. The proper set of constraints is found by considering the control vector that maximizes the performance index subject to the enforced equality constraints. The maximizing control vector at any particular iteration step may violate some of the inequality constraints that are not imposed at that particular step. The iterative procedure selects some of the violated constraints for addition to the imposed set by minimizing the Euclidean norm of the constraint violation vector. If a solution exists the violation is driven to zero. If a solution does not exist, the violation vector is minimized. This is a definite advantage when numerical errors make the problem "slightly infeasible."

The Shankland algorithm does require a positive-definite quadratic performance matrix, so it is not as flexible for performance criteria investigations as the Lemke method, in which the quadratic matrix can be set to zero for a linear performance criteria. However, the Shankland method requires considerably less storage space than the Lemke algorithm uses, since it does not store the complete complementary problem matrix. If Q and C are designated as the quadratic cost matrix and the complete constraint set matrix, respectively, their dimensions are indicative of the storage space required for Shankland's method, but the Lemke routine, as used, combines these matrices into the much larger $\overline{M}$ matrix with a large number of zeroes in the lower right corner.

$$M = \begin{bmatrix} Q & -C' \\ C & 0 \end{bmatrix} \qquad (6\text{-}1)$$

(Typically the zero matrix may be 40 x 40 or larger). It is possible to reprogram the Lemke algorithm to take advantage of the zero matrix, but the optimization of the computer programming is beyond the scope of this study.

The solution of each data frame is essentially the same for both algorithms. The Lemke routine is chosen for further analysis because of its flexibility, but it is not necessarily recommended for use in an operational system. The Lemke algorithm used in this study is one revised by Ravindran to use a special Revised Simplex search. This algorithm worked extremely well, except for very large M matrices of dimension near 100. (Ravindran's routine was originally limited to a dimension of 50). For the large dimensional cases, a large number of iterations caused a build-up of round off errors in the recursively calculated matrices, until reasonable solution accuracy was lost on some particular data frames. The more reasonable 60-dimensional problems produced solution accuracies of approximately seven significant digits. This accuracy is determined by comparison of the two sides of the complementary problem vector equation (Eq. 3-39). Similar numerical difficulties are experienced during a matrix decomposition routine used in the Shankland method when large dimensional optimizations are attempted.

A comparison of the successive frame solutions using the penalty function and the quadratic programming approaches is shown in

Figure 6-4 for framing Structure 1. Although it is more natural to think of the control variable in terms of acceleration, the curvature is plotted throughout these studies. The curvature is more closely related to the path and it includes the effects of both acceleration and velocity. For example, the curvature limits in Figure 6-4 of 0.0000875 and -0.0000175 ft^{-1} correspond to +3.4 and -0.58 G's at Mach 1 (V=1117 fps), or to +0.85 and -0.17 G's at Mach 0.5 (V=558 fps). To give the reader a feeling for the control magnitude, the acceleration limit corresponding to each curvature limit is shown in the figures and is based on a nominal velocity of 894 fps (Mach 0.8), unless otherwise specified. This is the velocity used in the aircraft simulations discussed in Chapter 7.

The framing process is illustrated also in Figure 6-4. Three frames are shown with a frame advance distance of 4000 feet. This same advance is used for most of the studied framing structures. It is chosen to be small compared to the frame lengths used, and it is held constant to minimize any interactions between other framing parameters. Only the portions of the optimal paths in each of the advance intervals is used for guidance in real time application.

The penalty function trajectory lies lower than the quadratic programming trajectory, but it also violates the clearance constraints. If the lower clearance values are acceptable, it is preferable to intentionally set the clearance level lower than to allow violations of the clearance level. This would provide more reliable control of the minimum clearance distance.

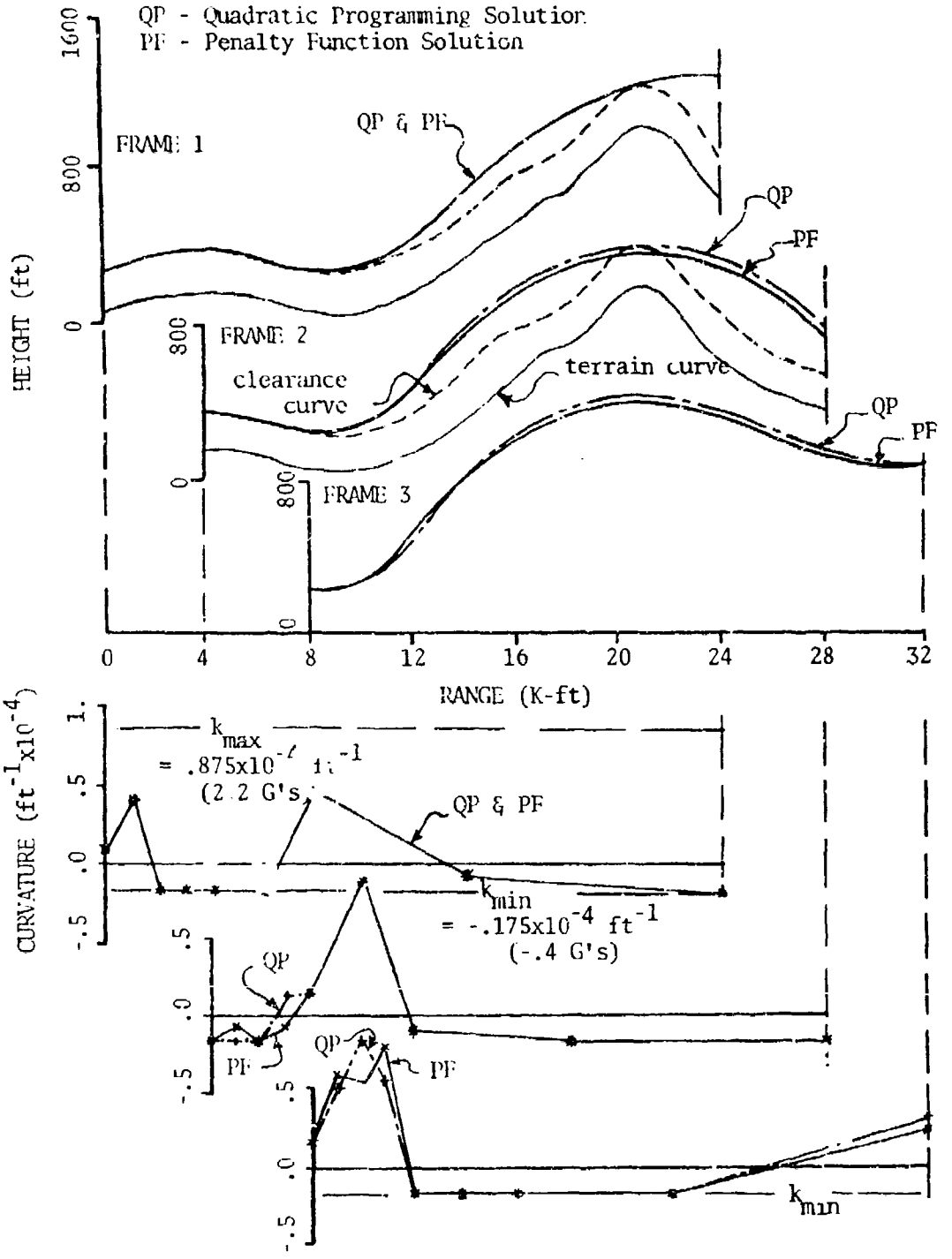

Figure 6-4 Penalty-Function vs. Quadratic Programming Solutions

6.3 Performance Criteria Study

An important concern in terrain following is the criterion for "closeness." Quadratic, linear, and min-max criteria, based on the clearance distance above the reference clearance curve, are considered here. The effect of the squared term in the quadratic cost function is to emphasize large clearance errors more than small errors. The min-max criteria goes even further in this direction.

6.3.1 Quadratic and Linear Performance Measures. The linear performance measure can be considered as a special case of the quadratic measure where the squared term coefficient, Q_n, of Eq.(3-2) is set to zero. Before the study of the coefficient values of Q_n and L_n was conducted, it was assumed that a change in the ratio of these coefficients could make a significant change in the solution. The values of Q_n and L_n are the same for each sample point, but to "normalize" the performance measure, these values were based on the number of sample points. That is, values of c_Q and c_L were specified and the Q_n and L_n were computed from these and the number of performance measure sample points, N_p.

$$Q_n = \frac{c_Q}{N_p} \tag{6-2}$$

$$L_n = \frac{c_L}{N_p} \tag{6-3}$$

Four sets of coefficient values are shown in Table 6-2, and the corresponding trajectories are essentially the same, even though

there are some slight differences in the curvature controls, as shown in Figure 6-5. The data in Table 6-2 are for seven frames based on Structures 2 through 5 of Table 6-3. The framing structures are identical except for the performance coefficients.

Table 6-2 Cost Coefficient Comparison

Framing Structure Nr.	c_Q	c_L	Total Nr. of Iterations	Computation Time (Sec)
2	.1	.0	210	9.0
3	.1	.001	206	8.9
4	.1	.1	291	9.8
5	.0	.1	329	10.7

Contrary to what was initially expected, the trajectories are quite insensitive to the values of the cost coefficients. After a little reflection this is not too surprising; the trajectories for the terrain following problem tend to be very constraint bound. The major portions of them are on some form of constraint boundary: a maximum pull up, a maximum push over, or a clearance curve boundary. The optimization problem, then, consists primarily of piecing these different types of trajectory arcs together at the proper points with suitable transition arcs. This is just the type of procedure that terrain-following investigators have attempted to do for some time now in the construction of ideal paths, but the schemes have not been applicable to real time implementation (except for that of Greaves).

Although the linear performance measure (last one in Table 6-2)requires slightly more computation time with the Lemke algorithm,

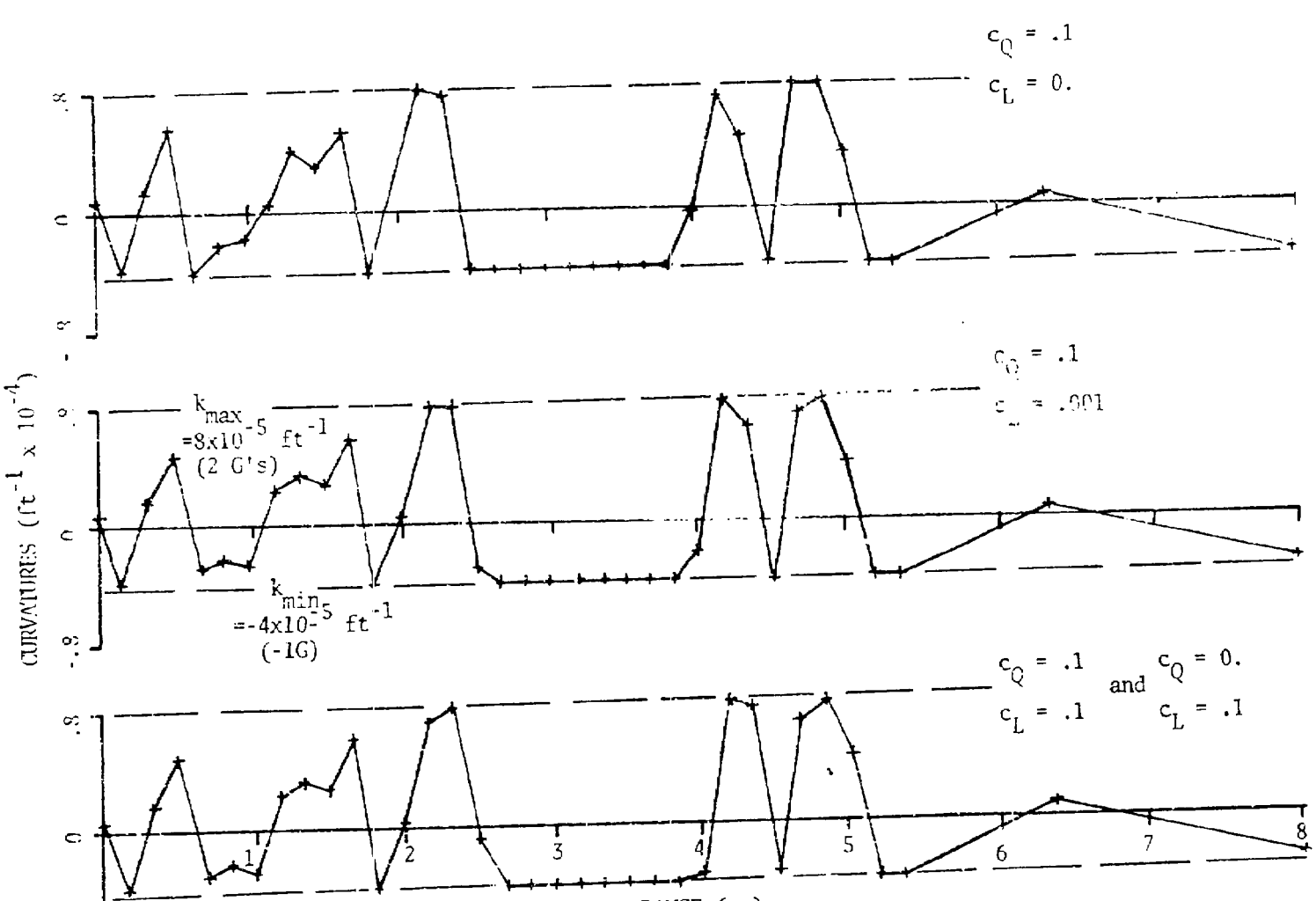

Figure 6-5 Control Comparison of Different Cost Coefficients

Table 6-3 Framing Structure for Reference Paths

Structure Nr.		1	2	3	4	5	6	7	8	9	10	11	12	13	14	15	16	17
Type of Study		Penalty Function	Performance Measure					Hard-Ride Frame Length			Soft-Ride Frame Length			Control Interval			Slope Constraint	
Frame Length	K-ft	24	24	24	24	24	24	12	20	28	20	32	44	20	20	20	20	20
Frame Advance	K-ft	4	4	4	4	4	4	4	4	4	4	4	4	4	4	4	8	8
LIMITS:																		
Curvature	$ft^{-1}x10^{-4}$	+.875 -.175	+.8 -.4	+.8 -.4	+.8 -.4	+.8 -.4	+.8 -.4	+.8 -.4	+.8 -.4	+.8 -.4	+.8 -.1	+.8 -.1	+.8 -.1	+.8 -.4	+.8 -.4	+.8 -.4	+.8 -.4	+.8 -.4
Acceleration*	G's	+ 2.2 - 0.4	+2. -1.	+2. -1.	+2. -1.	+2. -1.	+2. -1.	+2. -1.	+2. -1.	+2. -1.	+2. -.25	+2. -.25	+2. -.25	+2. -1.	+2. -1.	+2. -1.	+2. -1.	+2. -1.
Kink**	$ft^{-2}x10^{-8}$	±10.5	±12.	±12.	±12.	±12.	±6.	±12.	±12.	±12.	±4.5	±4.5	±4.5	±24.	±12.	±6.	±12.	±12.
Jerk*	G's/sec	±2.3	±2.7	±2.7	±2.7	±2.7	±1.3	±2.7	±2.7	±2.7	±1.0	±1.0	±1.0	±5.3	±2.7	±1.3	±2.7	±2.7
Nr. of Control Points		8	10	10	10	10	10	12	20	28	24	32	44	30	20	10	20	20
Complem. Prob. Dim.		28	32	32	32	32	61	36	60	84	40	64	88	80	60	40	80	60
SAMPLE INTERVALS†																		
Curvature		1[a,b]	1[b]	1[b]	1[b]	1[b]	2	1	1	1	2	2	2	.5[c]	1	2	1	1
Perf. Measure	K-ft	1	1	1	1	1	1	1	1	1	2	2	2	1	1	1	1	1
PERF. COEFFICIENT††:																		
c_L		0	0	.001	.1	.1	0	0	0	0	0	0	0	0	0	0	0	0
c_Q		10^4	.1	.1	.1	0	0	.1	.1	.1	.1	.1	.1	.1	.1	.1	.1	.1
Figure Number		2,3,4	6-5	6-5	6-5	6-5	6-6	6-7	6-7	6-7	6-8	6-8	6-8	6-9	6-9	6-9	6-10	6-10

* For V=984 fps ** Inherent limits from Δ & k_{lims}

† Exceptions to designated control interval sizes (K-ft) are: [a]5th & 6th = 2, [b]next to last = 6, and last = 10, [c]11th through 20th = 1; the clearance constraint interval = 1, the terrain data interval = 2, and no slope intervals are used except for Structure 16, for which it is 1 (with a slope limit of - .1).

†† c_M is zero except for Structure 6, for which it is 1.

it is worth noting that it does have significant advantages. The Lemke routine was used for this linear case because of its flexibility, but other linear programming algorithms could be used. Some would require less computer storage and would probably be faster, since the dimension of the overall programming problem would be reduced from that of the complementary problem.

6.3.2 Min-Max Criterion. Although minimizing the maximum vertical distance above the reference clearance path seems to be a reasonable criterion, it does stress one critical clearance distance on the data frame interval. Figure 6-6 shows the composite solutions from three successive data frames using the min-max criterion, with Q_n = L_n = 0, compared to the solutions for the quadratic criterion. These correspond to framing Structures 6 and 8, respectively, of Table 6-3. Notice that the optimal path for the min-max criterion does not follow the smoother portions of the clearance path as closely as does that of the other criterion, where the optimal path coincides with the clearance path unless the curvatures are too great. Another disadvantage of the min-max measure is that the upper-limit constraints on the clearance values increases the dimension of the programming problem (a linear one) with additional constraint equations. Since the difference in clearance maxima for the two paths in Figure 6-6 is less than two feet, the disadvantages outweigh the advantages for this performance measure.

6.4 Frame Length Study

The characteristic frame length was developed in Section 4.1 to estimate the minimum frame length required for good terrain

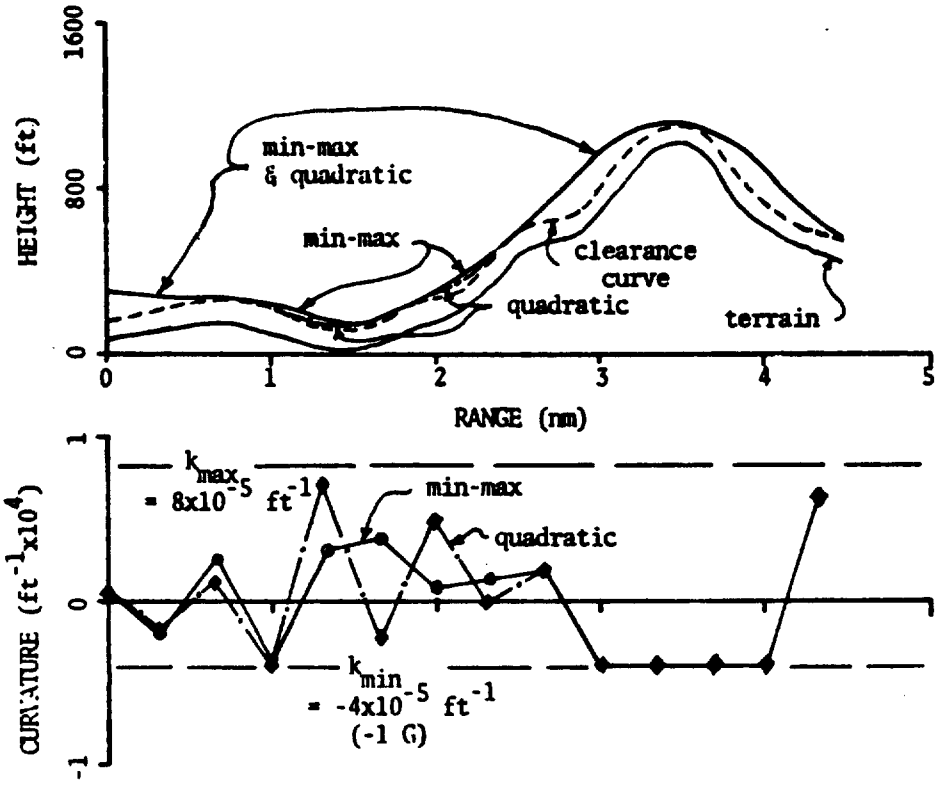

Figure 6-6 Min-Max vs. Quadratic Cost Solutions

following performance. This portion of the study tests the validity of that estimate. The computational details of the characteristic frame lengths and control intervals for the "hard" and "soft" rides are tabulated in Appendix B. The frame length values of 18,800 and 30,800 feet are based on a maximum-expected-obstacle height of 1000 feet and on the framing Structures 7 and 10 of Table 6-3.

To study the effects of frame length on the framing process, three different frame lengths are compared for each of the characteristic lengths. One length is approximately equal to the characteristic length, one is shorter, and one is longer. The

lengths used in the study are given in Table 6-4, along with a summary of other pertinent framing parameters. The complete sets of framing parameters are those for Structures 7 through 12 in Table 6-3. Table 6-4 also gives the characteristic control intervals and the actual intervals used for the optimization solutions.

Table 6-4 Frame Length Study Data

Type of Ride	Control Interval (ft)	Characteristic Interval (ft)	Characteristic Frame Length (K-ft)	Frame Length (K-ft)	Complem. Problem Dim.	Nr. of Frames in Run	Comput. Time Avg. Frame (Sec)	Comput. Time Total (Sec)
Hard	1000	1440	18.8	12	36	10	0.9	8.9
(-1,+2 G's)				20	60	8	2.4	21.5
V=894 fps)				28	84	6	6.2	37.1
Soft	2000	840	30.8	20	40	8	0.8	6.6
(-.25,+2 G's				32	64	5	1.6	8.2
V=894 fps)				44	88	2	3.1	6.2

The large control interval is used for the soft ride to reduce the number of sample points and, hence, the dimension of the optimization problem. The acceleration values shown in the figure are for two sets of curvature values at Mach 0.8. The same control interval is used for each case in a particular ride set; thus, the frame length is the only framing parameter varied in each set.

The hard ride optimal paths and controls are shown in Figure 6-7. The two longest frame lengths (20 and 28 K-ft) produce essentially the same paths. This indicates that any frame length greater than 20,000 feet is not needed. The shortest frame length

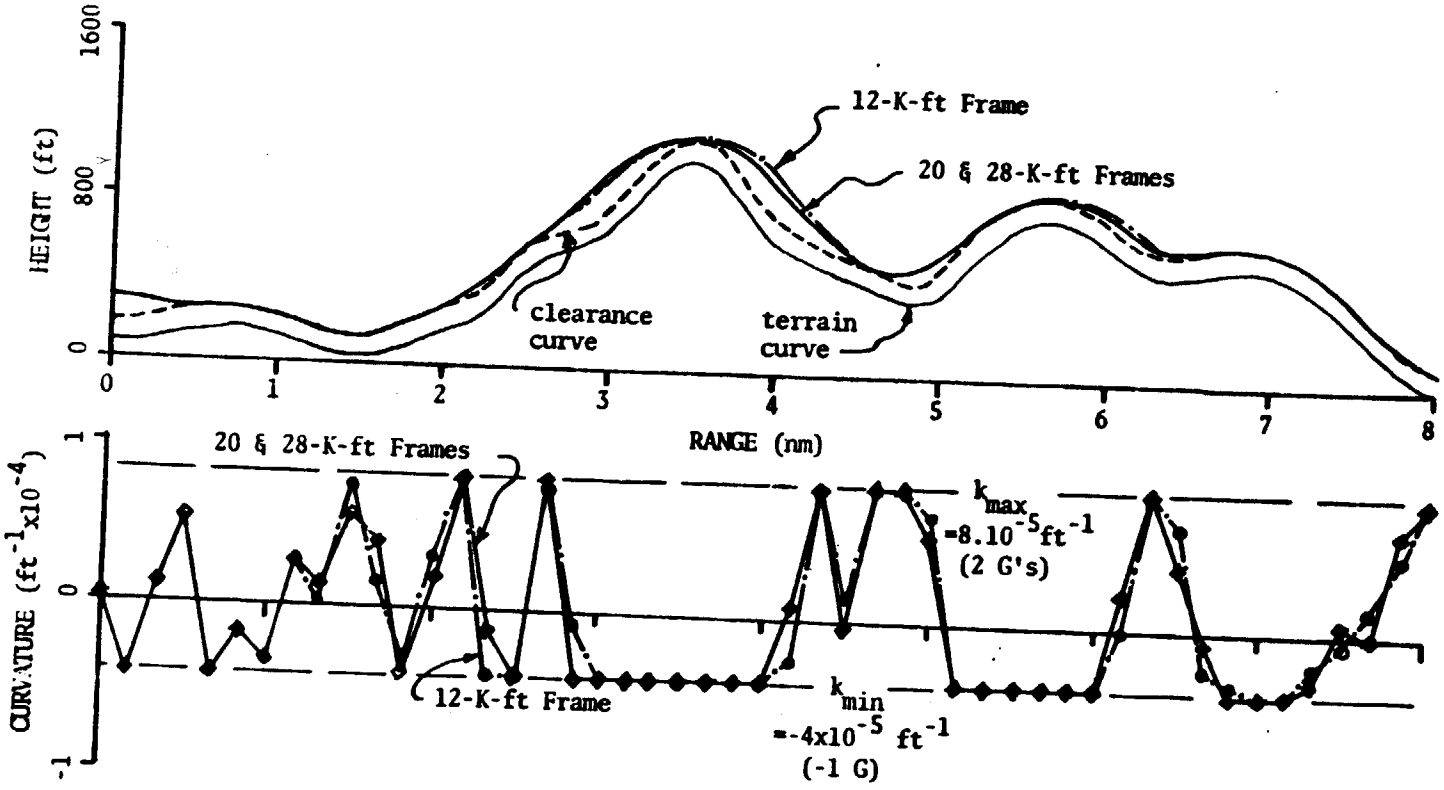

Figure 6-7 Hard-Ride Frame Length Comparison

represents a 40% range reduction from the mid-length case. The corresponding reduction in predictive capability produces small degradations in performance after the terrain peaks. The characteristic estimate of 18,800 feet agrees well with the length of 20,000 feet that provides good performance over the test terrain segment.

For the soft ride, the two paths corresponding to the two longest frame lengths are also essentially the same, even though there are minor variations in their curvature profiles, as shown in Figure 6-8. The shortest frame length is a reduction of 60% in range from the mid-length case. This large reduction causes a corresponding significant decrease in performance after the peaks. The use of a control interval significantly larger than the characteristic control interval may also be a factor contributing to the performance degradation. Once again, the characteristic frame length of 30,800 feet appears to be a good estimate of what is required for good performance in Figure 6-8 (approximately 32,000 feet).

The total time comparison for the soft ride in Table 6-4 is misleading due to the disproportionate length of the longest frame compared to the total range of the run (48,000 ft). Table 6-5 shows a more detailed comparison of the run times for the soft ride with the two longest frame lengths. (The shortest frame length run was not considered in this comparison since its performance was significantly worse). The average frame times are used to predict

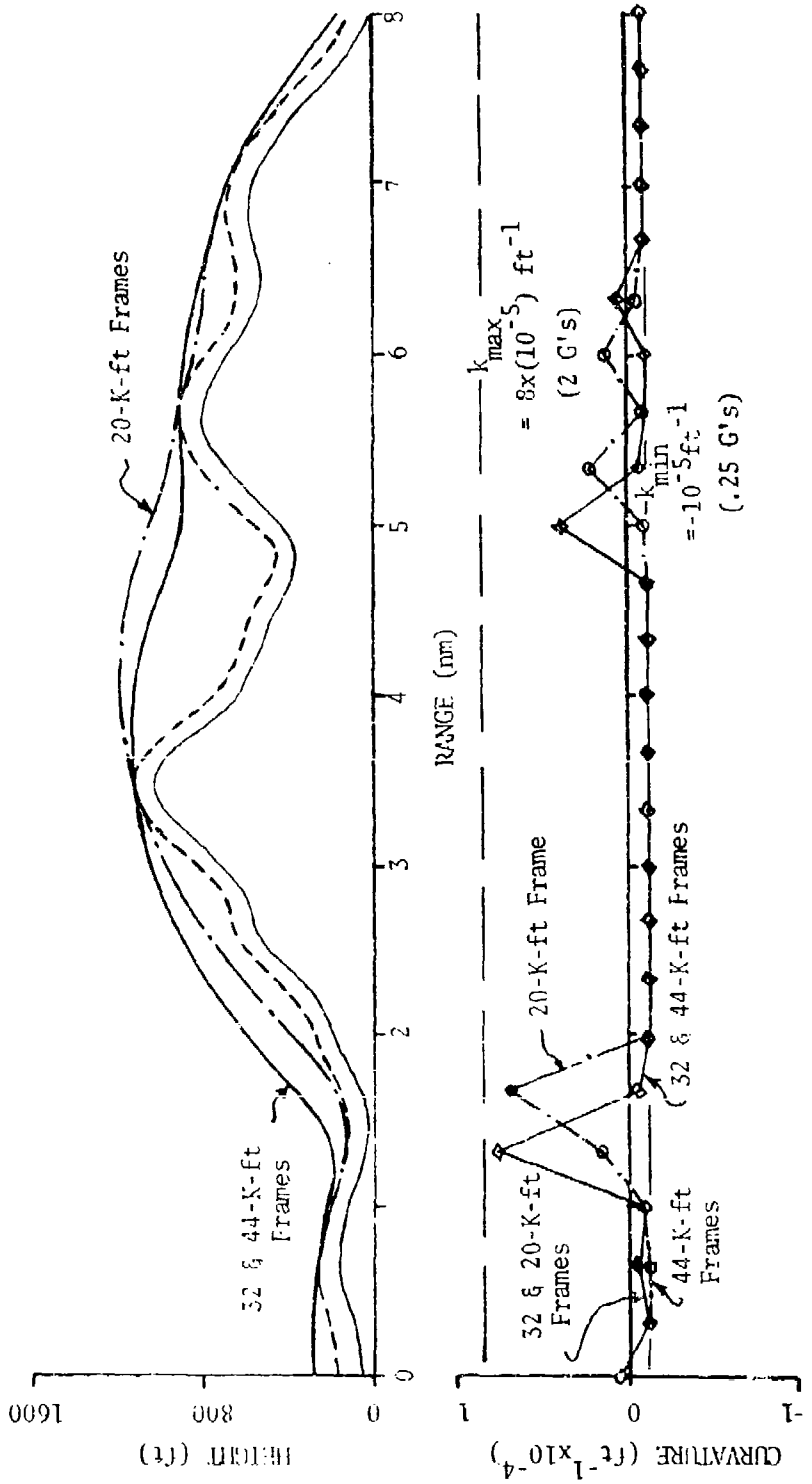

Figure 6-8 Soft-Ride Frame Length Comparison

computation times for two longer runs. Since the range covered by successive frame-advance intervals is the portion used for guidance, those corresponding portions must be comparable for two different frame lengths if the run time comparison is to be meaningful. As the total range of the run increases, the advance coverage for the cases shown in the table becomes more nearly equal. As expected, the longer frame length requires longer run times, just as it did for the hard ride comparison.

Table 6-5 Soft-Ride Computational Run Time Predictions

Run Length (K-ft)	Frame Length (K-ft)	Avg. Frame Time (Sec)	Number of Frames	Frame Advance Coverage (K-ft)	Total Time (*Predicted) (Sec)
48	32	1.6	5	16	8.2
	44	3.1	2	4	6.2
72	32	1.6	11	40	18.0*
	44	3.1	8	28	24.8*
96	32	1.6	17	64	27.8*
	44	3.1	15	52	46.5*

Comparison of Figures 6-7 and 6-8 indicates that as the maneuverability of the vehicle decreases the predictive capability of the control system must increase; i.e., the system must "look" further ahead. Furthermore, narrowing the acceleration span increases the vehicle's flight range, but it also increases the mean clearance of the path. The increase in possible flight range of the vehicle can be verified by considering the curvature profiles. The magnitudes of the curvature values are an indication of the induced

drag on the vehicle at any time. As the induced drag increases the flight range decreases for a given fuel supply. If total range is critical, a compromise must be made between the acceleration-limit span and the mean clearance altitude for the flight.

6.5 Control-Point Spacing

The spacing of the control points certainly affects the resulting trajectories in regions where the control is not on a curvature-constraint boundary for an extensive distance. This is illustrated in Figure 6-9 by three cases with different control intervals. All other framing parameters are held constant, as indicated in Table 6-3 by Structures 13 through 15. To prevent the problem dimension from becoming too large for the finest control-point spacing (500 feet), the last half of the frame uses a 1000-ft spacing.

On the fourth frame of the run with 500-ft spacing, computational difficulties were encountered. Because of solution inaccuracies due to round-off error accumulation from the third frame, the fourth frame had an infeasible solution--the path was slightly below the minimum clearance curve at the beginning of the frame. Therefore, this run only covered a total range of 28,000 feet, while only 14,000 feet of that range was covered by the 500-ft interval spacing of the control points. The majority of the remaining range is composed of pushover arcs. These portions are very predictable in nature. Therefore, the portion shown in the figure is fairly representative of the behavior with the fine control-interval spacing.

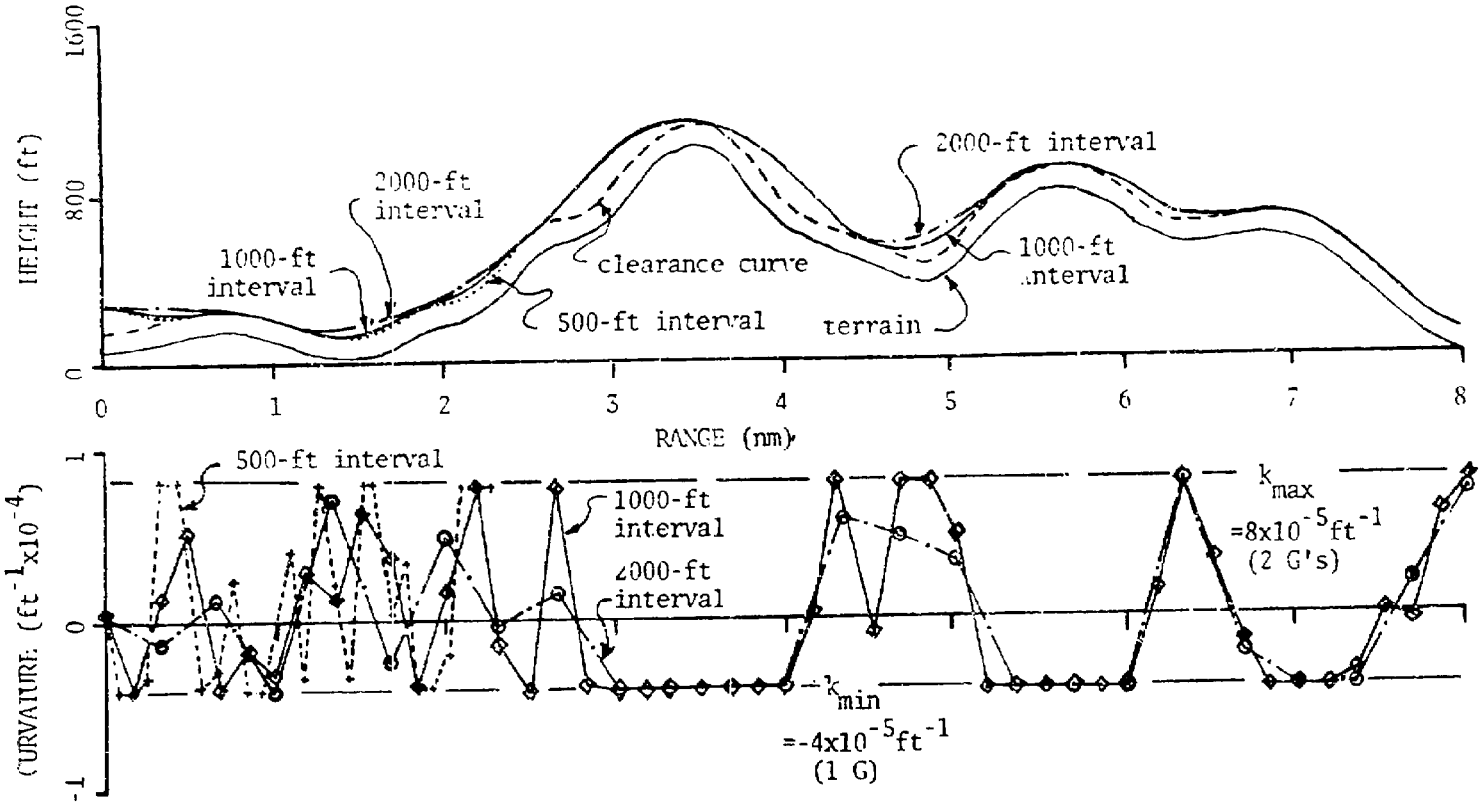

Figure 6-9 Control-Point Spacing Comparison

The behavior more closely resembles a bang-bang control than does either of the other two spacings. The finely spaced control has the largest kink values and the largest excursions in curvature. This places a much heavier stress on the tracking and flight-control systems, as well as the structural components of the vehicle. Vibration and fatigue may become serious problems for prolonged flights in this regime.

A comparison of the run times for the control interval study is shown in Table 6-6. The fine-spacing runs not only require much greater computation time and taxes the control system more heavily, but it decreases the total flight range, while lowering the trajectory only slightly in some regions. For these reasons, the numerical problems with this framing structure are not pursued further, although programming refinements could probably overcome the difficulties.

Table 6-6 Control-Point Spacing Parametric Data

Control Interval (ft)	Nr. of Control Points	Complementary Problem Dimension	Number of Frames	Computation Time (Sec) Average Per Frame	Total
500	30	80	$3\frac{1}{2}$	6.7	26.9
1000	20	60	8	2.4	21.5
2000	10	40	8	1.0	7.8

There must be a compromise between small control intervals to allow the path to follow the terrain more closely and large control intervals which reduce the computational and control rate

requirements. The particular vehicle and mission must be considered in making this decision.

6.6 Slope Constraints

Slope constraints on the flight path have usually been applied in previous designs to prevent the aircraft from descending too deeply into valleys, from which steep recoveries are required, followed by excessive overshoot of the terrain peaks. For this reason, slope constraints have not been applied in this study prior to this point. For some applications, definite requirements do exist for slope constraints, such as for transport aircraft or for a "let-down" from high altitude. The effect of a dive constraint (-0.1 minimum slope limit) on the optimal path is shown in Figure 6-10. No positive slope limit was imposed in this case. The slope-constrained path is compared to one without slope constraints; these two cases use framing Structures 16 and 17 of Table 6-3. The paths appear very much as one would expect, with flattened let-down segments in the regions where the negative slope constraints are active. However, the curvature profiles show that there is not sufficient time for the path to reach an equilibrium condition of zero curvature over any appreciable interval in these regions.

The addition of the dive constraint increased the complementary problem dimension from 60 to 80. The maximum desirable dimension for the Lemke-Ravindran routine appears to be approximately eighty, but other algorithms could probably handle higher dimensional problems, particularly the linear programming algorithms.

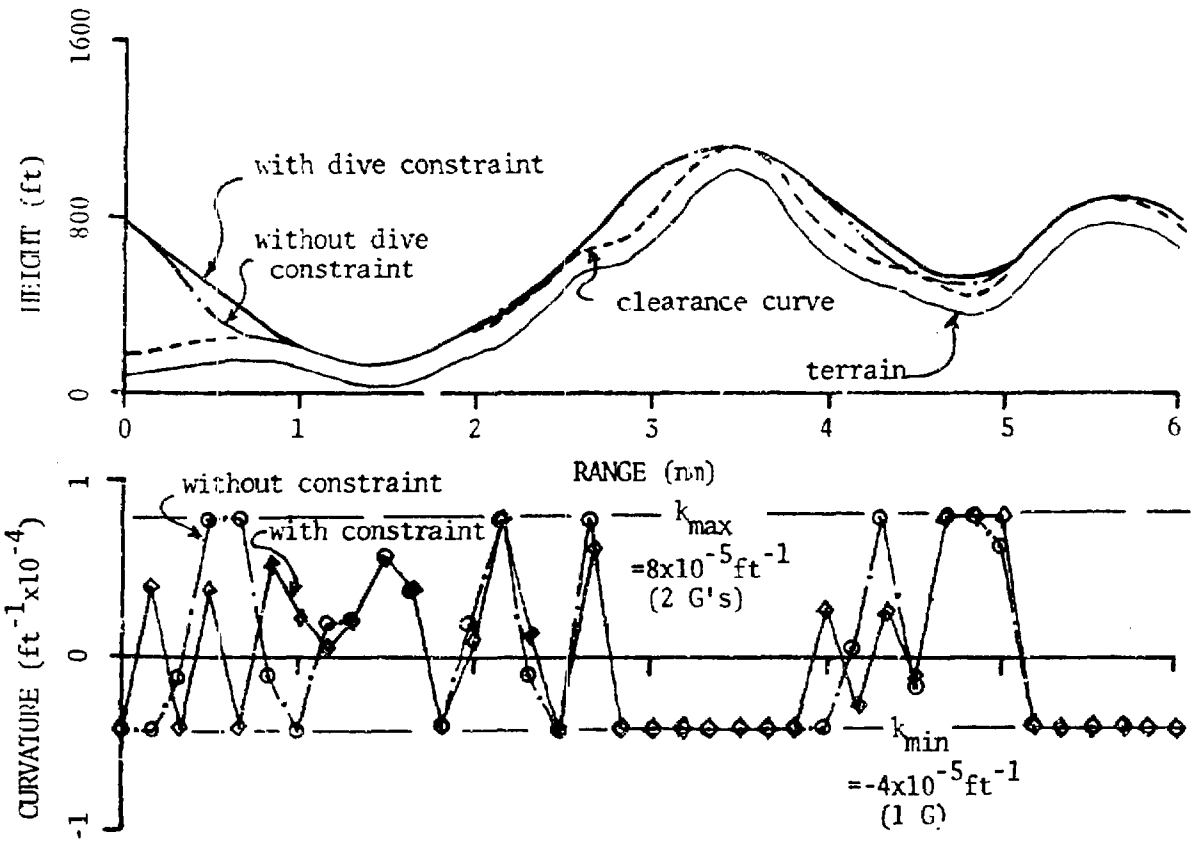

Figure 6-10 Dive Constraint Effects

The choice of various framing parameters should be based on overall system considerations, including tracker performance, which is discussed in the following chapter. It should be emphasized that most of the changes in framing parameters that may be desired for various trade-offs do not involve computer program changes; the only required changes are numerical data values. Therefore, the optimization scheme is very flexible.

7. SIMULATIONS OF THE TRACKER SYSTEM

A variety of tracker systems can be used to make the aircraft follow the optimal paths presented in the previous chapter. However, one of the goals of the optimization problem is to obtain a path that can be easily followed, and the solution of the optimization problem provides much more information than is available in other types of path processors. All derivatives of the optimal path are available to provide the tracker with some predictive capability. The block diagram for the general tracker system is shown in Figure 7-1.

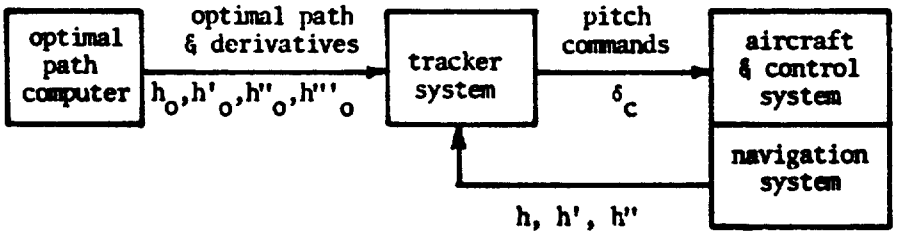

Figure 7-1 General Tracker System Diagram

The derivatives shown are with respect to range, rather than time, so the coordinate transformations of Eqs. (7-1) and (7-2) are required either in the navigation or tracker system.

$$t' = \frac{dt}{dR} = \frac{1}{\dot{R}} \tag{7-1}$$

$$x' = t' \dot{x} \tag{7-2}$$

This conversion is considered more appropriate than the use of the time domain, since terrain is fixed in the range domain and control of the path with respect to the terrain is the ultimate aim of the control

system. To test the optimal paths that have been generated for tracking feasibility, a simple tracker system is combined with a simulation of an aircraft. The specific tracker system studied is diagrammed in Figure 7-2.

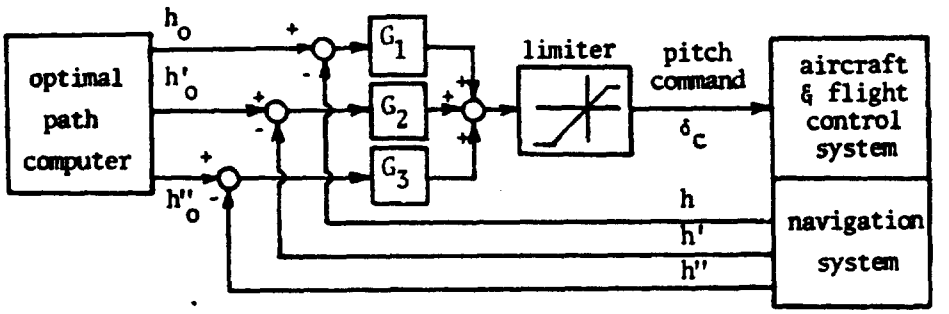

Figure 7-2 3-Channel Optimal-Path Tracker System

To determine pitch commands, three error signals are used: the altitude error and its first and second derivatives with respect to range. Each error is based on a comparison of the optimal-path value with the aircraft's actual value as determined by the navigation system. Since the optimal path is computed with continuous first and second derivatives, and the aircraft values are continuous, the error signals are also continuous. Since a range interval of optimal-path data is available prior to its use by the tracker system, a pure advance in range of the optimal curvature signal is feasible to compensate for lags in the overall aircraft system. However, the effects of lag are minor for the aircraft in this simulation, so this possibility is not pursued further.

The tracker system does not require "full state variable feedback", but it does require a coordinate transformation to convert the aircraft

motion from time dependency to range dependency. The nonlinear aircraft model has eight state variables, but only three variables are fed back for the tracker system employed here: h, h', and h''.

The simplifying assumptions made in the simulation are as follows:

1) The atmospheric density, ρ, and the speed of sound are constant,

2) The center-of-gravity of the aircraft does not change during the flight segment, and

3) Perfect navigation data on the aircraft state are available.

The particular aircraft data used for the simulation are for the F-4C, and the model is made as accurate as possible for the data available [12]. The simulation model incorporates a stability augmentation system (SAS) and a linear model of the control-surface actuator. A limiter is included to prevent the commands from driving the control surface past its physical stops, which allow a total stabilator rotation of 28°. The aerodynamic moment and forces are computed as linear combinations of the state variables, with the stability derivatives as coefficients; however, the nonlinear dynamic equations for aircraft motion are used. This provides a more accurate aircraft model than the completely linearized one frequently used to investigate aircraft control systems. The aircraft equations of motion and data are given in Appendix G. The nominal flight speed for all runs is Mach 0.8 at sea level (894 fps).

The spatial frequency content of the input signals to the tracker are determined strictly by the character of the optimal path. The curvature and kink limits, the control point spacing, and the terrain data affect the frequency content of the optimal path. Therefore, the set of tracker gains that minimizes the tracking errors is dependent upon the framing structure as well as the terrain. It is possible to change the gains in the tracker based upon the particular framing structure selected and upon the anticipated terrain roughness; however, a set of fixed gains worked well for all of the framing structures tested in this simulation.

The gain values used in the tracking simulation are approximately those obtained by a simple gradient parameter search [27] to minimize the sum of the squares of the tracking errors in each channel. Various test curvature control-profile functions were used as input signals to the tracker system in the process of adjusting the gains. The resulting gains are only appropriate for the particular aircraft system that is simulated here.

For two sets of gains, Table 7-1 lists the performance data for tracking an optimal path with a fairly oscillatory control curvature. The path is the one shown in Figure 6-9 with the 1000-ft control interval (Framing Structure 14 of Table 6-3). The first set of gains was chosen after a few trials based on the estimates of what would be appropriate if the aircraft behaved as a third order linear system. The second set is the result of the gradient search optimization that started from Set 1 values. Although the improvement in

Table 7-1 Tracker Gains & Performance

(Based on 241 Sample Points at 200 ft Intervals)

GAINS:		Set 1	Set 2
G_0		5.0	5.0
G_1		1.0	2.0
G_2		0.4	0.8
TRACKING ERRORS:			
Δh	max	+18.84 ft	+11.46 ft
	min	-19.08	-11.70
	RMS	9.21	6.50
Δs	max	+.02649 (+1.5°)	+.01268 (+0.7°)
	min	-.02828 (-1.6°)	-.01151 (-0.6°)
	RMS	.01143 (0.6°)	.00535 (0.3°)
Δk	max	$+.9782 \times 10^{-4} ft^{-1}$ (2.45 G)	$+.2053 \times 10^{-4} ft^{-1}$ (0.51 G)
	min	-.6932 (-1.75 G)	-.2409 (-0.60 G)
	RMS	.1877 (0.46 G)	.0800 (0.20 G)
ACCELERATIONS:		Optimal Path Values	
$a_{N_{pilot}}$	max	+2.00 G's	+2.11 G's	+1.94 G's
	min	-1.00	-1.49	-1.08
	RMS		1.01	0.93

performance obtained by the tracking optimization is not large, it is significant enough to add confidence in the use of the improved gain set.

The performance using Gain Set 2 for a variety of optimal-trajectory inputs is illustrated by the remaining figures in this chapter and the data are summarized in Table 7-2. Shown in each figure are four plots: first, the altitude or height error, then three comparisons of the optimal and aircraft path data--the heights, slopes, and curvatures. These plots indicate the error behavior in each of the three tracking channels. A soft-ride trajectory is shown in Figure 7-3, while Figures 7-4, 7-5 and 7-6 show hard-ride runs with basic control intervals of 2000, 1000 and 500 feet, respectively. These runs use framing Structures 11, 13, 14 and 15 (Table 6-3).

In Table 7-2, the minimum height error appears insensitive to variations in the jerk limits. However, the maximum and RMS height errors show a trend toward increasing errors with increasing jerk. The run with the finest control-point spacing appears to be an exception to this trend, but it is based on fewer sample points over a portion of the terrain that appears to cause smaller tracking errors, as can be observed from Figures 7-3 through 7-6. All other tracking errors follow the same trend. Furthermore, vehicle fuel economy and pilot ride comfort vary inversely with jerk and RMS acceleration. Therefore, it is desirable to keep the jerk and acceleration as low as possible, but restriction of this maneuvering capability also increases the RMS excess clearance for the flight, as indicated by

Table 7-2 Tracker Performance Data

(Based on 241 Sample Points at 200 ft Intervals)

Type of Ride	Soft	Hard		
OPTIMAL PATH PARAMETERS:				
Control Interval (ft)	2000	2000	1000	500
RMS Excess Clearance (ft)	233	91	86	81
LIMITS:				
max acceleration (G's)	+2.00	+2.00		
min acceleration (G's)	-0.25	-1.00		
inherent jerk(G's/sec)	±1.00	±1.33	±2.66	±5.33
TRACKING ERRORS:				
Δk max (ft)	+ 4.70	+ 9.94	+11.46	+ 7.32*
Δk min (ft)	-12.04	-11.84	-11.70	-10.32*
Δk RMS (ft)	3.14	5.98	6.50	5.04*
Δs max	+.00897 (+.5°)	+.01079 (+.6°)	+.01268 (+.7°)	+.01229*(+.7°)
Δs min	-.00837 (-.5°)	-.01091 (-.6°)	-.01151 (-.7°)	-.01304*(-.8°)
Δs RMS	.00238 (.1°)	.00442 (.3°)	.00535 (.3°)	.00695*(.4°)
Δk max ($ft^{-1}x10^5$)	+1.236 (+.31 G)	+1.508 (+.37 G)	+2.053 (+.51 G)	+2.546*(+.63 G)
Δk min ($ft^{-1}x10^5$)	-0.690 (-.17 G)	-1.260 (-.31 G)	-2.409 (-.60 G)	-3.963*(-.98 G)
Δk RMS ($ft^{-1}x10^5$)	.277 (.07 G)	.522 (.13 G)	.800 (.20 G)	1.502*(.37 G)
ACCELERATIONS:				
$a_{N_{pilot}}$ max (G's)	+1.94	+1.82	+1.94	+1.93*
$a_{N_{pilot}}$ min (G's)	-0.33	-1.03	-1.08	-1.07*
$a_{N_{pilot}}$ RMS (G's)	0.42	0.82	0.93	0.98*

* Based on 91 Sample Points.

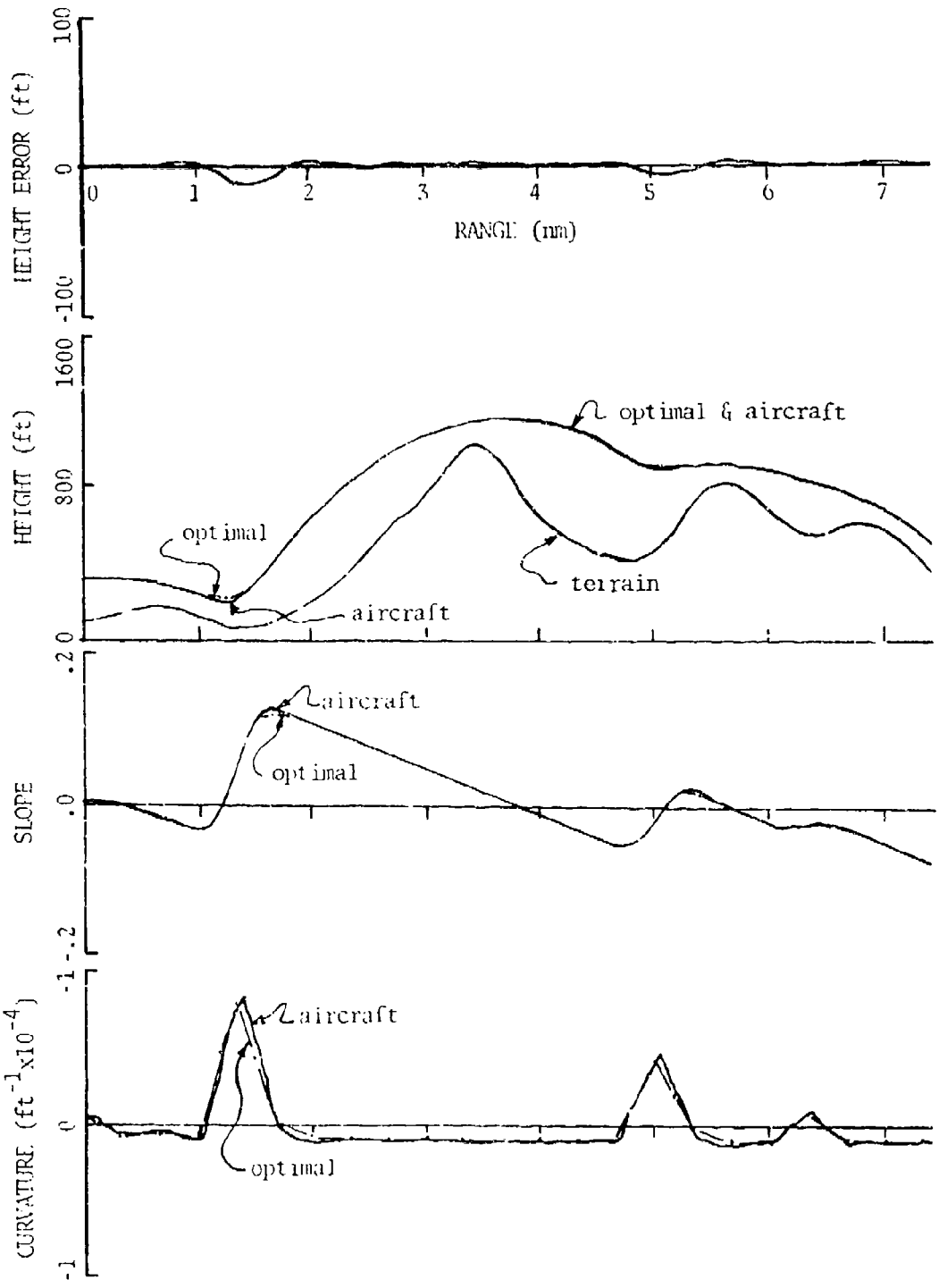

Figure 7-3 Soft-Ride Tracker Performance with 2000-ft Control Interval

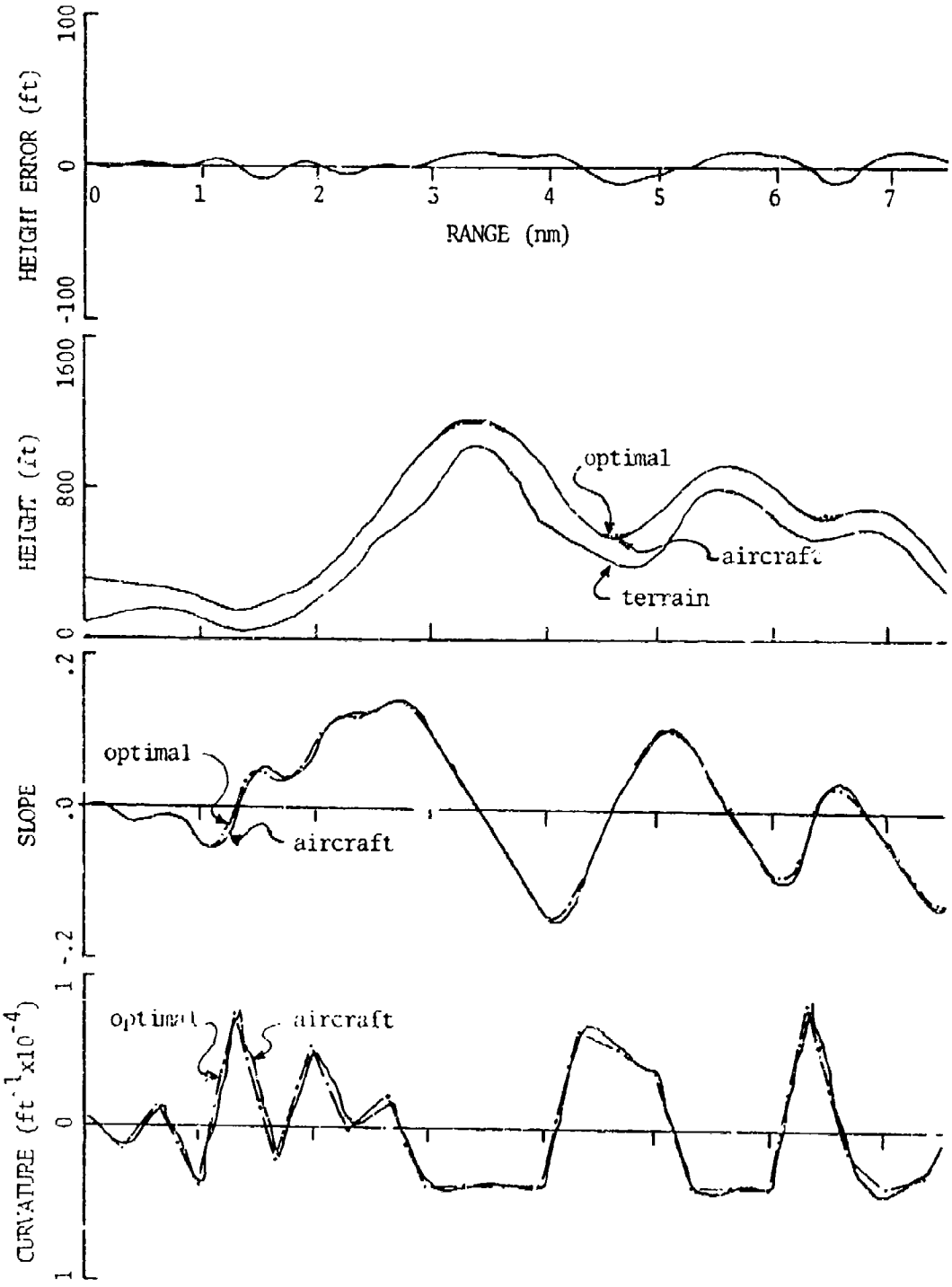

Figure 7-4 Hard-Ride Tracker Performance with 2000-ft Control Interval

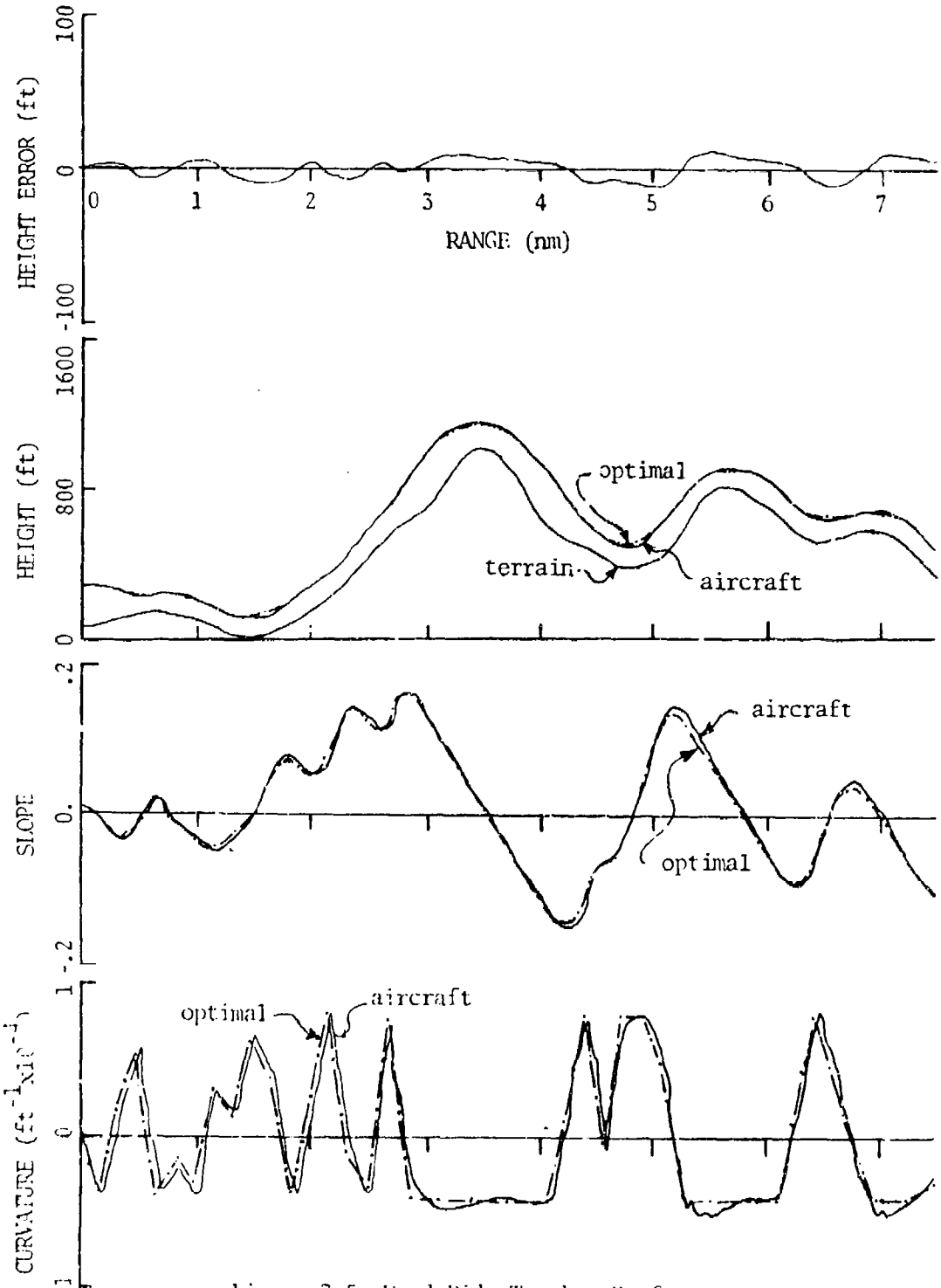

Figure 7-5 Hard-Ride Tracker Performance with 1000-ft Control Interval

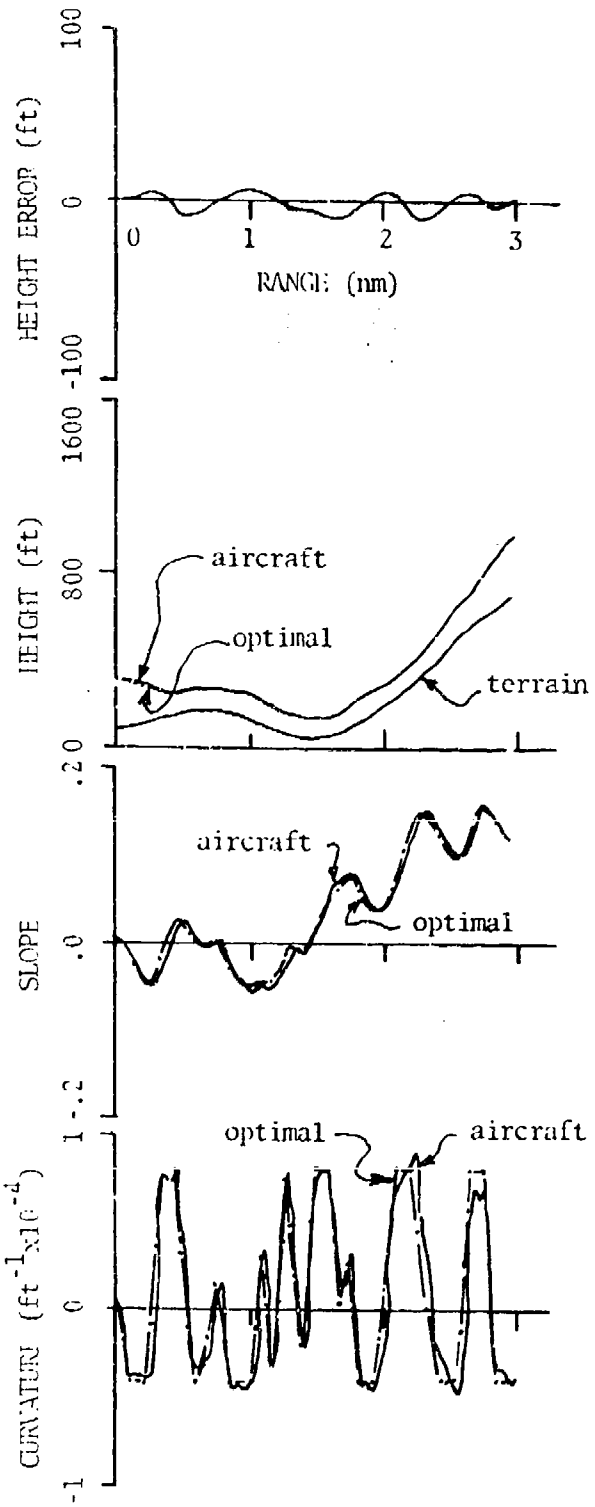

Figure 7-6 Hard-Ride Tracker Performance with 500-ft Control Interval

the values listed for the reference path in the table. Some compromise between the two effects is required.

The accelerations given in Table 7-2 are those measured at the pilots station. Since the pitch rates are small, there is little difference between those and the normal accelerations at the aircraft center-of-gravity. The objectives for this controller are to control very closely the extremes of the normal acceleration and the terrain clearance. The simulation results presented here indicate that this is done extremely well.

8. REAL TIME AIRBORNE APPLICATIONS

The overlapping frame process described in Chapter 4 was designed for real time airborne application, as illustrated in Figure 8-1. Three successive overlapping frames of terrain data

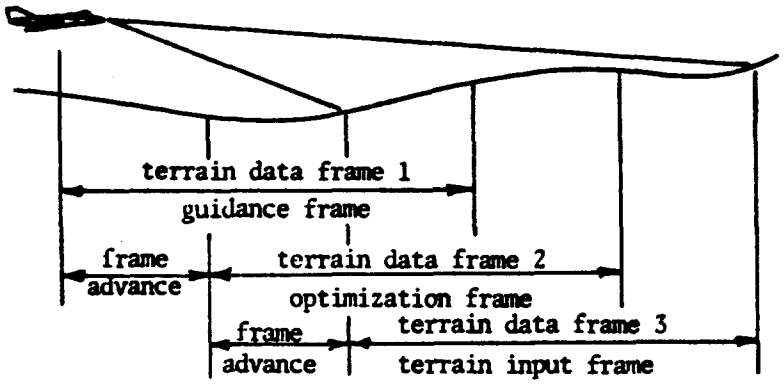

Figure 8-1 Real Time Framing

are depicted in the figure for a particular time, t. The time interval allowed for the optimization processing of one frame is Δt. Frame 1 contains information that is based on terrain data that was input to the system two time intervals earlier, at $t-2\Delta t$. The path optimizer began processing this terrain information one time interval earlier, at $t-\Delta t$. The optimal path solution that was computed is currently being used in the tracker system for guidance of the aircraft. Also, at time t, the Frame-2 terrain data is being processed by the optimization routine; it was input to the system one time interval earlier, at $t-\Delta t$. The terrain data in Frame 3 is currently being input and stored in the processing system. The terrain data can

be provided by a forward-looking radar, or it can be obtained from stored terrain map data if the aircraft position relative to the map is known.

During the time corresponding to each of the frame advance intervals, a complete optimization problem is solved, and a new set of terrain data is stored. These two distinct information processes can be done simultaneously, or on a time-shared basis, depending upon the processor structure available. The assumption that separate processors are available for the two tasks is made here. The process with the longer duration (probably the optimization) determines the maximum frame advance distance that can be used in real time.

If computation time were not a factor, computational errors could be maintained at a negligible level compared to the errors introduced into the system by the terrain and navigational sensors. However, in real time applications, the computational time is severely restricted, and the particular framing structure is the key to computational time and computational accuracy. There generally must be a trade off between computational time and accuracy. The framing structure described in Section 4.6 allows a great variety of combinations and trade offs. As previous results indicate, the computational time increases extremely rapidly with the increase in the dimension of the optimization problem. Since the performance is measured and the constraints are enforced at various sample points, the dimension of the problem is determined by the number of sample points, which depends upon both the frame length and various sample intervals. It

is desirable to reduce the number of sample points as much as possible, to minimize both the computational time and storage. The factors involved in this reduction are discussed below.

8.1 Total Number of Sample Points

From the various parametric studies discussed in previous chapters, the following conclusions can be drawn with respect to reducing the total number of sample points:

1) Slope constraints should not be applied unless there is a strong reason for limiting the flight path angle. Many flat and moderate terrains will not require slope limits, because the limits would not be normally encountered. If required, they can be sampled more coarsely than the clearance constraints, since the slope changes are more gradual.

2) The min-max criterion requires more constraints, in the form of upper bounds on the clearance distance, and should not generally be applied.

3) The linear programming problem may not require as large an optimization problem as the quadratic programming problem, so the linear performance criteria is recommended. Theoretically, the solution may not be unique for this problem--there may be more than one set of control points that give the same optimal performance measure, but any of these would be acceptable, or equally "close" to the terrain. Therefore, no effort is made to study non-uniqueness here.

4) The spacing of the clearance constraint points must be as fine as the finest control point spacing to prevent constraint

violations between constraint points from becoming significant. A similar argument can be given in regard to clearance constraint point spacing vs. terrain point spacing. The terrain and clearance curve intervals are assumed to be equal, and if the clearance-constraint interval is not at least as fine as the sample interval of the clearance curve, more extreme curvatures of the clearance curve can create significant violations between constraint points. The maximum constraint violation that can occur between sample points is approximately

$$c_v \approx \frac{1}{8} \Delta k \ (\Delta R)^2 \qquad (8\text{-}1)$$

where Δk is the difference in curvature between the two curves being considered, and ΔR is the constraint range interval. (The approximation is derived in Appendix H, based on constant curvature for each curve over the interval of violation).

5) Trade offs between ride-softness and specified minimum-clearance distance may be required to keep the problem dimension down. The more restrictive curvature limits of the softer ride require a longer frame length to predict clearance of the same height obstacle. Longer frames generally require more sample points of all kinds--unless the sample intervals are increased. But increasing the interval length increases the likelihood of constraint violations between sample points. A small percentage of violation will be much more acceptable for a high clearance trajectory than for a low clearance trajectory.

6) The feasibility of a real time scheme is dependent upon the aircraft performance: the speed, acceleration and slope limits. For example, a missile flying at Mach 2.5 at sea level (2792 fps) with acceleration limits of -1 and +3 G's would require curvature limits of +.000012 and -.000004 ft^{-1}. This would correspond to a characteristic frame length estimate of 54,900 feet (for the 1000 ft obstacle used previously). This long frame length would require a high dimensional optimization problem for realistic sample point intervals (probably about 500 ft for the terrain and clearance data). However, if the acceleration limits are changed to -5 and +15 G's, with all other data the same, the new estimate for frame length would be only 24,600 feet since the vehicle would be much more maneuverable.

8.2 Computational Requirements

Some conclusions can be drawn from the computational requirements of the test programs run on the CDC 6600 computer, but it is extremely difficult to compare these results directly with airborne computer requirements for the following reasons:

1) The test program has many optional features used in the parametric studies that would probably not be included in an operational program. Also, precomputation of many of the matrices used prior to flight could reduce significantly the inflight computation.

2) A direct linear programming algorithm would probably be used rather than the complementary problem, which requires more storage and probably more time.

3) The word length and processor structure of the airborne computer would be different, so equivalent programs might run at

different speeds on the two computers.

4) Input and output devices would be significantly different for the two computer systems. This would have a significant effect on the computational times. However, the use of central processor times tends to minimize this effect.

With the first two items above tending to offset any increases in the requirements due to the second two, the CDC 6600 execution times are some indication of the feasibility of this optimal-path-spline terrain-following scheme.

8.3 Evaluation of the Framing Structure for an Example Missile

It is difficult to draw any conclusions about the real time feasibility of the optimal-path scheme unless a particular frame structure is specified. The most rigorous test of the scheme is an extremely high speed vehicle, since the system must process the terrain data most rapidly. Therefore, the case of a very high-speed missile is considered, with a few variations in the framing structure. If the real time scheme is feasible for this missile it should certainly be feasible for slower vehicles. The test missile is the example mentioned in Section 8.1 and travels at Mach 2.5. The most difficult framing structure for processing corresponds to very restricted maneuverability of the missile, such as, soft-ride acceleration limits of -1 and +3 G's. Since the optimization problem must be limited, a frame length slightly shorter than the characteristic length of 54,900 feet is selected. A 2000-ft control interval is used, which is considerably longer than the characteristic interval

of 324 feet. Even with the longer control interval, the 50,000-ft frame length, with 25 equally spaced control points and 50-point clearance constraints, produces a complementary problem of dimension 100. The complete set of framing parameters is listed in Table 8-1 as Structure 18. The corresponding optimal path and curvature are shown in Figure 8-2. The performance appears to be good despite the restrictions placed on the framing structure and maneuverability. The computational times and performance data for the run are listed in Table 8-2. The "allowable" frame time is that which is required for the optimization processing to handle the terrain data as rapidly as the vehicle traverses the terrain. It is computed by dividing the frame advance distance by the nominal vehicle speed.

The RMS and maximum excess clearance values in the table for Structure 18 are rather high because of the acceleration limits. Therefore, the more maneuverable cases of Structures 19 and 20 are considered. The framing structures are listed in Table 8-1, while the performance data is in Table 8-2. The RMS and maximum excess clearance values are reduced substantially for both of the more maneuverable cases. The slightly longer frame length of Structure 19 shows an improvement in excess clearance over that for Structure 20; this can also be seen in the plot of the paths shown in Figure 8-3. However, the shorter advance distance for Structure 19 is borderline for real time application. The first frame takes slightly more computational time than the allowable frame time. The first frame always requires more time than the others during a run, because of

Table 8-1 Framing Structures for Missile Paths

Structure Number	Dim.	18	19	20	21
Type of Terrain		Moderately Rough σ_T= 364 ft			Smooth σ_T=137 ft
Type of Ride		Soft	Hard		
Expected Obstacle Ht.	ft	1000			500
Charact. Frame Length	K-ft	54.9	24.6	24.6	17.4
Frame Length	K-ft	50	26	24	24
Frame Advance	K-ft	24	14	16	12
LIMITS: Curvature	$ft^{-1}x10^{-4}$	+.12 -.04	+.6 -.2	+.6 -.2	+.6 -.2
Acceleration*	G's	+3 -1	+15 - 5	+15 - 5	+15 - 5
Kink**	$ft^{-2}x10^{-8}$	±.80	±8.0	±8.0	±4.0
Jerk*	G's/sec	±5.4	±54.1	±54.1	±27.0
Nr. of Control Pts.		25	26	24	12
Complem. Prob. Dim.		100	78	72	36
SAMPLE INTERVALS: Characteristic	K-ft	.324	1.444	1.444	1.022
Curvature		2	1	1	2
Performance Meas.		1	1	1	2
Clearance Const.		1	1	1	2
Terrain Data		2	2	2	2
PERFORMANCE COEFFS: C_L		0	0	0	0
C_Q		.1	.1	.1	.1
C_M		0	0	0	0
Figure Number		8-2	8-3	8-3	8-4

* For V = 2792 fps

** Inherent limits from Δ, k_{min} and k_{max}

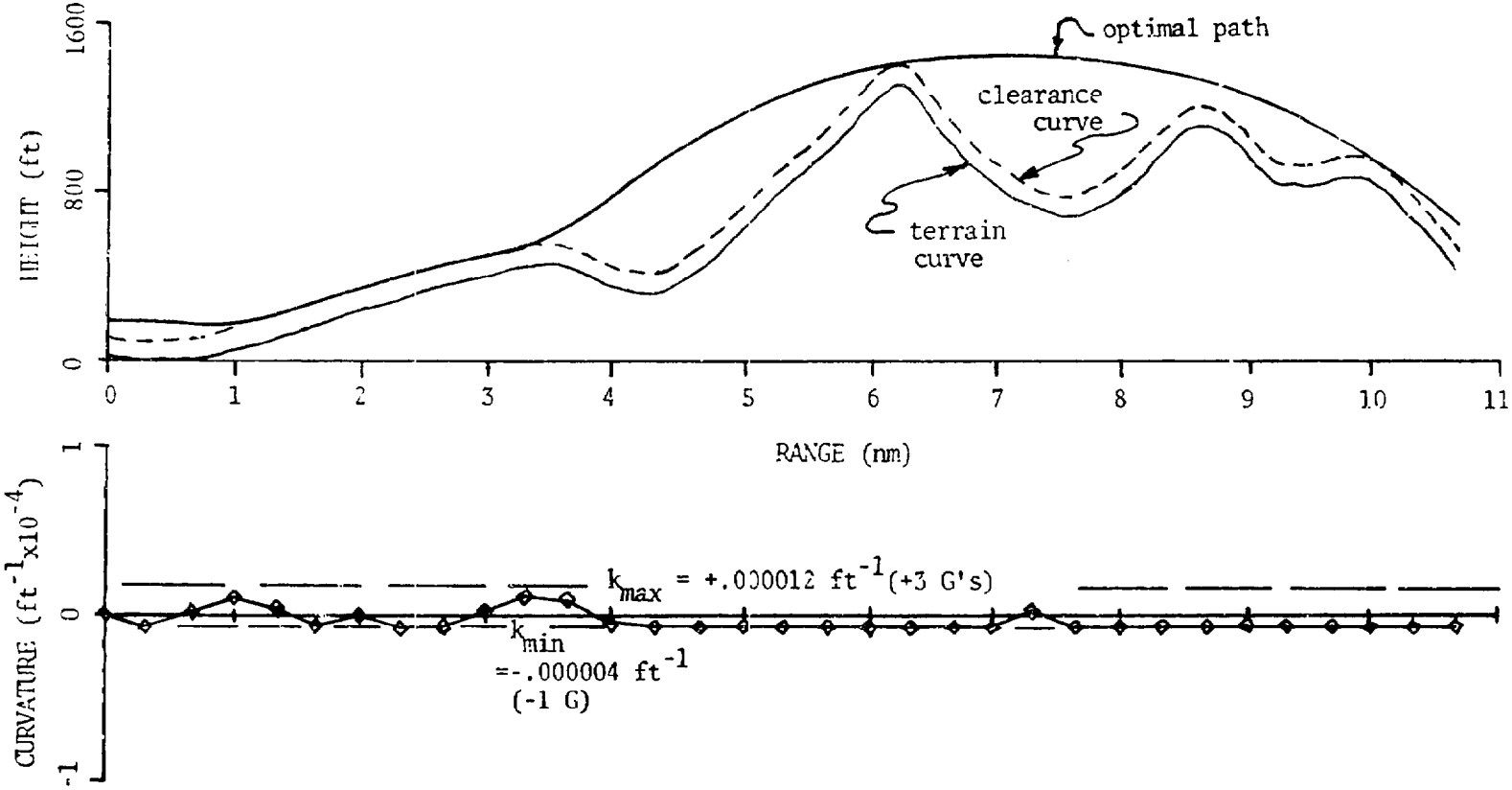

Figure 8-2 Example Missile Optimal Path for Soft-Ride

Table 8-2 Missile Reference Path Performance & Computational Times

Structure Number	18	19	20	21
Type of Terrain	Moderately Rough			Smooth
Type of Ride	Soft	Hard		
Frame Length (K-ft)	50	26	24	24
Frame Advance (K-ft)	24	14	16	12
Complem. Problem Dim.	100	78	72	36
Allowable Frame Time (sec)	8.6	5.0	5.7	4.3
COMPUTATIONAL TIMES: (Per Frame)				
Max	6.3	5.5	4.5	0.69
Min (sec)	1.3	3.4	2.4	0.46
Average	3.8	4.3	3.2	0.53
Number of Frames	2	4	4	27
EXCESS CLEARANCE HEIGHTS:	(For 321 Sample Points at Δ = 200 ft)			(226 Pts. Δ=1200 ft.)
e_{max}	664	313	384	52
e_{min} (ft)	-7	-8	-8	-6
e_{RMS}	292	105	121	9
Figure Number	8-2	8-3	8-3	8-4

the initialization of some of the matrices in the computer routine used. There is no reason that the matrices could not be initialized in flight prior to real time operation, to overcome this problem.

The short time for the second frame of Structure 18 appears to be just very fortuitous, as can be seen by comparison with the minimum times of the smaller dimensional problems. One more framing

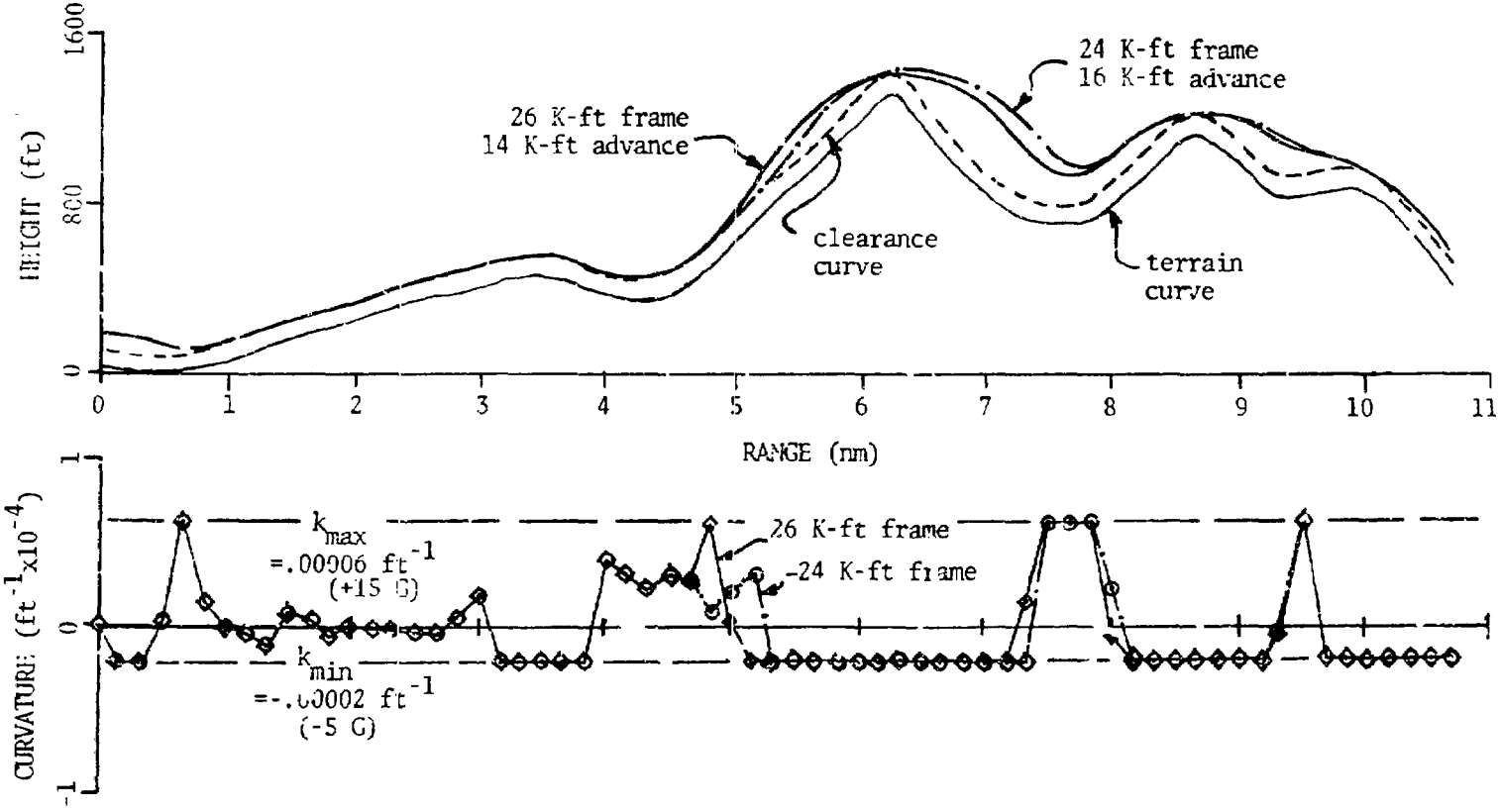

Figure 8-3 Example Missile Optimal Path for Hard-Ride

structure is considered for a flight over a different terrain segment. This second terrain is classified as smooth terrain, since it has a standard deviation of σ_T = 137 feet (compared to the σ_T = 364 feet of the previous terrain). Structure 21 of Table 8-1 is used in an effort to reduce the problem dimension without sacrificing performance. Both the frame length and the control interval selected are considerably greater than the corresponding characteristic values. The net result is a reduction by a factor of one-half in the complementary problem dimension, while the computational time reduction is considerably more than one-half, as indicated in Table 8-2. The performance over the smooth terrain is excellent, as illustrated in Figure 8-4, where the optimal path does not differ essentially from the minimum-clearance curve except in a few short regions. The expected obstacle heights are based on approximate peak heights of the terrain segments, but ll values of $3\sigma_T$ would be fairly good estimates, as can be observed from the values in Table 8-1.

Although some sacrifice in following the terrain closely may be required in some missions, the path optimization scheme appears to be quite feasible and flexible for real time applications.

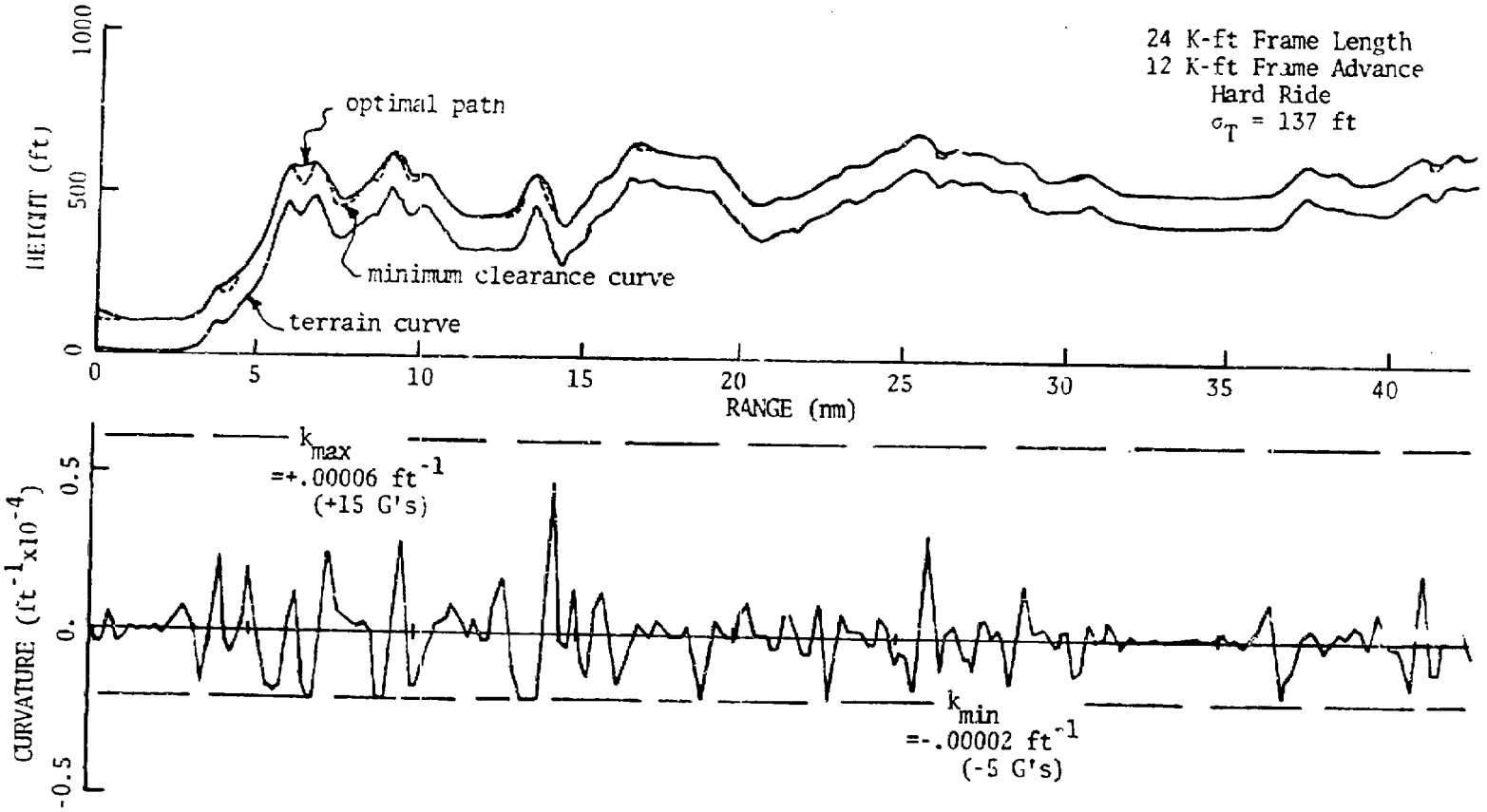

Figure 8-4 Example Missile Optimal Path for Smooth Terrain

9. CONCLUSIONS AND RECOMMENDATIONS

The concept of including an optimal path determination scheme into a terrain follower appears to be quite feasible in a modern, computer-equipped aircraft. It also offers a good deal of flexibility as a programmable control system. These conclusions are based on the following discussions of the various facets of the problem.

9.1 Splines and Clearance Paths

Although it is possible to treat both the terrain data and reference clearance path data as sets of discrete points, computational flexibility and more realistic path representations can be obtained through the use of cubic splines. The computation sample interval need not be restricted to the terrain data intervals if splines are used for interpolation between data points. The amount of computation required to interpolate between data points is a very small part of the overall computational requirements. Interpolation between data points also provides a basis for calculation of slant-clearance-distance paths, for which the nearest distance between the clearance and terrain curves is equal to the specified clearance value. This calculation gives a more accurate clearance than measuring a clearance path with the vertical distance equal to the specified clearance value; however, the slant procedure is more precise than usually needed. It was found that for typical terrain segments a simple estimate of points on the slant clearance path provided a good reference clearance path.

The estimate at any point is based on the local height, slope, and curvature of the terrain-spline curve.

9.2 Optimal Path Computations

The computation of the optimal path by either quadratic or linear programming algorithms is far superior to general optimization algorithms using penalty functions, primarily on the basis of computational time. The solution trajectories themselves agree fairly well, but the penalty function solutions have clearance constraint violations near terrain peaks. Although three types of performance criteria were analyzed: linear, quadratic, and min-max; the trajectories tend to be very constraint bound and rather insensitive to the particular performance measure. Piecing various constrained arcs together with appropriate transition arcs is the primary task of the optimization routine. If the programming problems were always feasible, the simplest performance criterion would be the most appropriate; the linear criterion and its resulting linear programming problem might have smaller computational requirements than the other performance measures. A revised simplex algorithm [14] would be a candidate for solving the linear problem, but Shankland's algorithm [29] which handles infeasibilities in the quadratic programming problem appears to be the most promising algorithm considered.

The data frame length must be chosen to give adequate predictive capability to the scheme. The frame length derived from the Characteristic Maneuver, which is based on a specified-obstacle-height and the aircraft acceleration limits, is a good estimate of "ideal" frame length for all of the cases considered here.

A great flexibility is possible in the selection of control point spacings and the various sample intervals used for performance measure and constraint satisfaction. Larger intervals yield smaller computational requirements, both in time and memory storage, but this is at the cost of theoretical optimal performance and accuracy. The control function suffers from lack of flexibility if the control point spacing is large, and the corresponding trajectory will have a higher RMS clearance value than would one with finer control-point spacing. However, if the control points are too closely spaced, ride comfort for the pilot will decrease, while tracking errors and fuel consumption will increase as the aircraft attempts to follow the computed optimal path. Also, greater overshoots of the desired acceleration limits will occur, along with the path overshoots. The number of control points and, hence, the computational requirements, can be reduced through a graduated control point spacing, where the near-frame (close to the aircraft) spacing is fine for control flexibility and the far frame spacing is coarse to predict gross positional changes that may be required. The final determination would depend upon the particular mission considered.

9.3 Tracker System Performance

The validation of the optimal path scheme required a realistic aircraft simulation and a candidate tracker system model. Since the optimal path was designed to provide a "trackable" path, an optimal tracker system was not considered necessary, rather, a simple feedback tracker system was tested. The tracker used inertial

path information plus two derivatives that were available from the optimal path solutions of data frames with appropriate framing structure. The tracker performed extremely well, with approximately a 6-ft RMS tracking error and a maximum tracking error of 12 feet, over a moderately rough terrain under hard-ride conditions (-1, +2 G's). This corresponded to errors of less than 12% of the specified minimum-clearance of 100 feet.

9.4 Overall System Performance

The overall performance of the system depends primarily upon how accurately the terrain data and the aircraft's position relative to the terrain can be determined. The choice of framing structure affects the sense of optimality in determining the optimal reference trajectory. A variety of possible trade offs are possible in an operational system--trade offs between closeness to the terrain and computational requirements. Performance can be adjusted, depending upon the particular aircraft and mission, by changing parameter values in the digital computer. Thus, the system is very flexible.

The overall system was compared to that of Greaves [11], since that system is the most advanced to date. All of the approaches discussed by Greaves compute slopes and accelerations of the "ideal" paths using difference equations. These correspond to parabolic path segments that will not necessarily be joined in a desirable way; i.e., they will not form a quadratic spline and they may be disjoint. (Whereas, the cubic spline approach produces slopes and accelerations for a smooth continuous path). Therefore,

the Greaves path may not be one that the aircraft can fly, and the system would require a very good (optimal) tracking system. Furthermore, the acceleration profiles of the optimal paths with the Greaves' method tend to be more bang-gang in character, since there are no transition arcs between maximum pullup and pushover arcs. This also makes his "ideal" path more difficult to track. The additional structure of the optimal spline paths provides sufficient predictive information for a very simple feedback tracker system, which can be optimized by gain selection for a truly nonlinear aircraft system, rather than through the use of linear approximations.

The sense of optimality of the two systems differs somewhat: the sense of Greaves system is rather obscure although it emphasizes the clearances near high terrain areas, while the spline-path system minimizes a weighted average clearance measure, where the weights can be directly adjusted in the computer program. Both systems have a tendency to make paths nearly horizontal at the peaks, but no strong reason for requiring it was observed. Conceptually, it is possible to add that constraint to either system, if necessary.

Although the system proposed by Greaves appears to be somewhat simpler in path processing, it is more complex in the tracking system. The approach of the optimal-spline-path system is a more unified approach for the overall system.

9.5 Recommendations

1) Further studies of the optimal-spline-path terrain following system should be made to select the best programming algorithm.

These studies might also include the effects of radar shadowing, in which the terrain data that is input to the optimization processor is limited to that available on a direct line of sight. The optimization algorithm does not change, but the data that it must use is modified from the true terrain values. Thus, the probability of infeasible programming problems increases.

2) The optimal path generator can be used as a design aid to provide rapid generation of standard reference trajectories for any desired terrain segment. These standards can be used to evaluate proposed controllers and modifications to those controllers.

3) The optimal reference trajectories can be used for frequency analysis to determine what frequency spectra the flight control system must be capable of handling during terrain following. The path optimization processor acts as a low-pass filter to attenuate the amplitudes of any high frequency terrain components. The frequency spectrum of the processed path is what the flight control system must be capable of handling. The framing structure used in determining the reference path will affect the frequency content of the path. The characteristics of an existing flight-control system can be used to determine a compatible frame structure for the terrain following controller, or from desired flight profiles, the framing structure and corresponding flight-control system requirements can be developed.

4) The concepts of the optimal-path follower can be extended to terrain avoidance. If only lateral motion is involved in the

terrain avoidance mode (with an altitude hold), the extension merely involves a transfer of the problem from the vertical plane to a horizontal plane. The performance measure would be referenced to a navigation path, valley, or ridge line that the vehicle is attempting to follow. If a combination of terrain-avoidance and terrain-following is desired, the optimization problem will, at least, double in size. Furthermore, linearization of the coupling effects between lateral and vertical motion relative to the terrain must be employed.

5) The spline-tracker concept discussed in Chapter 7 has broader applications than merely to that of an optimal-path follower. A reference spline path can be generated in a great variety of ways. For example, the spline path could be a navigation track passing through specified "way points." In that case, the lateral flight control system would track the navigation path, which would be defined by a fairly small set of discrete values, and yet represent a very smooth path. A great variety of maneuvers could be accomplished in a similar manner by merely specifying certain points on a three-dimensional path as guidance parameters. The control system would then track a bi-variant spline fit through the points. Techniques of this type would be quite useful in digital command-guidance systems.

APPENDIX A

OPTIMIZATION PROBLEM EQUATION DERIVATIONS

The first part of this Appendix contains a derivation of the equations for the path state variables as affine functions of the curvature-control-point values. Then, the cost gradients with respect to the control-point values are derived. (The gradients are used only in the general optimization routine.) From the path state relationships, the equations for the quadratic programming problem and the corresponding complementary problem are derived.

A.1 Path State Equations

The path state variables, as described by differential equations, are the path height h and the slope s, while the independent variable is range R, and the control function is the curvature k. The h, s, and k variables for the cubic spline path are functions of the set of discrete control values k_n.

$$h'(R;k_n) \equiv \frac{dh}{dR}(R;k_n) = s(R;k_n) \tag{A-1}$$

$$s'(R;k_n) \equiv \frac{ds}{dR}(R;k_n) = k(R;k_n) \tag{A-2}$$

$$k(R;k_n) = (1-\sigma)k_i + \sigma k_{i+1} = k_i + \sigma(k_{i+1} - k_i) \tag{A-3}$$

for $R \in [R_i, R_{i+1}]$, where the "normalized" range increment is

$$\sigma \equiv \frac{R-R_i}{R_{i+1}-R_i} \tag{A-4}$$

over the control interval

$$\Delta_i \equiv R_{i+1}-R_i \tag{A-5}$$

The kink, p, can also be considered as a state variable, but it is defined directly as a function of the control set k_n.

$$p_i = \frac{1}{\Delta_i} (k_{i+1}-k_i) \tag{A-6}$$

One can convert the two differential equation relationships into simple functions of the k_n by integration. Note that on the horizontal range interval Δ_i,

$$d\sigma = \frac{1}{\Delta_i} dR \tag{A-7}$$

When Eq. (A-3) is substituted into Eq. (A-2) and the resulting equation is integrated over the normalized interval $[0,\sigma]$, in terms of the dummy variable z, the result is

$$\begin{aligned} s(R) &= s(R_i) + \Delta_i \int_0^{\sigma} [k_i + z(k_{i+1}-k_i)]\, dz \\ &= s(R_i) + \Delta_i \left[k_i\sigma + \frac{1}{2} \Delta k_i \sigma^2\right] \end{aligned} \tag{A-8}$$

where

$$\Delta k_i \equiv k_{i+1}-k_i \tag{A-9}$$

At the end of the control interval, where $\sigma=1$,

$$s(R_{i+1}) = s(R_i) + \frac{\Delta_i}{2}(k_i+k_{i+1}) \tag{A-10}$$

Recursive use of this equation for i=0, 1, 2, ..., n yields

$$s(R_n) = s(R_0) + \frac{1}{2} \sum_{i=0}^{n-1} \Delta_i (k_i+k_{i+1}) \tag{A-11}$$

Thus for $R \in [R_n, R_{n+1}]$

$$s(R) = s(R_0) + \frac{1}{2} \sum_{i-0}^{n-1} \Delta_i (k_i+k_{i+1}) + \Delta_i [k_i\sigma + \frac{1}{2} \Delta k_i \sigma^2] \tag{A-12}$$

Similarly, the height equation can be integrated using Eq. (A-8)

$$h(R) = h(R_i) + \Delta_i \int_0^{\sigma} [s(R_i) + \Delta_i(k_i z + \frac{1}{2}\Delta k_i z^2)]dz$$

$$= h(R_i) + \Delta_i s(R_i)\sigma + \frac{\Delta_i^2}{2} k_i \sigma^2 + \frac{\Delta_i^2}{6}\Delta k_i \sigma^3 \qquad \text{(A-13)}$$

and for the full interval (σ=1)

$$h(R_{i+1}) = h(R_i) + \Delta_i s(R_i) + \frac{\Delta_i^2}{6}(2k_i + k_{i+1}) \qquad \text{(A-14)}$$

When Eqs. (A-14) and (A-10) are used recursively, for i=0, 1, 2, ..., n,

$$h(R_n) = h(R_0) + \sum_{m=0}^{n-1} \Delta_m [s(R_0) + \frac{1}{2} \sum_{i=0}^{m-1} \Delta_i (k_i + k_{i+1})]$$

$$+ \frac{1}{6} \sum_{i-0}^{n-1} \Delta_i^2 [2k_i + k_{i+1}]$$

$$= h(R_0) + (\sum_{m=0}^{n-1} \Delta_m)\, s(R_0) + \frac{1}{2} \sum_{m=0}^{n-1} \sum_{i=0}^{m-1} \Delta_m \Delta_i (k_i + k_{i+1})$$

$$+ \frac{1}{6} \sum_{i=0}^{n-1} \Delta^2{}_i [2k_i + k_{i+1}] \qquad \text{(A-15)}$$

The equation for $R\epsilon[R_n, R_{n+1}]$ is determined from Eqs. (A-13), (A-11) and (A-15)

$$h(R) = h(R_0) + (\sum_{m=0}^{n-1} \Delta_m) s(R_0) + \frac{1}{2} \sum_{m=0}^{n-1} \sum_{i=0}^{m-1} \Delta_m \Delta_i (k_i + k_{i+1})$$

$$+ \frac{1}{6} \sum_{i=0}^{n-1} \Delta_i^2 (2k_i + k_{i+1}) + \Delta_n s(R_0)\sigma + \frac{1}{2} \sum_{i=0}^{n-1} \Delta_n \Delta_i (k_i + k_{i+1})\sigma$$

$$+ \frac{1}{6} \Delta_i^2 [(3-\sigma)k_i + k_{i+1}\sigma]\sigma^2 \qquad \text{(A-16)}$$

Finally, the excess clearance distance at R is also a function of the set of k_i

$$e \equiv e(R;k_i) = h(R;k_i) - c(R) \tag{A-17}$$

Where c is the minimum-clearance curve height.

A.2 Cost Gradients

The cost function is

$$J = \sum_{n=1}^{N_p} (Q_n e_n^2 + L_n e_n + T P_n e_n^2) + m \tag{A-18}$$

where

$$T \equiv \begin{cases} 1 \text{ if } e_n < 0 \\ 0 \text{ if } e_n \geq 0 \end{cases} \tag{A-19}$$

and N_p is the total number of points in the performance sample set.

The partial derivative of e_n with respect to the i^{th} control point value, k_i, is

$$\frac{\partial e_n}{\partial k_i} = \frac{\partial h_n}{\partial k_i} \tag{A-20}$$

The cost gradient is

$$\frac{\partial J}{\partial k_i} = \sum_{n=1}^{N_p} \frac{\partial J}{\partial e_n} \frac{\partial e_n}{\partial k_i} = \sum_{n=1}^{N_p} \frac{\partial J}{\partial e_n} \frac{\partial h_n}{\partial k_i} \tag{A-21}$$

where

$$\frac{\partial J}{\partial e_n} = 2(Q_n + T P_n) e_n + L_n \tag{A-22}$$

When the partial derivatives of Eq. (A-15) are taken with respect to the k_i

$$\frac{\partial h_n}{\partial k_1} = \frac{\partial h(R_n,k_i)}{\partial k_i} = \begin{cases} 0 & \text{,for } R_n \epsilon [R_0, R_{i-1}) \\ \frac{\Delta_{i-1}^2}{6}\sigma^3 & \text{,for } R_n \epsilon [R_{i-1}, R_i) \\ \frac{\Delta_i^2}{6}[(\frac{\Delta_{i-1}}{\Delta_i}+\sigma)(\frac{\Delta_{i-1}}{\Delta_i}+2\sigma)+(1-\sigma)\sigma^2], & \\ & \text{,for } R_n \epsilon [R_i, R_{i+1}) \\ \frac{\Delta_i^2}{6}[(\frac{\Delta_{i-1}}{\Delta_i}+1)(3\frac{(R_n-R_{i+1})}{\Delta_i}+2+\frac{\Delta_{i-1}}{\Delta_i})] & \\ & \text{,for } R_n \epsilon [R_m, R_{m+1}) \end{cases} \quad \text{(A-23)}$$

where $m \geq i+1$.

A.3 Quadratic Programming Problem Equations

In the following development, two distinct types of indices will be used: sample point superscripts and control point subscripts. The sample points can be used for constraint enforcement as well as performance measurement. The control points are the specific points where curvature control values are selected. The state variable values at the control points can be generated recursively by Eqs. (A-10) and (A-14), while the sample point values are determined from the appropriate control point values by Eqs. (A-12) and (A-13). These equations lead to equations of the following forms.

$$h^n = \sum_{i=0}^{N_k} \alpha_i^n k_i + \gamma^n \quad \text{(A-24)}$$

$$s^n = \sum_{i=0}^{N_k} \beta_i^n k_i + \rho^n \quad \text{(A-25)}$$

$$h_m = \sum_{i=0}^{N_k} \alpha_{mi} k_i + \gamma_m \tag{A-26}$$

$$s_m = \sum_{i=0}^{N_k} \beta_{mi} k_i + \rho_m \tag{A-27}$$

By comparing the above four equations with Eqs. (A-8) and (A-13), one can obtain recursive relations for the coefficients that are functions only of incremental range from the last control point at R_m to the sample point at R^n, $\sigma^n = (R^n - R_m)/\Delta_m$.

$$\alpha_i^n = \alpha_{mi} + \Delta_m \sigma^n \beta_{mi} + \Delta_m^2 \frac{(\sigma^n)^2}{6} [(3-\sigma^n)\delta_{mi} + \sigma^n \delta_{(m+1)i}] \tag{A-28}$$

$$\gamma^n = \gamma_m + \Delta_m \sigma^n \rho_m \tag{A-29}$$

$$\beta_m^n = \beta_{mi} + \Delta_m [(\sigma^n - \frac{(\sigma^n)^2}{2})\delta_{mi} + \frac{(\sigma^n)^2}{2} \delta_{(m+1)i}] \tag{A-30}$$

$$\rho^n = \rho_m = s_0 \tag{A-31}$$

where δ is the Kronecker delta:

$$\delta_{mi} = \begin{cases} 0, & \text{for } m \neq i \\ 1, & \text{for } m = i \end{cases} \tag{A-32}$$

Now the inequality constraint equations can be developed, where the zero indices indicate specified initial condition values.

$$c^n = h^n - c^n = \sum_{j=1}^{N_k} \alpha_i^n k_i + \alpha_0^n k_0 + \gamma^n - c^n \geq 0 \tag{A-33}$$

or

$$-\sum_{i=1}^{N_k} \alpha_i^n k_i \leq \alpha_0^n k_0 + \gamma^n - c^n \tag{A-34}$$

Also, curvature constraints must be included:

$$k_i \leq k_{max} > 0 \quad , \text{for } i \varepsilon \P_k \tag{A-35}$$

$$k_i \geq k_{min} < 0 \quad , \text{for } i \varepsilon \P_k \tag{A-36}$$

$\P_k$ is the index set of the control points; similarly $\P_c$, $\P_s$, $\P_d$, $\P_m$, and $\P_p$ are the index sets of the sample points for constraints on minimum-clearance, climb slope, dive, and maximum-clearance (for min-max), and for the performance measure, respectively.

In terms of the control points, the climb constraints are

$$s^n = \sum_{i=1}^{N_k} \beta_i^n k_i + \beta_0^n k_0 + s_0 \leq s_{max} > 0 \quad , \text{for } n \varepsilon \P_s \tag{A-37}$$

and the dive constraints are

$$s^n \geq s_{min} < 0 \quad , \text{for } n \varepsilon \P_d \tag{A-38}$$

When the min-max criterion is used, the following additional constraints are imposed, where m is a parameter value to be determined by the optimization.

$$e_n \leq m \quad , \text{for } n \varepsilon \P_m \tag{A-39}$$

If direct kink constraints are imposed, they are

$$p_{min} \leq p_n \leq p_{max} \quad , \text{for } n \varepsilon \P_k \tag{A-40}$$

The equations for e, s and p can be written in the following vector-matrix form, with k an N_k-dimensional vector,

$$e = Ek + F \tag{A-41}$$

$$s = Sk + W \tag{A-42}$$

$$p = Pk \tag{A-43}$$

where, for $n \in \P_i$, (i=p,c or m); $\ell \in \P_j$, (j=s or d); and r, $q \in \P_k$

$$E_i = [\alpha_q^{\ n}] \quad \text{, an } N_i \text{ x } N_k \text{ matrix} \qquad \text{(A-44)}$$

$$S_i = [\beta_q^{\ \ell}] \quad \text{, an } N_j \text{ x } N_k \text{ matrix} \qquad \text{(A-45)}$$

$$F_i = \alpha_0^{\ n} k_0 + \gamma^n - c^n \quad \text{, an } N_i \text{ vector} \qquad \text{(A-46)}$$

$$W_i = \beta_0^{\ \ell} k_0 \quad \text{, an } N_j \text{ vector} \qquad \text{(A-47)}$$

$$P = [\eta_q^{\ r}] \quad \text{, an } N_k \text{ x } N_k \text{ matrix} \qquad \text{(A-48)}$$

The elements of P are

$$\eta_q^{\ r} = \frac{1}{\Delta q} (\delta_{(r-1)q} - \delta_{rq}) \qquad \text{(A-49)}$$

The following combined constraint equation (A-50) can be expanded to include the possibility of min-max upper-bound-clearance constraints.

$$C' K \leq D \qquad \text{(A-50)}$$

C is an $(N_k + 1_m)$ x $(N_c + N_m + 4N_k + N_s + N_d)$ matrix if $2N_k$ kink constraints are enforced and D is an $(N_c + N_m + 4N_k + N_s + N_d)$ vector. In partitioned form the equation is

$$\begin{bmatrix} E_m & -1_m \\ -E_c & 0 \\ I_k & 0 \\ -I_k & 0 \\ -S_d & 0 \\ S_s & 0 \\ P & 0 \\ -P & 0 \end{bmatrix} \begin{bmatrix} K \\ m \end{bmatrix} \leq \begin{bmatrix} -F_m \\ F_c \\ 1_k\, k_{max} \\ -1_k\, k_{min} \\ -1_d\, S_{min} + W_d \\ 1_s\, S_{max} - W_s \\ 1_k\, p_{max} \\ 1_k\, p_{min} \end{bmatrix} \qquad \text{(A-51)}$$

where $l_m = 1$ if $N_m \neq 0$, otherwise $l_m = 0$; and $\underline{1}_i$ is an N_i vector with unit elements, while I_i is an indentity matrix of dimension N_i.

Similarly the performance function can be written in matrix form, where $\bar{Q}$ is a diagonal matrix with the Q_n values as the diagonal elements. (If all the Q_n are equal $\bar{Q}$ can be considered a scalar). The e and $\bar{L}$ are vectors with e_n and L_n as elements, for $n \epsilon \P_p$.

$$J = \frac{1}{2} \; e'\bar{Q}e + \bar{L}'e + m \tag{A-52}$$

The form of Eq. (A-41) can be substituted for e into Eq. (A-52).

$$J = \frac{1}{2} \; K'E'\bar{Q}EK + [F'\bar{Q} + \bar{L}']EK + m + \frac{1}{2} \; F'\bar{Q}F + \bar{L}'F \tag{A-53}$$

The last two terms are invariant with respect to the parameters K and m, so the set of K and m values that minimize J also maximize P.

$$\begin{aligned} P &= -\frac{1}{2} \; K'E'\bar{Q}EK - [F'\bar{Q}+\bar{L}']EK - m \\ &= -\frac{1}{2} \; K'BK + A' - m \end{aligned} \tag{A-54}$$

where

$$B = E'\bar{Q}E \tag{A-55}$$

$$A = -[F'\bar{Q} + \bar{L}'] \tag{A-56}$$

A.4 Complementary Problem Equations

The non-negativity constraints on the variables in the Lemke formulation of the complementary problem require a "biased" control parameter set of the form in Eq. (A-57)

$$x_i \equiv k_i - k_{min} \geq 0 \qquad i \epsilon \P_k \tag{A-57}$$

Thus, the excess clearance vector for the performance measure sample set, $\P_p$, is N_p dimensional:

$$\begin{aligned} e_p &= E_p K + F_p = E_p(x+\underline{1}_k \, k_{min}) + F_p \\ &= E_p x + D_p \end{aligned} \tag{A-58}$$

where

$$D_p \equiv E_p \underline{1}_k k_{min} + F_p \tag{A-59}$$

The constraint set of Eq. (A-35) can be expressed in terms of x, but the non-negativity of x replaces the lower-bound constraint on k.

$$\begin{bmatrix} E_m & -1_m \\ -E_c & 0 \\ I_k & 0 \\ -S_d & 0 \\ S_s & 0 \\ P & 0 \\ -P & 0 \end{bmatrix} \begin{bmatrix} x \\ m \end{bmatrix} \leq \begin{bmatrix} -(E_m \underline{1}_k k_{min} + F_m) \\ (E_c \underline{1}_k k_{min} + F_c) \\ (k_{max} - k_{min}) \underline{1}_k \\ (S_d \underline{1}_k k_{min} + W_d) - \underline{1}_d s_{min} \\ -(S_s \underline{1}_k k_{min} + W_s) \underline{1}_s s_{max} \\ \underline{1} p_{max} - P \underline{1}_k k_{min} \\ -\underline{1}_k p_{min} + P \underline{1}_k k_{min} \end{bmatrix} \tag{A-60}$$

which can be written in the form of Eq. (A-61)

$$G \begin{bmatrix} x \\ m \end{bmatrix} \geq H \tag{A-61}$$

This inequality is converted to an equality with a $(N_m+N_c+3N_k+N_d+N_s)$- dimensional slack variable vector, u.

$$u = G \begin{bmatrix} x \\ m \end{bmatrix} - H \geq 0 \tag{A-62}$$

The performance measure can also be expressed in terms of the x variable vector. For the augmented variable vector $\bar{x}' = [x\ m]$,

$$Z = L'\bar{x} + \frac{1}{2} \bar{x}'Q\bar{x} \tag{A-63}$$

Compare this with Eq. (A-52), after substituting from Eq. (A-58)

$$J = \frac{1}{2} x'E_p'\bar{Q}E_p x + [k_{min}\underline{1}_k'E_p'\bar{Q} + F_p'\bar{Q} + \bar{L}']E_p x + m + \frac{1}{2} k_{min}^2 \underline{1}_k'E_p'\bar{Q}E_p\underline{1}_k + [F_p'\bar{Q} + \bar{L}']E_p\underline{1}_k k_{min} + (\frac{1}{2}F_p'\bar{Q}+\bar{L}')F_p \tag{A-64}$$

The following matrices are required

$$Q = \begin{bmatrix} E_p'\bar{Q}E_p & 0 \\ 0 & 0 \end{bmatrix} \tag{A-65}$$

$$L = \begin{bmatrix} E_p(\bar{Q}D_p + \bar{L}) \\ 1_m \end{bmatrix} \tag{A-66}$$

where

$$D_p \equiv [E_p 1_k k_{min} + F_p] \tag{A-67}$$

Now upon application of the Kuhn-Tucker conditions, the Lemke complementary problem arises, with non-negative multipliers v and y (dual variables).

$$\begin{bmatrix} v \\ u \end{bmatrix} = \begin{bmatrix} Q & -G' \\ G & 0 \end{bmatrix} \begin{bmatrix} \bar{x} \\ y \end{bmatrix} + \begin{bmatrix} L \\ -H \end{bmatrix} \tag{A-68}$$

The large matrix and vector are

$$M \equiv \begin{bmatrix} Q & -G' \\ G & 0 \end{bmatrix} \tag{A-69}$$

$$q = \begin{bmatrix} L \\ -H \end{bmatrix} \tag{A-70}$$

The partitioned forms of these matrices are shown in Eqs. (A-71) and (A-72), with the dimensions of each partition indicated adjacent to the matrix.

$$
M = \begin{array}{c} \\ N_k \\ l_m \\ N_m \\ N_c \\ N_k \\ N_d \\ N_s \\ N_k \\ N_k \end{array}
\begin{array}{c}
\begin{array}{ccccccccc} N_k & l_m & N_m & N_c & N_k & N_d & N_s & N_k & N_k \end{array} \\
\left[\begin{array}{ccccccccc}
E_p'QE_p & 0 & E_m' & -E_c' & I_k' & -S_d' & S_s' & P' & -P' \\
0 & 0 & -\underline{1}_m' & 0 & 0 & 0 & 0 & 0 & 0 \\
-E_m & \underline{1}_m & 0 & 0 & 0 & 0 & 0 & 0 & 0 \\
E_c & 0 & 0 & 0 & 0 & 0 & 0 & 0 & 0 \\
-I_k & 0 & 0 & 0 & 0 & 0 & 0 & 0 & 0 \\
S_d & 0 & 0 & 0 & 0 & 0 & 0 & 0 & 0 \\
-S_s & 0 & 0 & 0 & 0 & 0 & 0 & 0 & 0 \\
-P & 0 & 0 & 0 & 0 & 0 & 0 & 0 & 0 \\
P & 0 & 0 & 0 & 0 & 0 & 0 & 0 & 0
\end{array}\right]
\end{array}
\qquad \text{(A-71)}
$$

$$
q = \begin{array}{c}
\left[\begin{array}{l}
E_p\ (\overline{QD})_p + \overline{L}) \\
\underline{1}_m \\
-(E_m \underline{1}_k k_{min} + F_m) \\
(E_c \underline{1}_k k_{min} + F_c) \\
(k_{max} - k_{min})\underline{1}_k \\
(S_d \underline{1}_k k_{min} + W_d) - \underline{1}_d s_{min} \\
-(S_s \underline{1}_k k_{min} + W_s) + \underline{1}_s s_{max} \\
\underline{1}_k p_{max} - P \underline{1}_k k_{min} \\
-\underline{1}_k p_{min} + P \underline{1}_k k_{min}
\end{array}\right]
\end{array}
\begin{array}{l}
N_k \\
1 \text{ or } 0 \\
N_m \\
N_c \\
N_k \\
N_d \\
N_s \\
N_k \\
N_k
\end{array}
\qquad \text{(A-72)}
$$

APPENDIX B

CHARACTERISTIC MANEUVER FRAME LENGTH ESTIMATE

The characteristic maneuver was defined in Section 4.2, and is shown in Figure B-1.

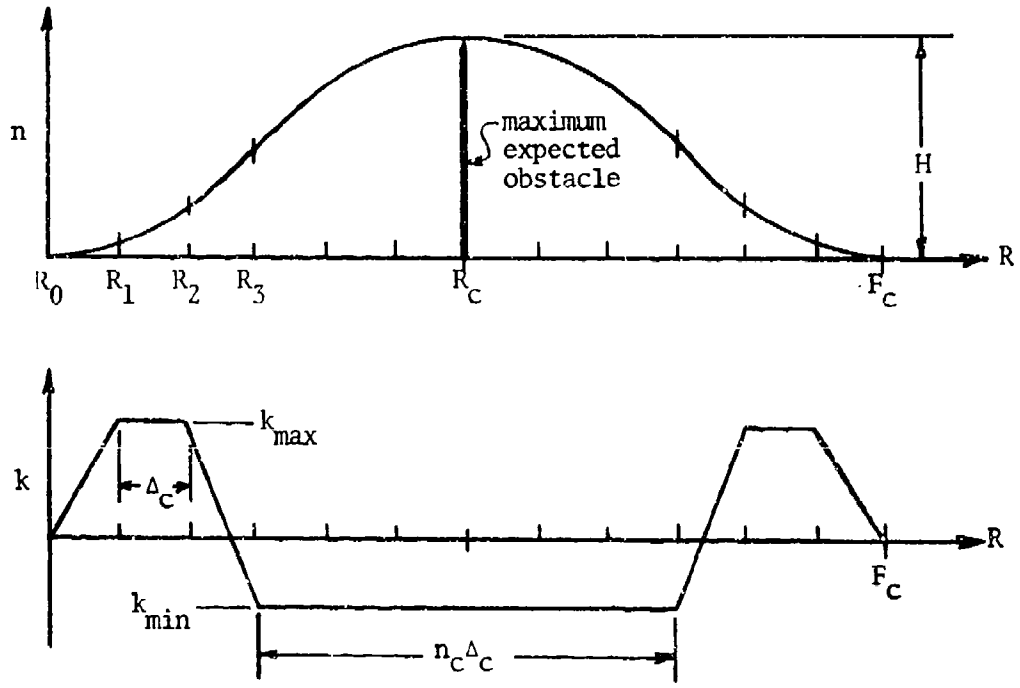

Figure B-1 Characteristic Maneuver

Specified for the maneuver are

k_{min} - minimum curvature

k_{max} - maximum curvature

H - maximum expected obstacle height.

The characteristic frame length, F_c, is the total range distance required by the maneuver and is determined after computing the

characteristic range interval, Δ_c. The slope and height differential equations are integrated piece-wise to the mid range, R_c. The total frame length is twice the value of R_c.

ARC 1 $R_0 = 0$ and $R_1 = \Delta_c$

$$\text{For } R \in [R_0, R_1],\ k(R) = \frac{k_{max}}{\Delta_c} R \tag{B-1}$$

$$S(R) = \int_{R_0}^{R} k(r)dr = \int_{R_0}^{R} \frac{k_{max}}{\Delta_c} rdr = \frac{k_{max}}{\Delta_c} \left[\frac{r^2}{2}\right]_0^R = \frac{k_{max}R^2}{2\Delta_c} \tag{B-2}$$

$$h(R) = \int_{R_0}^{R} s(R)dr = \int_{R_0}^{R} \frac{k_{max}r^2}{2\Delta_c} dr = \frac{k_{max}}{6\Delta_c} [r^3]_0^R = \frac{k_{max}R^3}{6\Delta_c} \tag{B-3}$$

$$S(R_1) = \frac{k_{max}\Delta_c}{2} \tag{B-4}$$

and

$$h(R_1) = \frac{k_{max}\Delta_c^2}{6} \tag{B-5}$$

ARC 2

$R_1 = \Delta_c$ and $R_2 = 2\Delta_c$

$$\text{For } R \in [R_1, R_2],\ k = k_{max} \tag{B-6}$$

$$S(R) = S(R_1) + \int_{R_1}^{R} k_{max}dr = \frac{k_{max}\Delta_c}{2} + k_{max}(R-\Delta_c) \tag{B-7}$$

$$h(R) = h(R_1) + \int_{R_1}^{R} k_{max}(r-\frac{\Delta_c}{2})dr = \frac{k_{max}\Delta_c^2}{6} + \frac{k_{max}}{2}[(r-\frac{\Delta_c}{2})^2]_{\Delta_c}^{R} \tag{B-8}$$

$$S(R_2) = k_{max}\frac{3}{2}\Delta_c \tag{B-9}$$

$$h(R_2) = k_{max}\frac{7}{6}\Delta_c^2 \tag{B-10}$$

ARC 3

$R_2 = 2\Delta_c$ and $R_3 = 3\Delta_c$

$$\text{For } R \in [R_2, R_3],\quad k(R) = k_{max} + \frac{(R-2\Delta_c)}{\Delta_c}(k_{min}-k_{max}) \tag{B-11}$$

$$S(R) = S(R_2) + \int_{R_2}^{R} [k_{max} + \frac{(r-2\Delta_c)}{\Delta_c} (k_{min}-k_{max})]dr$$

$$= k_{max}\frac{3}{2}\Delta_c + k_{max}[r-2\Delta_c]_{2\Delta_c}^{R} + \frac{(k_{min}-k_{max})}{2\Delta_c}[(r-2\Delta_c)^2]_{2\Delta_c}^{R}$$

$$= k_{max}[\frac{3}{2}\Delta_c + (R-2\Delta_c)] + \frac{(k_{min}-k_{max})}{2\Delta_c}[(R-2\Delta_c)^2] \quad \text{(B-12)}$$

$$h(R) = h(R_2) + \int_{R_2}^{R} \{k_{max}[\frac{3}{2}\Delta_c + (r-2\Delta_c)] + \frac{(k_{min}-k_{max})}{2\Delta_c}[(r-2\Delta_c)^2]\}dr$$

$$= k_{max}\frac{7}{6}\Delta_c^2 + k_{max}[\frac{3}{2}\Delta_c(R-2\Delta_c) + \frac{1}{2}(R-2\Delta_c)^2]$$

$$+\frac{(k_{min}-k_{max})}{6\Delta_c}[(R-2\Delta_c)^3] \quad \text{(B-13)}$$

$$S(R_3) = (2k_{max} + \frac{1}{2}k_{min})\Delta_c \quad \text{(B-14)}$$

$$h(R_3) = (3k_{max} + \frac{1}{6}k_{min})\Delta_c^2 \quad \text{(B-15)}$$

ARC 4

$R_3 = 3\Delta_c$ and $R_c = (3+\frac{n_c}{2})\Delta_c$, where n_c is to be determined.

For $R \in [R_3, R_c]$, $\quad k(R) = k_{min}$ (B-16)

$$S(R) = S(R_3) + \int_{R_3}^{R} k_{min}dr = (2k_{max}+\frac{1}{2}k_{min})\Delta_c + k_{min}(R-3\Delta_c) \quad \text{(B-17)}$$

$$h(R) = h(R_3) + \int_{R_3}^{R} \{(2k_{max} + \frac{1}{2}k_{min})\Delta + k_{min}(r-3\Delta_c)\}dr$$

$$= (3k_{max}+\frac{1}{6}k_{min})\Delta_c^2 + (2k_{max}+\frac{1}{2}k_{min})\Delta_c(R-3\Delta_c)$$

$$+ \frac{1}{2}k_{min}(R-3\Delta_c)^2 \quad \text{(B-18)}$$

$$S(R_c) = [2k_{max} + \frac{1}{2}(n_c+1)k_{min}]\Delta_c \tag{B-19}$$

$$h(R_c) = [(3+n_c)k_{max} + \frac{1}{24}(4+6n_c+3n_c^2)k_{min}]\Delta_c^2 \tag{B-20}$$

Now the boundary conditions can be applied to determine Δ_c and n_c.

$$S(R_c) = 0 \tag{B-21}$$

$$h(R_c) = H \tag{B-22}$$

From Eqs. (B-19) and (B-21)

$$n_c = -(4\frac{k_{max}}{k_{min}} + 1) \tag{B-23}$$

Since $k_{min} < 0$, n_c will be a positive number when $k_{max} > -\frac{k_{min}}{4}$

The central range value is

$$R_c = (3+\frac{n_c}{2})\Delta_c = \frac{F_c}{2} \tag{B-24}$$

Thus, from (B-23) and (B-24)

$$F_c = \Delta_c\,(5 - 4\frac{k_{max}}{k_{min}}) \tag{B-25}$$

All that remains is to determine Δ_c from Eqs. (B-20), (B-22) and (B-23)

$$\Delta_c^2 = \frac{H}{(3+n_c)k_{max}+\frac{1}{24}(4+6n_c+3n_c^2)k_{min}}$$

$$= \frac{24H}{48k_{max}(1-\frac{k_{max}}{k_{min}})+k_{min}} \tag{B-26}$$

$$\Delta_c = \sqrt{\frac{24H}{48k_{max}(1-\frac{k_{max}}{k_{min}})+k_{min}}} \tag{B-27}$$

EXAMPLES:

1. Aircraft Soft Ride: $k_{min} = -10^{-5}$ ft^{-1}, $k_{max} = .00008$, H = 1000 ft

$\Delta_c = 834$ ft

$F_c = 37\Delta_c = 30{,}800$ ft

$n_c = 31$

2. Aircraft Hard Ride: $k_{min} = -.00004$, $k_{max} = .00008$, H = 1000 ft

$\Delta_c = 1440$ ft

$F_c = 13\Delta_c = 18{,}800$ ft

$n_c = 7$

3. Missile Soft Ride: $k_{min} = -.000004$, $k_{max} = .000012$, H = 1000 ft

$\Delta_c = .324$ ft

$F_c = 17\Delta_c = 54{,}900$ ft

$n_c = 11$

4. Missile Hard Ride: $k_{min} = -.00002$, $k_{max} = .00006$, H = 1000 ft

$\Delta_c = 1444$ ft

$F_c = 17\Delta_c = 24{,}600$ ft

$n_c = 11$

5. Missile Hard Ride over Smooth Terrain:

$k_{min} = -.00002$, $k_{max} = .00006$, H = 500 ft

$\Delta_c = 1022$ ft

$F_c = 17\Delta_c = 17{,}400$ ft

$n_c = 11$

APPENDIX C

CURVATURE RELATIONSHIPS

To determine the relationship between the path curvature and the normal acceleration (normal to the path), consider height to be a function of range, which is in turn a function of time.

$$h = h(R(t)) \tag{C-1}$$

The curvature is

$$k \triangleq \frac{d^2h}{dR^2} = \frac{d}{dR(t)} \left(\frac{dh}{dR(t)}\right) \tag{C-2}$$

But by the chain rule

$$\frac{d}{dR}( ) = \frac{d}{dt}( )\frac{dt}{dR} = (\dot{})t' = \frac{(\dot{})}{\dot{R}} \tag{C-3}$$

So

$$k = \frac{d}{dt}\left(\frac{\dot{h}}{\dot{R}}\right)\frac{1}{\dot{R}} = \frac{\ddot{h}\dot{R}-\dot{h}\ddot{R}}{\dot{R}^3} \tag{C-4}$$

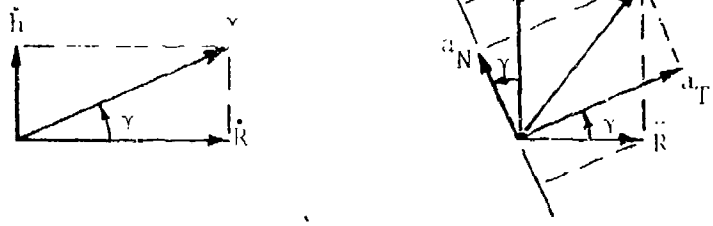

Figure C-1 Velocities and Accelerations

From Figure C-1 it can be seen that

$$\dot{R} = v \cos\gamma \tag{C-5}$$

and

$$a_N = \ddot{h} \cos\gamma - \ddot{R} \sin\gamma = \frac{\ddot{h}\dot{R}}{v} - \frac{\ddot{R}\dot{h}}{v} \tag{C-6}$$

Therefore

$$k = \frac{\ddot{h}\dot{R} - \ddot{R}\dot{h}}{v^3 \cos^3\gamma} = \frac{a_N}{v^2 \cos^3\gamma} \tag{C-7}$$

or

$$k = \frac{a_N}{v^2} \sec^3\gamma \tag{C-8}$$

The instantaneous radius of curvature, r_c, is equal to the radius of a circle that coincides with an infinitesimal segment of the path.

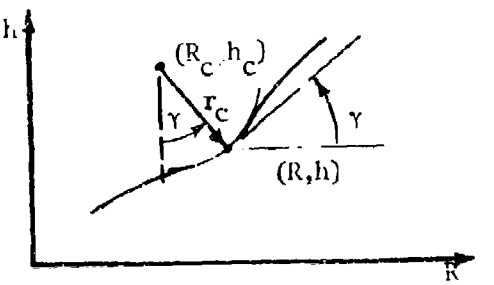

Figure C-2 Radius of Curvature

The coordinates of the path point, for fixed center (R_c, h_c) and fixed radial length, r_c, are

$$R = R_c + r_c \sin\gamma \tag{C-9}$$

$$h = h_c - r_c \cos\gamma \tag{C-10}$$

for

$$\gamma = \tan^{-1}\left(\frac{dh}{dR}\right) \tag{C-11}$$

The slope is

$$\frac{dh}{dR} = \tan\gamma \tag{C-12}$$

while its derivative is

$$\frac{d^2h}{dR^2} = \sec^2\gamma \frac{d\gamma}{dR} \tag{C-13}$$

The differential of Eq. (C-9) can be solved for

$$\frac{d\gamma}{dR} = \frac{1}{r_c} \sec\gamma \tag{C-14}$$

Thus, the relationship between the curvature and radius of curvature is

$$k = \frac{1}{r_c} \sec^3\gamma \tag{C-15}$$

APPENDIX D

DIRECT-SLOPE SPLINE FITTING METHOD

The non-dimensional range variable is

$$\sigma(x) \triangleq (x-x_i)/a_i \tag{D-1}$$

where the dimensional range increment is

$$a_i \triangleq x_{i+1} - x_i \tag{D-2}$$

The ratio of successive increments is

$$H_i \triangleq \frac{a_i}{a_{i+1}} \tag{D-3}$$

and the change in dependent variable over an increment is

$$Y_i \triangleq y_{i+1} - y_i \tag{D-4}$$

The cubic spline and its first two derivatives can then be written

$$y(x) = y_i + A_i\sigma + B_i\sigma^2 + C_i\sigma^3 \tag{D-5}$$

$$y'(x) = \frac{1}{a_i}\left[A_i + 2B_i\sigma + 3C_i\sigma^2\right] \tag{D-6}$$

$$y''(x) = \frac{1}{a_i^2}\left[2B_i + 6C_i\sigma\right] \tag{D-7}$$

Continuity at the knot where $\sigma_{i+1} = 0$ and $\sigma_i = 1$ requires

$$y_{i+1} = y_i + A_i + B_i + C_i \tag{D-8}$$

$$y'_{i+1} = \frac{A_{i+1}}{a_{i+1}} = \frac{1}{a_i}\left[A_i + 2B_i + 3C_i\right] \tag{D-9}$$

$$y''_{i+1} = \frac{2B_{i+1}}{a^2_{i+1}} = \frac{1}{a_i^2}\left[2B_i + 6C_i\right] \tag{D-10}$$

Eqs. (D-8) and (D-9) can be rewritten as a system of two simultaneous equations:

$$\begin{bmatrix} 1 & 1 \\ 2 & 3 \end{bmatrix} \begin{bmatrix} B_i \\ C_i \end{bmatrix} = \begin{bmatrix} Y_i & -A_i \\ H_i A_{i+1} & -A_i \end{bmatrix} = \begin{bmatrix} Y_i - Y'_i a_i \\ a_i (y'_{i+1} - y'_i) \end{bmatrix} \quad \text{(D-11)}$$

When this system is solved

$$\begin{bmatrix} B_i \\ C_i \end{bmatrix} = \begin{bmatrix} 3 & -1 \\ -2 & 1 \end{bmatrix} \begin{bmatrix} Y_i - y'_i a_i \\ H_i A_{i+1} - A_i \end{bmatrix} = \begin{bmatrix} 3Y_i - a_i (2y'_i + y'_{i+1}) \\ -2Y_i + a_i (y'_i + y'_{i+1}) \end{bmatrix} \quad \text{(D-12)}$$

the expressions for B_i, C_i and B_{i+1} can be substituted into Eq. (D-10)

$$2H_i^2 [3Y_{i+1} - a_{i+1}(2y'_{i+1} + y'_{i+2})] = 2[3Y_i - a_i(2y'_i + y'_{i+1}) - 6Y_i + 3a_i(y'_i + y'_{i+1})] \quad \text{(D-13)}$$

or

$$y'_i + 2(1+H_i) y'_{i+1} + H_i y'_{i+2} = 3\left(\frac{Y_i}{a_i} + H_i \frac{Y_{i+1}}{a_{i+1}}\right) \quad \text{(D-14)}$$

Then the complete set of equations for all the unknown y'_i can be written

$$\begin{bmatrix} 2(1+H_1) & H_1 & 0 & \cdots & & \\ 1 & 2(1+H_2) & H_2 & 0 & \cdots & \\ 0 & 1 & 2(1+H_3) & H_3 & 0 & \\ \cdots & 0 & 1 & 2(1+H_4) & H_4 & 0 \\ & & & \vdots & & \\ & \cdots & 0 & 1 & 2(1+H_{n-3}) & H_{n-3} \\ & & \cdots & 0 & 1 & 2(1+H_{n-2}) \end{bmatrix} \begin{bmatrix} y'_2 \\ y'_3 \\ y'_4 \\ \vdots \\ \\ \vdots \\ y'_{n-1} \end{bmatrix}$$

is equal to

$$\begin{bmatrix} 3(\Sigma_1+H_1\Sigma_2)-y'_1 \\ 3(\Sigma_2+H_2\Sigma_3) \\ 3(\Sigma_3+H_3\Sigma_4) \\ \vdots \\ \\ \vdots \\ 3(\Sigma_{n-2}+H_{n-2}\Sigma_{n-1}-H_{n-2}y'_n) \end{bmatrix} \tag{D-15}$$

where

$$\Sigma_i \triangleq \frac{Y_i}{a_i} \tag{D-16}$$

Now if a procedure similar to that given in Section 5.2 is followed to bi-diagonalize the above matrix, simple recursive equations can be derived: 1) Divide the first equation by the first coefficient. 2) Subtract it from the second equation, then divide the resulting equation by the first non-zero coefficient. 3) Repeat the process of step 2 for each successive pair of equations, until the result is in the form

$$\begin{bmatrix} 1 & c_2 & 0 & \cdots & & \\ 0 & 1 & c_3 & 0 & \cdots & \\ \cdots & 0 & 1 & c_4 & 0 & \cdots \\ & & & \vdots & & \\ & \cdots & 0 & 1 & c_{n-3} & 0 \\ & & \cdots & 0 & 1 & c_{n-2} \\ & & & \cdots & 0 & 1 \end{bmatrix} \begin{bmatrix} y'_2 \\ y'_3 \\ y'_4 \\ \vdots \\ \\ \vdots \\ y'_{n-1} \end{bmatrix} = \begin{bmatrix} W_2 \\ W_3 \\ W_4 \\ \vdots \\ \vdots \\ W_{n-2} \\ W_{n-1}-c_{n-1}y'_n \end{bmatrix} \tag{D-17}$$

where

$$c_1 \triangleq 0 \tag{D-18}$$

and

$$W_1 \triangleq y'_1 \tag{D-19}$$

for i=1, 2, ..., n-2 the forward recursion equations are

$$c_{i+1} = \frac{H_i}{2(1+H_i)-c_i} \tag{D-20}$$

$$W_{i+1} = \frac{3(\Sigma_i+H_i\Sigma_{i+1})-W_i}{2(1+H_i)-c_i} \tag{D-21}$$

Finally, the backward recursion equations yield,

for i = n-1, n-2, ..., 2

$$y'_i = w_i - c_i y'_{i+1} \tag{D-22}$$

All data necessary to compute the spline or its derivatives at any point, $\sigma\varepsilon[0,1]$, are now available:

$$y(\sigma) = y_i + \sigma^2(3-2\sigma)[y_{i+1}-y_i] + [(\sigma-2\sigma^2+\sigma^3)y'_i + (\sigma^3-\sigma^2)y'_{i+1}]a_i \tag{D-23}$$

$$y'(\sigma) = \frac{6\sigma}{a_1}(1-\sigma)[y_{i+1}-y_i] + [(1-4\sigma+3\sigma^2)y'_i+(3\sigma^2-2\sigma)y'_{i+1}] \tag{D-24}$$

$$y''(\sigma) = \frac{6(1-2\sigma)}{a_i^2}[y_{i+1}-y_i]+\frac{2}{a_i}[(3\sigma-2)y'_i+(3\sigma-1)y'_{i+1}] \tag{D-25}$$

$$y''' = \frac{-12}{a_i^3}[y_{i+1}-y_i] + \frac{6}{a_i^2}[y'_i+y'_{i+1}] \tag{D-26}$$

Equal Intervals

It is interesting to note the special form of Eq. (D-15) when the spline intervals are all equal ($H_i = 1$).

$$\begin{bmatrix} 4 & 1 & 0 & \cdots & & & \\ 1 & 4 & 1 & 0 & & & \\ 0 & 1 & 4 & 1 & 0 & & \\ \cdots & 0 & 1 & 4 & 1 & & \\ & & & & \vdots & & \\ & & & 0 & 1 & 4 & 1 \\ & & & \cdots & 0 & 1 & 4 \end{bmatrix} \begin{bmatrix} y'_2 \\ y'_3 \\ y'_4 \\ \vdots \\ \\ \vdots \\ y'_{n-1} \end{bmatrix} = \begin{bmatrix} 3(\Sigma_1+\Sigma_2)-y'_1 \\ 3(\Sigma_2+\Sigma_3) \\ 3(\Sigma_3+\Sigma_4) \\ \\ \\ \\ 3(\Sigma_{n-3}+\Sigma_{n-2}) \\ 3(\Sigma_{n-2}+\Sigma_{n-1})-y'_n \end{bmatrix} \quad \text{(D-27)}$$

The corresponding recursion equations (D-20) and (D-21) become, for i=1, 2, ..., n-2:

$$c_{i+1} = \frac{1}{4-c_i} \quad \text{(D-28)}$$

$$W_{i+1} = \frac{3(\Sigma_i+\Sigma_{i+1})-W_i}{4-c_i} \quad \text{(D-29)}$$

Ahlberg [1, pg 16] shows that a second order difference equation can be used as an alternate method of generating the c_i and W_i coefficients for the equal interval case.

$$d_i = 4d_{i-1}-d_{i-2} \qquad \text{for } i=2, 3, \ldots, n-2 \quad \text{(D-30)}$$

$$d_0 = 1 \quad \text{(D-31)}$$

$$d_1 = 4 \quad \text{(D-32)}$$

For i=1, 2, ..., n-2

$$c_{i+1} = \frac{d_{i-1}}{d_i} \tag{D-33}$$

and

$$W_{i+1} = \frac{3(\Sigma_i+\Sigma_{i+1})-W_i}{d_i} \tag{D-34}$$

with $W_1 = y'_1$.

APPENDIX E

OFFSET-LOOP-POINT REJECTION METHOD

When the instantaneous radius of curvature is less than the offset distance, the offset curve will have a loop as shown in Figure E-1.

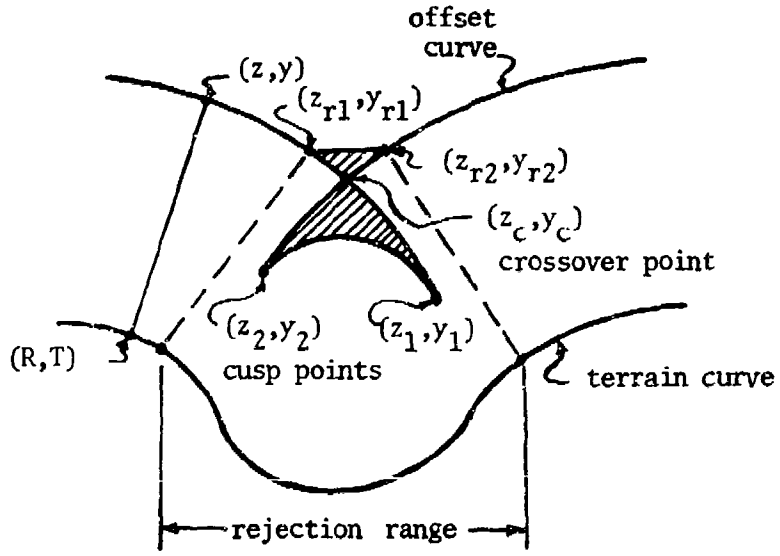

Figure E-1 Offset Loop

Each point on the terrain curve, (R,T), corresponds to a point on the offset curve, (z,y). Since a smooth clearance curve is desired, the portions of the offset curve near the cusps and the crossover point should not be used for points on the clearance curve. One possible method for selecting clearance curve points near a loop is to establish a rejection range, as indicated in the figure by points (z_{r_1},y_{r_1}) and (z_{r_2},y_{r_2}). These points could be located such that they are some prescribed percentage of the intervals $[z_2,z_c]$ and $[z_c,z_1]$. The clearance curve could then be fit

through (z_{r1},y_{r1}), (z_{r2},y_{r2}) and other points outside the rejection range. The proposed rejection procedure is outlined below.

Rejection Procedure

1. Determine if an offset loop is present either by

$$z_{i+1} < z_i \quad \text{when } R_{i+1} > R_i, \text{ or}$$

$$\frac{dz}{dR} = 1 - \frac{\theta^3 k}{s^2+1} < 0 \tag{E-1}$$

for

$$\theta \triangleq n \cos\gamma \tag{E-2}$$

and

$$s = \tan\gamma \tag{E-3}$$

where n is the offset distance, s is the terrain slope, k is the curvature, and γ is the path angle.

2. Compute the cusp points using a binary chop method.

3. Compute the crossover point, lying between the two cusps, by a Newton-Raphson two-dimensional search, by moving two points together, starting from the cusp points.

4. Select the appropriate distances between the cusp points and the crossover point as the rejection interval limits (30% of the distance from crossover to cusp worked reasonably well).

APPENDIX F

SLANT CLEARANCE ESTIMATE

The clearance estimate derived here is a "local" one, in that only the properties of the terrain curve at a single point, T, are used. The radius of curvature, r, is assumed to be constant in the immediate vicinity of the point. Two cases are considered: those of positive and negative terrain curvature.

F.1 Positive Curvature

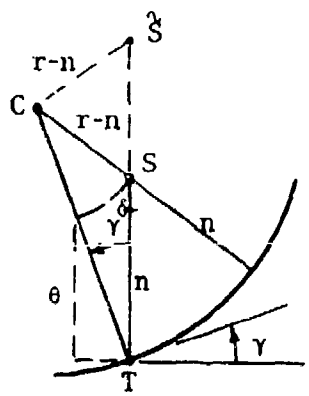

Figure F-1 Positive Curvature Clearance Estimate

The point C is the instantaneous center of curvature for the arc, and S represents the estimated point that has a slant clearance distance of n from the terrain curve (as measured along the normal). The vertical clearance distance of the point S is $C_V=(n+\delta)$. From the cosine law for the triangle CST

$$(r-n)^2 = C_V^2 + r^2 - 2rC_V \cos\gamma \qquad (F-1)$$

This expression can be solved for C_v by the quadratic formula.

$$C_v = r\cos\gamma \pm \sqrt{(r\cos\gamma)^2 - n(2r-n)} \tag{F-2}$$

But

$$\theta \triangleq n\cos\gamma \tag{F-3}$$

so

$$C_v = \frac{r\theta}{n} \pm \sqrt{\left(\frac{r\theta}{n}\right)^2 - n(2r-n)} \tag{F-4}$$

This estimate should only be used if $r > n$, otherwise the normal offset curve has a loop, and estimates about point T are unreliable. Therefore

$$-n(2r-n) < 0 \tag{F-5}$$

and

$$\frac{r\theta}{n} > \sqrt{\left(\frac{r\theta}{n}\right)^2 - n(2r-n)}$$

when the radical is real. So there are two positive roots, with the larger one corresponding to point S shown in Figure F-1. The desired root is

$$C_v = \frac{r\theta}{n} - \sqrt{\left(\frac{r\theta}{n}\right)^2 - n(2r-n)} \tag{F-6}$$

F.2 Negative Curvature

When the path curvature is negative the radius of curvature also has a negative sign

$$r = \frac{1}{K}\sec^3\gamma \tag{F-7}$$

Thus, with $r < 0$, and $C_v = n+\delta$

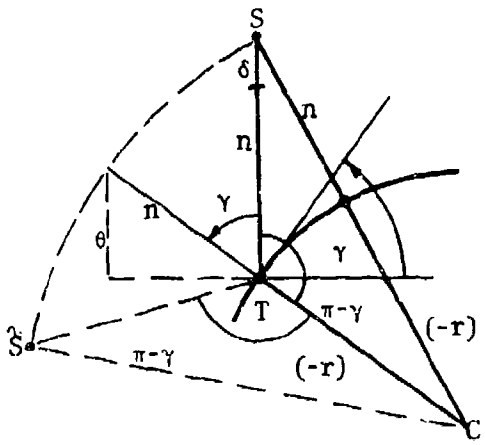

Figure F-2 Negative Curvature Clearance Estimate

Once again, the cosine law for triangle CST yields

$$(n-r)^2 = C_v^2 + r^2 - 2C_v(-r)\cos(\pi-\gamma) \tag{F-8}$$

or

$$(r-n)^2 = C_v^2 + r^2 - 2C_v r\cos\gamma \tag{F-9}$$

This equation is exactly the same as Eq. (F-1) so the solutions are again

$$C_v = \frac{r\theta}{n} \pm \sqrt{\left(\frac{r\theta}{n}\right)^2 - n(2r-n)} \tag{F-4}$$

However, by convention, this time r is negative; for the desired positive root, now the positive sign must be chosen.

Since now

$$-n(2r-n) > 0 \tag{F-10}$$

$$\left|\frac{r\theta}{n}\right| < \sqrt{\left(\frac{r\theta}{n}\right)^2 - n(2r-n)} \tag{F-11}$$

while the negative root corresponds to $\hat{S}$ in Figure F-2.

Finally, we can solve for the clearance difference, δ, in a general expression

$$\delta = \left(\frac{r\theta}{n} - n\right) - \text{sgn}(r)\sqrt{\left(\frac{r\theta}{n}\right)^2 - n(2r-n)}$$

$$= \left(\frac{r\theta}{n} - n\right) - \text{sgn}(r)\sqrt{\left(\frac{r\theta}{n} - n\right)^2 - 2r(n-\theta)} \qquad \text{(F-12)}$$

In general, the total vertical clearance is

$$C_V = \frac{r\theta}{n} - \text{sgn}(r)\sqrt{\left(\frac{r\theta}{n} - n\right)^2 - 2r(n-\theta)} \qquad \text{(F-13)}$$

APPENDIX G

AIRCRAFT SIMULATION

This Appendix contains the equations used in the aircraft simulation. Most of the symbols used in this Appendix are not used elsewhere in the thesis, therefore the symbols are defined below.

C_D Total drag coefficient

C_{D_o} Trim drag coefficient

C_{D_x} Partial derivative of the drag coefficient with respect to various "x" variables

C_L Total lift coefficient

C_{L_o} Trim lift coefficient

C_{L_x} Partial derivative of the lift coefficient with respect to various "x" variables

C_m Total moment coefficient

C_{m_o} Trim moment coefficient

C_{m_x} Partial derivative of the moment coefficient with respect to various "x" variables

D Drag

F Thrust

I_y Aircraft moment of inertia (in pitch)

L Lift

M Moment, in pitch, about the aircraft center of gravity

$\bar{M}$ Mach number

R Horizontal range

S Surface reference area

V Total velocity magnitude

$\bar{a}$	Speed of sound
$\bar{b}$	Distance from aircraft center of gravity to thrust line
$\bar{c}$	Aircraft reference chord length
c.g.	Center of gravity of the aircraft
d	Specific drag force
f	Specific thrust force
g	Specific gravitational force
h	Altitude
k	Path curvature
l	Specific lift force
m	Mass of aircraft
q	Pitching rate with respect to time (positive-nose up)
s	Path slope
u	Component of velocity along the longitudinal (x) stability axis
w	Component of velocity along the normal (z) stability axis (positive downward)
x	Longitudinal stability coordinate
$\underline{x}$	State variable vector
z	Normal stability coordinate (positive downward)
Δ	Indicates a change from the reference condition
α	Angle of attack
α_0	Trim angle of attack
γ	Flight-path angle
γ_0	Angle of x stability axis from the horizontal
δ_c	Command signal to longitudinal flight controller

δ_S Stabilator (pitch control surface) deflection angle (positive, trailing edge down)

δ_{SAS} Stabilator input signal from stability augmentation system (SAS)

ρ Atmospheric density

θ Pitch angle

ϵ Thrust alignment angle

G.1 General Aircraft Equations of Motion

The seven-dimensional state variable vector is

$$\underline{x}' = [u, w, \theta, q, h, \delta_{SAS}, \delta_S] \qquad \text{(G-1)}$$

The stability axis system is fixed with respect to the aircraft as shown in Figure G-1. It coincides with the trim, or steady-state, wind axis system.

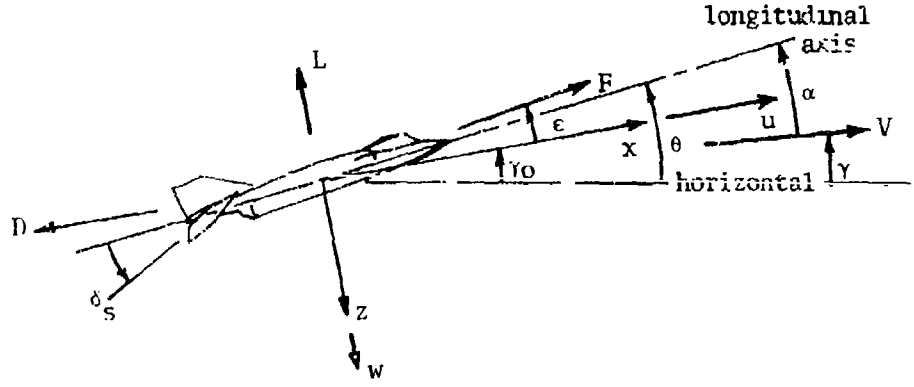

Figure G-1 Stability Axis System

Normally $\gamma_o = 0$ for the reference condition. The equations of motion with respect to time are

$$\dot{R} = u \cos \gamma_o + w \sin \gamma_o \tag{G-2}$$

$$\dot{u} = f_x + g_x - d - qw \tag{G-3}$$

$$\dot{w} = f_z + g_z - \ell + q u \tag{G-4}$$

$$\dot{\theta} = q \tag{G-5}$$

$$\dot{q} = C_{\Lambda M} V^2 C_M + M_F \tag{G-6}$$

$$\dot{h} = u \sin \gamma_o - w \cos \gamma_o \tag{G-7}$$

$$\dot{\delta}_{SAS} = C_{SAS}\, \dot{q} - \delta_{SAS} \tag{G-8}$$

$$\dot{\delta}_s = C_s\, (\delta_{SAS} - \delta_s + \delta_c) \tag{G-9}$$

where C_{SAS} and C_s are constants and

$$f_x \triangleq \frac{T}{m} \cos \epsilon \tag{G-10}$$

$$f_z \triangleq \frac{T}{m} \sin \epsilon \tag{G-11}$$

$$M_F \triangleq \frac{T \bar{b}}{I_y} \tag{G-12}$$

$$g_x \triangleq g_o \sin \gamma_o \tag{G-13}$$

$$g_z \triangleq g_o \cos \gamma_o \tag{G-14}$$

$$\ell \triangleq C_\Lambda V^2 C_L \tag{G-15}$$

$$d \triangleq C_\Lambda V^2 C_D \tag{G-16}$$

and the aerodynamic coefficients are

$$C_\Lambda \triangleq \frac{\rho_o S}{2m} \tag{G-17}$$

$$C_{\Lambda M} \triangleq \frac{\rho_o S \bar{c}}{2 I_y} \tag{G-18}$$

$$C_L \cong C_{L_o} + C_{L_\alpha} \Delta\alpha + C_{L_{\bar{M}}} \Delta\bar{M} + C_{L_\delta} \Delta\delta_s \tag{G-19}$$

$$C_D \cong C_{D_o} + C_{D_\alpha} \Delta\alpha + C_{D_{\bar{M}}} \Delta\bar{M} + C_{D_\delta} \Delta\delta_s \tag{G-20}$$

$$C_m \cong C_{m_o} + C_{m_\alpha} \Delta\alpha + C_{m_{\bar{M}}} \Delta\bar{M} + C_{m_\delta} \Delta\delta_s + \frac{\bar{c}}{2V_o} (C_{m_q} q + C_{m_{\dot{\alpha}}} \dot{\alpha}) \tag{G-21}$$

These additional relationships also apply:

$$V^2 = u^2 + w^2 \tag{G-22}$$

$$\Delta\alpha = \tan^{-1} \frac{w}{u} \tag{G-23}$$

$$\alpha = \alpha_o + \Delta\alpha \tag{G-24}$$

$$\gamma_o = \theta - \alpha_o \tag{G-25}$$

For this problem the atmospheric density, ρ_o, and Mach number are assumed constant for the flight. Note also, that α_o is constant, but γ_o is time varying. Furthermore,

$$\dot{\alpha} = \frac{u\dot{w} - w\dot{u}}{V^2} \tag{G-26}$$

The time differential equations can be converted to range dependence by multiplication by the factor

$$t' \triangleq \frac{dt}{dR} = \frac{1}{\dot{R}} \tag{G-27}$$

Thus

$$\underline{x}' = t' \, \underline{\dot{x}} \tag{G-28}$$

The path slope is

$$s = \frac{dh}{dR} = \dot{h}t' = \frac{\dot{h}}{\dot{R}} \tag{G-29}$$

and the curvature of the path is

$$k = \frac{d^2h}{dR^2} = \ddot{h}(t')^2 + \dot{h}t'' = \frac{\ddot{h}\dot{R} - \dot{h}\ddot{R}}{\dot{R}^3} \tag{G-30}$$

G.2 Normalization

The variables were normalized for computation according to the following system:

1 VU = 1117.1 fps (Mach 1 at Sea Level)

1 DU = 2000 ft

$$1\ TU = \frac{1\ DU}{1\ VU} = 1.79035 \text{ sec}$$

$$1\ AU = \frac{1\ VU}{1\ TU} = 623.9562096 \text{ fps}^2 = 19.3955924 \text{ Gs}$$

G.3 F-4C Aircraft Data (from Reference 12)

Mach .8 at Sea Level (V = 894 fps)

$\alpha_o = .3^o$ $\quad \delta_{S_o} = .3^o$

$C_{L_o} = .076$, $\quad C_{D_o} = .018$

$C_{L_\alpha} = 3.3$, $\quad C_{D_\alpha} = .08$, $\quad C_{m_\alpha} = -.28$

$C_{L_{\bar{M}}} = 0.$, $\quad C_{D_{\bar{M}}} = 0.$, $\quad C_{m_{\bar{M}}} = -.04$

$C_{L_{\delta_S}} = .34$, $\quad C_{D_{\delta_S}} = 0$ (not given), $\quad C_{m_{\delta_S}} = -.49$

$C_{m_{\dot{\alpha}}} = -1.0$

$C_{m_q} = -2.3$

$\varepsilon = 5.25^o$

$S = 530 \text{ ft}^2$

$m = 38{,}925 \text{ lb} = 1209.978 \text{ slug}$

$b_{pilot} = 16.2 \text{ ft}$

$\bar{c} = 16.04 \text{ ft}$

$I_y = 122{,}193 \text{ slug ft}^2$

APPENDIX H

CONSTRAINT VIOLATIONS BETWEEN SAMPLE POINTS

There are no curvature violations between sample points, because the curvature is a linear spline. Neither are there any kink violations, since the kink is always constant over each sample interval. However, there can be clearance and slope constraint violations. The maximum clearance-constraint violation is illustrated in Figure H-1.

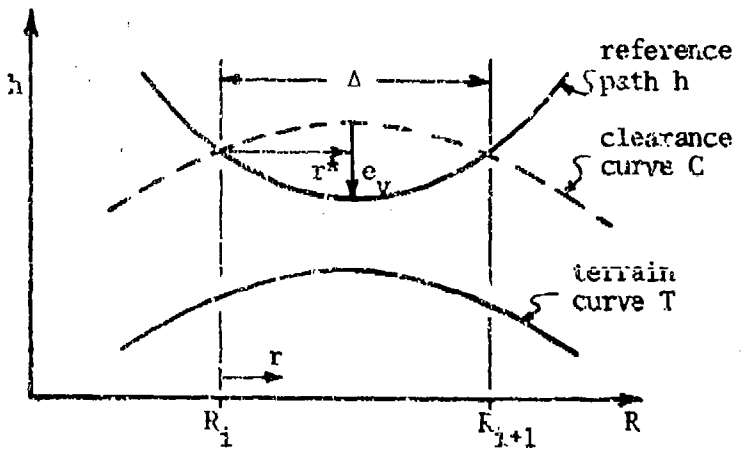

Figure H-1 Maximum Clearance-Constraint Violation

The maximum violation occurs for a maximum pull-up path directly above a minimum curvature terrain peak. When the clearance curve has the same curvature as the terrain curve, the equations for the path and clearance curve over the interval of violation, $r \in [0,\Delta]$, are

$$h_i(r) = h_i + s_i r + \frac{1}{2} k_{max} r^2 \qquad \text{(H-1)}$$

$$c(r) = c_i + d_i r + \frac{1}{2} k_{T_{min}} r^2 \qquad \text{(H-2)}$$

Since the excess clearance is

$$e(r) = h(r) - c(r) \tag{H-3}$$

and

$$h_i = c_i \tag{H-4}$$

$$h_{i+1} = c_{i+1} \tag{H-5}$$

Thus

$$e(r) = (s_i - d_i)r + \frac{r^2}{2}(k_{max} - k_{T_{min}}) \tag{H-6}$$

But at $r=\Delta$, Eqs. (H-1) and (H-2) become

$$h_{i+1} = h_i + s_i\Delta + \frac{1}{2} k_{max}\Delta^2 \tag{H-7}$$

$$h_{i+1} = h_i + d_i\Delta + \frac{1}{2} k_{T_{min}}\Delta^2 \tag{H-8}$$

The difference between these two equations is divided by Δ to yield

$$s_i - d_i = -\frac{\Delta}{2}[k_{max} - k_{T_{min}}] \tag{H-9}$$

Then from Eqs. (H-6) and (H-9)

$$e(r) = \frac{1}{2}(r^2 - r\Delta)(k_{max} - k_{T_{min}}) \tag{H-10}$$

The extreme value of e occurs when

$$0 = \frac{\partial e}{\partial r} = \frac{1}{2}(2r - \Delta)(k_{max} - k_{T_{min}}) \tag{H-11}$$

or

$$r^* = \frac{1}{2}\Delta \tag{H-12}$$

$$e(r^*) = -\frac{\Delta^2}{8}(k_{max} - k_{T_{min}}) < 0 \tag{H-13}$$

The maximum violation is

$$e_v = -e(r^*) = \frac{\Delta^2}{8}(k_{max} - k_{T_{min}}) \tag{H-14}$$

If there are slope constraints active on the interval of violation, the violation will have an even smaller bound than that of Eq. (H-14). In this case, the curvature of the path cannot remain at a maximum value over the entire interval without violating the slope constraint at one end of the interval.

A bound on the maximum slope-constraint violation can be determined from the geometry of Figure H-2.

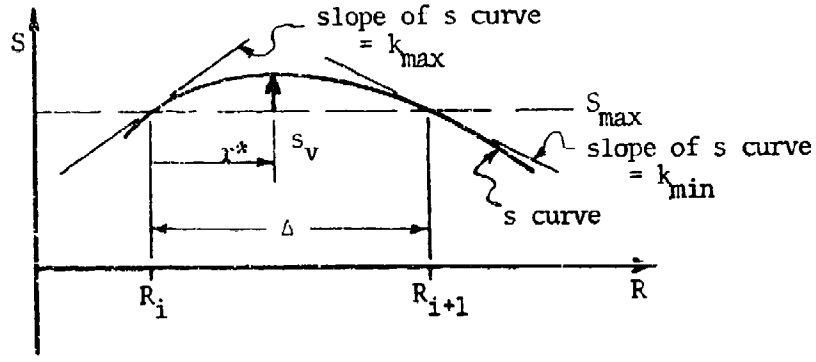

Figure H-2 Maximum Slope-Constraint Violation

Over the interval of violation, the curvature goes from a maximum to a minimum as r goes from zero to Δ.

$$k(r) = k_{max} - \frac{1}{\Delta}(k_{max}-k_{min})\, r \tag{H-15}$$

The path slope is the integral of this equation.

$$s(r) = s_{max} + k_{max} r - \frac{1}{2\Delta}(k_{max}-k_{min})\, r^2 \tag{H-16}$$

The violation is

$$s_v(r) = s(r)-s_{max} = k_{max} r - \frac{1}{2\Delta}(k_{max}-k_{min})\, r^2 \tag{H-17}$$

The extreme value occurs for

$$0 = \frac{\partial s_v}{\partial r} = k_{max} - \frac{1}{\Delta} (k_{max}-k_{min})\, r \tag{H-18}$$

or

$$r^* = \frac{k_{max}\,\Delta}{k_{max}-k_{min}} \tag{H-19}$$

Thus, the bound on the maximum-slope violation is

$$s_{v_{max}} = \frac{k_{max}^2\,\Delta}{2(k_{max}-k_{min})} \tag{H-20}$$

Similarly, a bound on the minimum-slope violation magnitude can be computed

$$s_{v_{min}} = \frac{k_{min}^2\,\Delta}{2(k_{max}-k_{min})} \tag{H-21}$$

REFERENCES

1. Ahlberg, J.H., E.N. Nilson, and J.L. Walsh, The Theory of Splines and Their Applications. Academic Press, N. Y. 1967.

2. Asseo, S.J. and P.J. Brodnicki. ADLAT VI Aircraft Control System Studies for Terrain Following / Terrain Avoidance, AFAL-TR-71-134, Air Force Avionics Lab., April 1971 (AD 517-289).

3. Ball, S.A., Jr. F-111 Operation in the Terrain-Following Mode. Eleventh Symposium Guidance and Control Panel, AGARD, NATO, Brussels, Belgium, 2 Sept 1970.

4. Bergmann, G.E. and G.L. DeBacker. Terrain Following Criteria (Final Report). AFFDL-TR-73-135, Air Force Flight Dynamics Lab., WPAFB, Ohio, 1 June 1974.

5. Beltrami, Edward J. An Algorithmic Approach to Nonlinear Analysis and Optimization. Academic Press, N. Y. 1970.

6. Brostrom, Kenneth E. Terrain Following Evaluation Simulation. Proceedings of NAECON Conference, Dayton, Ohio, pp 219-224, 10-12 June 1975.

7. Bryson, A. E., Jr. and J.L. Speyer. Optimal Programming Problems with Bounded State Space. AIAA Journal, Vol. 6, pp 1448-1491, Aug 1968.

8. Canon, M.D., C.D. Cullum, and E. Polak. Theory of Optimal Control and Mathematical Programming. McGraw Hill, N. Y. 1970.

9. Davidon, William C. Variance Algorithm for Minimization. Computer Journal, Vol. 32, pp 406-410, Oct 1968.

10. Denham, W.F. and A.E. Bryson, Jr. Optimal Programming Problems with Inequality Constraints, II: Solution by Steepest Ascent. AIAA Journal, Vol. 2, No. 1, pp 25-34, Jan 1964.

11. Greaves, C.J. Theoretical Development of an Optimum Aircraft Control System. Dissertation, Rensselaer Polytechnic Institute, Troy, N. Y., Aug 1968.

12. Heffley, Robert K. and W.F. Jewell. Aircraft Handling Qualities Data. NASA CR-2144, Dec 1972.

13. Hennig, G.R. A Numerical Method for the Solution of Optimal Control Problems with Bounded State Variables. Dissertation, DS/EE/71-1, Air Force Institute of Technology, WPAFB, Ohio, 1971.

14. Hillier, F.S. and G.J. Lieberman. Introduction to Operations Research. Holden-Day Inc., San Francisco, 1967.

15. Jacobson, D.H. and M.M. Lele. Transformation Technique for Optimal Control Problems with State Variable Inequality Constraints. Joint Automatic Control Conference, 10th, University of Colorado, Boulder, Colo., 5-7 Aug 1969, Preprints of Technical Papers, N. Y., AIChE, pp 52-59, 1969.

16. Jeffrie, Howard L. A Scoring Criterion for the Evaluation of Terrain Following System Performance. M.S. Thesis, St. Louis University, Mo., 1967.

17. Kelley, H.J. and W.F. Denham. An Accelerated Gradient Method for Parameter Optimization with Nonlinear Constraints. Space Flight Mechanics Specialist Conference, University of Denver, Colo., 6-8 July 1966.

18. Kisslinger, R.L. and G.J. Versch. Survivable Flight Control System, Interim Report No. 1, Studies, Analyses and Approach. AFFDL-TR-71-20, Supplement 2, Air Force Flight Dynamics Lab., WPAFB, Ohio, May 1971.

19. Lasdon, L.S., A.D. Warren, and R.K. Rice. An Interior Penalty for Inequality Constrained Optimal Control Problems. IEEE Transactions on Automatic Control, Vol. AC-12, No. 4, pp 388-395, Aug 1967.

20. Martensson, Krister. A Constraining Hyperplane Technique for State Variable Constrained Optimal Control Techniques. Joint Conference on Automatic Control, 14th, Columbus, Ohio, 20-22, June 1973, Preprints of Technical Papers, N. Y., IEEE, pp 154-163, 1973.

21. Merriam, C.W., III. Optimization Theory and the Design of Feedback Control Systems. McGraw Hill, N. Y., 1964.

22. Poirier, C.P. Cubic Spline Programs. Scientific System Analysis Section, Computer Center, (4950/ADDS), WPAFB, Ohio

23. Quinlivan, R.P., G. Tye and H.H. Westerholt. Analytical Investigation of Control Requirements for High Speed Low Altitude Penetration -- Final Report Brief. FDL-TDR-64-104, Air Force Flight Dynamics Lab., WPAFB, Ohio, Dec 1964.

24. Quinlivan, R.P. and H.H. Westerholt. Investigation of Flight Control Requirements for Terrain Following (Summary). AFFDL-TR-66-65, Air Force Flight Dynamics Lab., WPAFB, Ohio, July 1966.

25. Quinlivan, R.P. Terrain Following Controller Flight Test -- First Technical Report. AFFDL-TR-67-114, Part I, Air Force Flight Dynamics Lab., WPAFB, Ohio, June 1967.

26. Ravindran, Arunachalan. A Computer Routine for Quadratic and Linear Programming Problems. (Algorithm 431) Communications of ACM, Vol. 15, No. 9, pp 818-820, Sept 1972.

27. Ritchey, V.S., J.D. Kendrick and R.A.K. Mitchell. Terrain Following Aircraft Controller, E.E. Term Project, Air Force Institute of Technology, WPAFB, Ohio, Sept 1974.

28. Schoenberg, I.J. (Editor). Approximations with Special Emphasis on Spline Functions. Proceedings of a Symposium Conducted by the Mathematical Research Center, United States Army, at the University of Wisconsin, 5-7 May 1969, Academic Press, N. Y. 1969.

29. Shankland, D.G. Quadratic Programming Using Generalized Inverses. Technical Report, AFIT TR-75-2, Physics Dept., Air Force Institute of Technology, WPAFB, Ohio, May 1975.

30. UNIVAC Cubic Spline Routines, UNIVAC 1108 Mathematics - Statistics Library.

31. Weir, David H. Computation and Analysis of Flight Control System Command Inputs. AFFDL TR-65-119, Air Force Flight Lynamics Lab., WPAFB, Ohio, Jan 1966.

END 5-76